Investigating Novel Roles for *gdf6* and *crx* in Retinal Development and Disease

by

Lindsey Dawn March

A thesis submitted in partial fulfillment of the requirements for the degree

of

Master of Science

in

Molecular Biology and Genetics

Department of Biological Sciences

University of Alberta

Abstract

The growth and development of an organ is a multi-step process. It involves initial specification of the progenitor cells to become a particular cell type, proliferation of those cells for organ growth, and organization of the cells into a final functional tissue. The growth and development of the vertebrate eye is an exquisite example of this process. Specification of the eye field early in development, proliferation of retinal progenitor cells and eye morphogenesis, differentiation of mature neural (retinal) and non-neural cell types that make up the eye, and organization of multiple cell types into functional tissues are required for correct eye development.

Bone morphogenetic proteins (BMPs) have diverse roles in development, including regulation of differentiation, proliferation and cell survival. Mutations in BMP genes are associated with a spectrum of blinding ocular abnormalities, including MAC (microphthalmia, anophthalmia, colobomata) and Leber's congenital amaurosis (LCA). We used a microphthalmic zebrafish line, with a mutation in the BMP ligand *gdf6a*, to investigate the development of microphthalmia. $gdf6a^{-/-}$ mutants have ectopic retinal apoptosis that is rescued by pharmaceutical treatment with an anti-apoptotic compound. Interestingly, the rescue of retinal apoptosis in the $gdf6a^{-/-}$ mutants does not rescue eye-size, and only partially recovers visual activity. We concluded that mutations in *gdf6a* must disrupt

multiple developmental processes that contribute to eye development, one of which is retinal progenitor cell survival, and that these are the underlying causes of microphthalmia in this model.

The vertebrate retina is a highly organized and laminar structure, the development of which is conserved among all vertebrates. The retina contains 6 neuronal cell types and one glial cell type. Differentiation of these cell types from retinal progenitor cells requires the transcription factor *cone-rod homeobox* (*crx*). *crx* is a member of the highly conserved *orthodenticle*-related (*otx*) gene family of transcription factors and lesions in human *CRX* have been associated with photoreceptor degeneration disorders such as LCA, retinitis pigmentosa and cone-rod dystrophy. We hypothesized that zebrafish *crx*$^{-/-}$ mutants would display a loss of photoreceptor identity. Contrary to our hypothesis, zebrafish *crx*$^{-/-}$ mutant retinas have a wild-type appearance. Zebrafish *crx,* and a paralog of *crx, otx5,* have similar expression patterns in the retina. Knocking down *otx5* in *crx*$^{-/-}$ mutants revealed a loss of photoreceptor identity. We show that *crx* and *otx5* have overlapping functions in the retina, and that Crx and Otx5 cooperatively specify photoreceptor identity in the zebrafish retina.

Preface

This thesis is an original work by Lindsey Dawn March. The research project, of which this thesis is part, received research ethics approval from the University of Alberta Animal Policy and Welfare Committee. The author has met the Canadian Council on Animal Care (CCAC) mandatory training requirements for animal users on the Care and Use of Animals in Research, Teaching and Testing.

Portions of Chapter 3 have been contributed by the author to the following publications:

Asai-Coakwell, M., March, L., Dai, X.H., Duval, M., Lopez, I., French, C.R., Famulski, J., De Baere, E., Francis, P.J., Sundaresan, P., Sauve, Y., Koenekoop, R.K., Berry, F.B., Allison, W.T., Waskiewicz, A.J. and Lehmann, O.J., 2013. Contribution of growth differentiation factor 6-dependent cell survival to early-onset retinal dystrophies. Hum Mol Genet. 22, 1432-42.

French, C.R., Stach, T.R., March, L.D., Lehmann, O.J. and Waskiewicz, A.J., 2013. Apoptotic and proliferative defects characterize ocular development in a microphthalmic BMP model. Invest Ophthalmol Vis Sci. 54, 4636-47.

Pant, S.D., March, L.D., Famulski, J.K., French, C.R., Lehmann, O.J. and Waskiewicz, A.J., 2013. Molecular mechanisms regulating ocular apoptosis in zebrafish *gdf6a* mutants. Invest Ophthalmol Vis Sci. 54, 5871-79.

All data presented in this thesis are the author's original work.

Acknowledgements

Table of Contents

List of Tables

List of Figures

List of Abbreviations

3C: chromosome conformation capture

A: adenine

AIDS: autoimmune deficiency syndrome

Apaf1: apoptotic protease-activating factor 1

Bak: Bcl-2 antaginist or killer

Bambi: BMP and activin membrane bound inhibitor

Bax: Bcl-2-associated X protein

BCIP: 5-bromo-4-chloro-3-indolyl-phosphate

BMAL: brain muscle ARNT-like 1

BMP: bone morphogenetic protein

BMPR-I: BMP receptor, type I

BMPR-II: BMP receptor, type II

bp: base pair

BRE: BMP-responsive element

BSA: bovine serum albumin

C: cytosine

cDNA: complementary DNA

CDS: coding sequence

ChIP: chromatin immunoprecipitation

CLOCK: circadian locomotor output cycles kaput

CMZ: ciliary marginal zone

Crx: cone-rod homeobox

Ct: threshold cycle

DEPC: diethylpyrocarbonate treated water

DIG: digoxigenin

DMSO: dimethyl sulfoxide

DNA: deoxyribonucleic acid

dpf: days-post-fertilization

dsDNA: double-stranded DNA

DTT: dithiothreitol

EF1a: elongation factor 1 alpha

EFTF: eye field transcription factors

EM: embryo media

ERG: electroretinogram

FC: fold change

G: guanine

GCL: ganglion cell layer

gdf6a: growth differentiation factor 6a

gDNA: genomic DNA

GOI: gene of interest

HD: homeodomain

HIV: human immunodeficiency virus

hpf: hours-post-fertilization

HRMA: high resolution melt curve analysis

INL: inner nuclear layer

IPL: inner plexiform layer

IPTG: isopropyl β-D-1-thiogalactopyranoside

JRP: juvenile retinitis pigmentosa

LB: Luria broth

LCA: Leber's congenital amaurosis

MAC: microphthalmia, anophthalmia, colobomata

MAPK: mitogen activated protein kinase

MO: morpholino oligonucleotide

MOMP: mitochondrial outer membrane permeabilization

mRNA: messenger RNA

N: number of biological repeats

NBT: 4-nitro blue tetrazoluim

Npas3: neuronal PAS domain protein 3

Nr2e3: photoreceptor-specific orphan nuclear receptor

NRE: Nrl-responsive element

Nrl: neural leucine zipper

nt: nucleotides

OKR: optokinetic response

OMR: optomotor response

ONL: outer nuclear layer

OPL: outer plexiform layer

ORF: open reading frame

OT: optic tectum

Otd: orthodenticle

Otx: orthodenticle-related homeobox gene

Otx2: orthodenticle homeobox 2

Otx5: orthodenticle homeobox 5

PBS: phosphate buffered saline

PBSDTT: 1X PBS, 1% DMSO, 0.1% Tween-20, 0.1% Triton X-100

PBST: PBS + 0.1% Tween-20

PCR: polymerase chain reaction

PFA: paraformaldehyde

PINE: pineal negative regulatory element

Prkca: protein kinase c α

PTU: N-phenylthiourea

qPCR: quantitative real-time PCR

RAR: retinoic acid receptor

RC: relative concentration

RGC: retinal ganglion cell

RNA: ribonucleic acid

Rorβ: RAR related orphan receptor

RPC: retinal progenitor cell

RPE: retinal pigmented epithelium

RT-PCR: reverse transcriptase PCR

RVD: repeat variable di-residue

SD: standard deviation of the Ct

SD$_{FC}$: standard deviation of the FC

SDS: sodium dodecyl sulfate

SD$_{\Delta Ct}$: standard deviation of the ΔCt

SEM: standard error of the mean

Shh: sonic hedgehog

SOC: super optimal broth with catabolite repression

SSC: saline sodium citrate buffer

T: thymine

Tak1: Tgfβ-activated kinase 1

TALEN: transcription activator-like effector nuclease

TBST: tris buffered saline + Tween-20

Tcm: total cataract with microphthalmia

TFM: tissue freezing media

TGFβ: transforming growth factor-β

T$_m$: melting temperature

tRNA: transfer RNA

Trβ2: thyroid hormone receptor β2

UTR: untranslated region

Vax2: ventral homeobox 2

VBA: visually mediated background adaptation

WISH: whole mount mRNA in situ hybridization

WSP: wolbachia surface protein motif

XGAL: 5-bromo-4-chloro-3-indolyl-β-D-galactopyranoside

ZFN: zinc-finger nuclease

ΔCt: average change in Ct

ΔΔCt: calibrated Ct

Chapter 1

Introduction

Zebrafish Eye Development

Eye development, retinal structure and visual processing are well conserved among all vertebrates. Several animal models have been used throughout history to study the structure and function of the vertebrate retina. The first description of the cellular structure of the retina was by Spanish neuroscientist and Nobel laureate Santiago Ramón y Cajal in 1888. Cajal used the rapid Golgi staining method to label only a few cells, allowing him to observe and describe, in detail, the structure and form of the retinal cells and processes in the avian retina (Cajal, 1972). Since then, the retina has been studied in multiple vertebrate species including, but not limited to, zebrafish, *Xenopus,* newt, chick, mouse and primates (Cajal, 1972).

The high degree of evolutionary conservation of vertebrate eye development allows the study of retinal biology in a teleost zebrafish (*Danio rerio*) model. Zebrafish are also well suited as a model for studying retinal biology for the following reasons: zebrafish embryos develop externally and display embryonic transparency, allowing easy access and manipulation of the embryonic retina; zebrafish lay large clutches of embryos (200 – 1000 per breeding pair); zebrafish have a relatively short life-cycle relative to other vertebrate models (sexual maturity is reached by three months of age) and are relatively easy and affordable to maintain; and the zebrafish genome has been sequenced, with a number of freely-accessible online genomic resources available. In zebrafish, retinal neurogenesis persists beyond the embryonic period and responds to retinal damage by replacing lost neurons. Understanding the regenerative response in the zebrafish retina has the potential to lead to strategies for restoring vision in humans with visual system disorders. The diurnal zebrafish retina contains large numbers of rod and cone photoreceptors, the neurogenesis of which are both temporally and spatially distinct. This makes the teleost retina a better

model of the human retina than a nocturnal model system with limited colour vision, such as rodents (reviewed in Stenkamp, 2007).

Zebrafish Eye Morphogenesis

Zebrafish eye field specification occurs during gastrulation, as early as 6 hours post fertilization (hpf; Seo et al., 1998). After eye field separation, the optic primordia evaginate laterally from the anterior neuroepithelium at 12 hpf producing bilateral optic vesicles. Between 13 – 15 hpf the optic vesicles flatten and reorient from horizontal wings to vertical pads on either side of the anterior neuroepithelium. Invagination and rotation of the optic vesicle to form a double-walled optic cup occurs from 15 – 36 hpf (Li et al., 2000; Schmitt and Dowling, 1994). The exterior layer of the optic cup is fated to become the retinal pigmented epithelium (RPE) and the inner layer fated to become the neural retina. Signaling cues from the optic vesicle to the overlying ectoderm induce lens placode formation at 15 hpf and the lens detaches from the overlying ectoderm by 24 hpf (Figure 1.1; Dahm et al., 2007; Donner et al., 2006). During invagination and subsequent eye morphogenesis, the presence of a transient ventral fissure (the optic or choroid fissure) allows for the vascular entry into and axonal exit from the retina (Barishak, 1992; Li et al., 2000).

Vertebrate Eyefield Specification

Shortly after gastrulation, the presumptive eye field is specified at the medial anterior neural plate by the overlapping expression of a set of highly conserved eye field transcription factors (EFTFs). These EFTFs are *Pax6, Lhx2, Rx* and *Six3* (Heavner and Pevny, 2012; Walther and Gruss, 1991). The EFTF, *Pax6,* is a paired domain-containing transcription factor (Walther and Gruss, 1991), and heterozygous lesions in the *Pax6* gene result
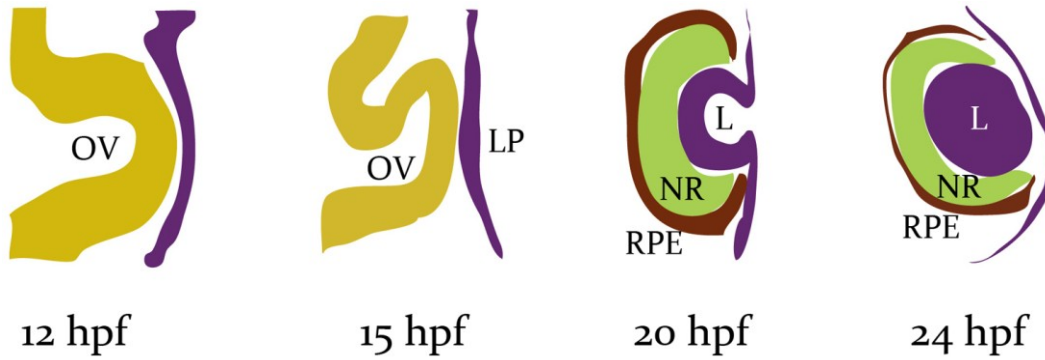
Figure 1.1: Zebrafish eye morphogenesis. At 12 hpf, the optic vesicle (OV) evaginates from the anterior neuroepithelium, approaching the overlying ectoderm. Reorientation of the OV occurs at 15 hpf, and the lens placode (LP) is induced in the overlying ectoderm. By 20 hpf the OV invaginates, forming a double-layered optic cup, with the inner layer fated to become the neural retina (NR) and the outer layer fated to become the retinal pigmented epithelium (RPE). The lens (L) detaches by 24 hpf.

in anophthalmia (no eye) or aniridia (absent iris) in human patients and mouse models (Glaser et al., 1994; Hill et al., 1991). Mice deficient in *Lhx2* can generate optic vesicles, but not optic cups (Porter et al., 1997). *Pax6* expression is maintained in mouse *Lhx2*^{-/-} mutants and, conversely, *Lhx2* expression is maintained in mouse *Pax6*^{-/-} mutants. These data indicate that these genes have independent, essential roles, but they are separately insufficient for eye development (Porter et al., 1997). Lesions in *Rx* have been identified in mouse models and human patients with anophthalmia (Voronina et al., 2004; Zhang et al., 2000) and *Rx*^{-/-} mice lack expression of EFTF genes in the presumptive eye field (Zhang et al., 2000). Finally, loss of *Six3* expression in the mouse eye field results in loss of neural retina formation (Liu et al., 2010).

The neural ectoderm transcription factors Otx2 and Sox2 are also critical for specification of the eye field. Heterozygous mutations in human *SOX2* are often associated with anophthalmia (Fantes et al., 2003), and heterozygous mutations in human *OTX2* cause a range of phenotypes from anophthalmia to retinal dystrophy (Ragge et al., 2005). Additionally, in vitro data suggests that *Otx2* and *Sox2* act cooperatively to promote *Rx* expression (Danno et al., 2008). Taken together, these data suggest a model for eye field specification wherein the cooperative action of Otx2 and Sox2 transcription factors activate *Rx* expression in the presumptive eye field. Next, Rx activates the expression of the rest of the EFTF genes, *Pax6, Six3,* and *Lhx2*. The overlapping expression of *Rx, Pax6, Six3* and *Lhx2* now specify the eye field.

Functional compartmentalization of the optic vesicle is obtained by the spatially restricted expression of tissue-specific genes whose expression are controlled by signaling networks. The optic vesicle is compartmentalized into three distinct tissues: [1] the morphogen *Sonic*

5

hedgehog (*Shh*) is secreted from the ventral midline and promotes *Pax2* expression in tissues destined to become optic stalk; [2] *Fgf* signaling from the overlying ectoderm activates *Vsx2* expression in the putative neural retina; [3] Dorsal *Wnt* signaling promotes *Mitf* expression in the future RPE (reviewed in Heavner and Pevny, 2012).

Zebrafish Retinal Neurogenesis and Organization

The vertebrate neural retina is a highly organized and conserved laminar tissue that contains six neuronal and one glial cell type. These cells are organized into three nuclear layers (the outer nuclear layer [ONL], inner nuclear layer [INL] and retinal ganglion cell layer [GCL]) and two synaptic layers (the outer plexiform layer [OPL] and inner plexiform layer [IPL]; Figure 1.1). The ONL contains the light-detecting rod- and cone-photoreceptor cells. Upon photoactivation, photoreceptor cells relay an electrical signal to the bipolar cells located in the INL, which in turn transmit the signal to the retinal ganglion cells (RGCs) in the GCL (Luo et al., 2008). The axons of the RGCs exit the retina via the optic nerve and send their axon projections to the visual processing center of the brain, the optic tectum. Horizontal and amacrine cell bodies are located in the INL and their axons project into the OPL and IPL respectively. The nuclei of Müller glial cells are located in the INL, but their projections spread throughout all retinal cell layers (Stenkamp, 2007). Müller glia mainly have a supportive role in the retina, but after injury they have been shown to dedifferentiate into multipotent progenitor cells that can differentiate into multiple cell types (Bernardos et al., 2007).

All neuronal retinal cells are derived from a single, uniform population of common multi-potent retinal progenitor cells (RPCs). Retinal cells are born in a stereotypical order with fan-shaped waves of
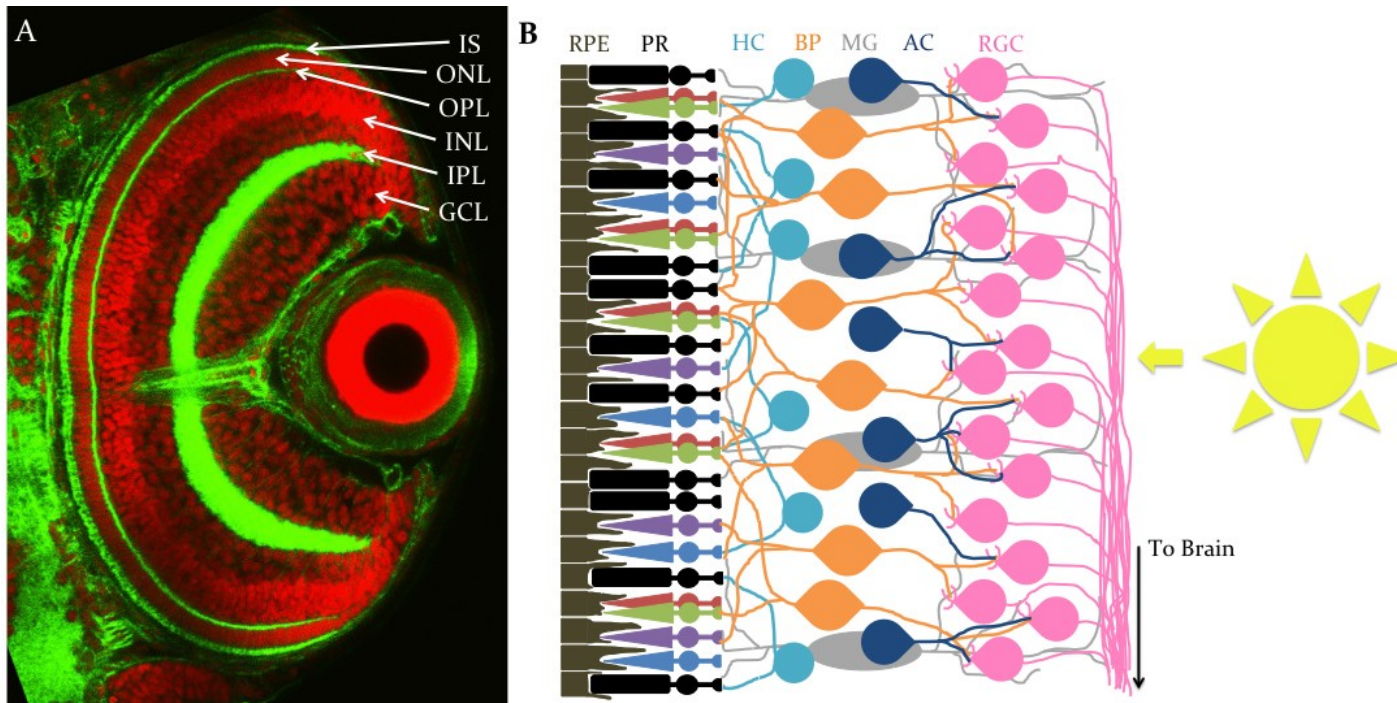
Figure 1.2: The retina is a highly organized laminar tissue. (A) Cross-section through a 3 dpf zebrafish retina (Phalloidin: green; ToPro3: red). (B) Diagram showing the six neuronal and one glial cell types of the retina, and the retinal pigmented epithelium (RPE). The outer nuclear layer (ONL) contains rod and cone photoreceptors (PR), the inner nuclear layer contains the bipolar interneurons (BP) and the horizontal (HC) and amacrine (AC) cell bodies. The ganglion cell layer (GCL) contains the retinal ganglion cells (RGC) that send their axonal projections to the visual processing centers of the brain via the optic nerve. Müller glial cells (MG) span the length of the retina. IS: photoreceptor inner segment; OPL: outer plexiform layer; IPL: inner plexiform layer.

neurogenesis sequentially producing each neural layer. RGCs exit the cell cycle between 24 – 36 hpf, interneurons of the INL (horizontal, amacrine and bipolar cells) exit the cell cycle from 36 – 48 hpf, and cone photoreceptors exit the cell cycle from 48 – 72 hpf (Hu and Easter, 1999). Neurogenesis of each retinal layer begins in a ventronasal patch of first-born cells followed by a fan-shaped wave of differentiation spreading from the ventronasal patch to the nasal-, dorsal-, then temporal retina (Raymond et al., 1995; Schmitt and Dowling, 1996). Rod photoreceptors are slower to mature (Raymond, 1985) and rods are continuously generated and inserted into the teleost retina throughout development (Raymond and Rivlin, 1987). Rod differentiation follows a developmental program distinct from cones, and arises from a secondary wave of neurogenesis originating from a population of mitotically active INL cells (Otteson and Hitchcock, 2003). The first rod nuclei are observable at 8 dpf, and rod outer segments can be first observed at 12 dpf (Branchek and Bremiller, 1984).

Retinotectal Mapping

Correct mapping of the connections between the eye and the brain are critical for our ability to interpret a visual image. Regional expression of retinal patterning genes is restricted to four quadrants of the eye, demarking the nasal, dorsal, temporal and ventral quadrants. The optic tectum (OT) is similarly divided into anterior, posterior, lateral and medial quadrants. The placement of the RGC axons from each quadrant of the eye to the corresponding quadrant of the optic tectum is critical for the brain to interpret the image we see. Axons from the nasal retina map to the posterior OT, and axons from the temporal retina map to the anterior OT. Similarly, axons from the dorsal retina map to the lateral OT, and axons from the ventral retina map to the medial OT. This precise axonal

placement relies on gradients of Eph receptors and their Ephrin ligands, which promote either attractive or repulsive cues between the RGC axons and the surrounding tissue.

EphrinA ligands and EphA receptors provide repulsive cues and are expressed in opposing gradients in the OT (*ephA,* anterior; *ephrinA,* posterior) and the retina (*ephA,* temporal; *ephrinA,* nasal). As a result, *ephA*-expressing RGC axons from the temporal retina are repelled by the *ephrinA*-expressing posterior OT, and map to the anterior OT where *ephrinA* expression is lowest. Conversely, *ephrinA*-expressing nasal RGC axons are attracted to the posterior OT, where *ephA* expression is lowest. Similarly, the EphrinB ligands and EphB receptors are also expressed in opposing gradients in the OT (*ephB,* lateral; *ephrinB,* medial) and retina (*ephB,* ventral; *ephrinB,* dorsal). These ligand-receptor interactions are attractive, thus the *ephB*-expressing RGC axons from the ventral retina are attracted to the medial OT where *ephrinB* expression is highest, and the *ephrinB*-expressing dorsal RGC axons are attracted to the lateral OT, where *ephB* expression is highest (reviewed in Lemke and Reber, 2005).

Vertebrate Dorsal-Ventral Retinal Patterning

To set up the dorsal-ventral and nasal-temporal axes of the retina, genes are expressed in opposing gradients often with mutual inhibition. Bone morphogenetic protein (BMP) signaling specifies the dorsal retinal identity. The BMP ligands *Bmp2, Bmp4* and *Gdf6* are expressed at high levels in the dorsal retina (Behesti et al., 2006; French et al., 2009; Sakuta et al., 2006). BMP signaling activates expression of the T-Box transcription factor *Tbx5,* which in turn activates the expression of dorsal axon guidance molecules (Koshiba-Takeuchi et al., 2000). Shh-signaling in the ventral retina induces *ventral homeobox 2 (Vax2)* expression in the ventral retina

(Take-uchi et al., 2003). Additionally, there is evidence that Vax2 activates the expression of ventral axon guidance molecules (Schulte et al., 1999). Overexpression of dorsal-specific *Bmp4* results in a dorsalized retina and reduces the expression of *Vax2* (Koshiba-Takeuchi et al., 2000). Conversely, overexpression of *Vax2* results in the down-regulation of dorsal-specific *Tbx5* (Schulte et al., 1999), supporting a model of mutual inhibition of opposing transcription factors.

Photoreceptor Development

Photoreceptors are central to our ability to convert light into the neural messages that result in our visual experience. Cone photoreceptors respond to bright light and come in varieties with distinct spectral sensitivities to mediate high resolution, colour vision. Rod photoreceptors respond to low light and can be up to 100-fold more light sensitive than cones. Rods do not discriminate spectral information, but their high light sensitivity allows for exquisite night vision (Luo et al., 2008). Photoreceptors contain light-absorbing visual pigments called opsins that are linked to the chromophore 11-*cis*-retinal. Photoisomerization of 11-*cis*-retinal activates a signal cascade that results in hyperpolarization of the neuron in a process called phototransduction (Luo et al., 2008). Rods have one type of visual pigment, rhodopsin, and cones may have a number of different visual pigments that absorb light at particular wavelengths. Humans and diurnal primates have three types of cone opsin: [1] S opsin (short-wave-sensitive) that absorbs blue light, [2] M opsin (medium-wave-sensitive) that absorbs green light and [3] L opsin (long-wave-sensitive) that absorbs red light. Most mammals only have S- and M opsin (Swaroop et al., 2010). In addition to blue, green and red sensitive opsins, zebrafish have an

additional short-wave-sensitive opsin that absorbs ultraviolet light (Robinson et al., 1993).

The generation of functional, mature neurons from RPCs proceeds in a stepwise fashion that restricts lineage choices at each step and commits cells to a particular fate (Agathocleous and Harris, 2009). Photoreceptor differentiation can be divided into 5 basic steps: [1] proliferation of RPCs, [2] RPC competence restriction, [3] cell fate specification and commitment, [4] photoreceptor-specific gene expression and [5] axon growth, synapse formation and outer segment biogenesis (Swaroop et al., 2010). The molecular mechanisms that promote RPCs to develop into photoreceptor precursors (steps 1-3) remain relatively uncharacterized. Notch proteins are transmembrane receptors that interact with transmembrane ligands on neighboring cells. Activation of Notch signaling results in the cleavage of its intracellular domain, which functions as a transcription factor. It is known that Notch signaling maintains the cycling of RPC pools and Notch inhibition drives commitment of RPCs to a photoreceptor cell fate (Jadhav et al., 2006), but the molecular mechanisms that downregulate Notch signaling to generate photoreceptor precursors are unclear.

The events that promote a photoreceptor precursor to differentiate into a rod or cone are more characterized. There are six key transcription factors involved in photoreceptor differentiation. These are orthodenticle homeobox 2 (Otx2), cone-rod homeobox (Crx), neural retina leucine zipper (Nrl), photoreceptor-specific orphan nuclear receptor (Nr2e3), RAR-related orphan receptor β (Rorβ) and thyroid hormone receptor β2 (Trβ2). *Otx2* is expressed in retinal progenitors during final mitosis and in early photoreceptor precursor cells (Swaroop et al., 2010), and is a key inducer of photoreceptor cell fate (Koike et al., 2007; Nishida et al., 2003). *Crx* is expressed early in postmitotic photoreceptor precursors and acts

downstream of *Otx2* (Koike et al., 2007; Nishida et al., 2003). It is involved in the terminal differentiation of photoreceptor cells and promotes the expression of photoreceptor-specific genes (Hennig et al., 2008). Nrl and Nr2e3, in conjunction with Crx, promote rod photoreceptor cell fate by suppressing cone photoreceptor gene expression (Oh et al., 2008). Rorβ regulates both rod and cone differentiation through regulation of *Nrl* expression, and *Rorβ* is expressed in all layers of the retina (Jia et al., 2009). It also acts in conjunction with Crx to promote S cone cell fate (Srinivas et al., 2006). *Trβ2* expression mediates M cone differentiation (Ng et al., 2001) and coordinates cone opsin patterning (Lu et al., 2009).

The 'transcriptional dominance' model of photoreceptor differentiation requires the coordinated and precisely balanced action of these six key transcription factors (Figure 1.2). Several of these factors may be expressed in a photoreceptor precursor, engaging in a 'tug-of-war' for transcriptional dominance that determines the cell fate (Swaroop et al., 2010). *Otx2* expression biases RPCs to a photoreceptor precursor cell fate and promotes a default S cone cell fate, unless their fate is directed into rods by expression of *Nrl*. In photoreceptor precursors, Otx2 activates expression of *Crx,* and Rorβ promotes transcription of *Nrl*. Recent evidence also suggests that Otx2 plays an active role in promoting *Nrl* expression as well (Roger et al., 2014), and when the amount of Nrl protein reaches a threshold level it can recruit Crx to activate *Nr2e3* expression. Together, *Nr2e3* and *Nrl* expression inhibit S cone cell fate and restricts the lineage to rod precursors. *Trβ2* expression inhibits S cone cell fate and promotes M cone cell fate in cells not fated to become rods (Figure 1.2; Swaroop et al., 2010).
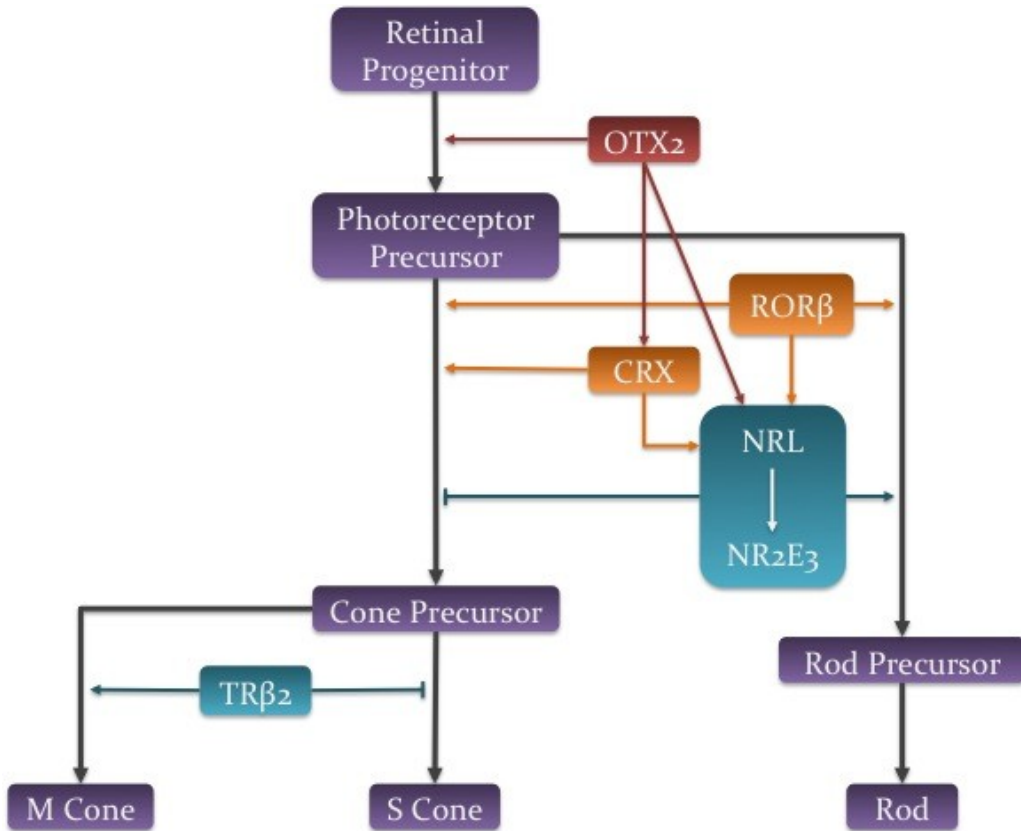
Adapted from Swaroop *et al.*, 2010

Figure 1.3: The "transcriptional dominance" model of photoreceptor differentiation. A photoreceptor precursor forms under the influence of *Otx2* expression. This precursor will develop into an S cone in the default state. Downstream of *Otx2* is *Crx*, which promotes terminal differentiation of the photoreceptor precursor cell into a rod or a cone. *Nrl* and *Nr2e3* expression will induce a rod cell fate and suppress a cone cell fate. Otx2 and Rorβ activate expression of *Nrl*, and Nrl protein, in cooperation with Crx, activates expression of *Nr2e3*. If *Nrl* and *Nr2e3* are not expressed, the photoreceptor precursor follows the default pathway to become an S cone, unless TRβ2 is present to induce an M cone cell fate. This diagram illustrates the main control centers in photoreceptor differentiation, but there are numerous other factors involved in the cell fate decisions and all control centers are subject to modifying regulators.

Development of Vision

While most of the research presented in this thesis focuses on the embryonic retinal development of zebrafish, it is also important to understand how this translates into the ability to see. These associations are made possible by performing a number of behavioral assays that test visual ability and correlating them with known genetic and developmental information. The startle response (abrupt movement in response to a visual stimuli) is the first visually evoked behavioral response, and while it demonstrates the ability to differentiate between light and dark, it says nothing about form vision (Easter and Nicola, 1996; Fleisch and Neuhauss, 2006). In zebrafish, the first post-mitotic retinal cells (the RGCs) are post-mitotic at 28 hpf, with their axons making connections to the optic tectum by 48 hpf (Easter and Nicola, 1996). Cone outer segments are seen at 55 hpf (Schmitt and Dowling, 1999) with functional synapses by 65 hpf (Gestri et al., 2012), the time point at which the startle response is first elicited (Easter and Nicola, 1996).

Optokinetic responses (OKR) are tracking eye movements elicited by surrounding motion that indicate form vision, and are first observed at 3 dpf (Easter and Nicola, 1996; Fleisch and Neuhauss, 2006). Functional signal transduction to second-order neurons occurs by 3.5 dpf, coinciding with the emergence of OKR and indicating that a focused image is being formed on the retina (Easter and Nicola, 1996). What this means is that simple light/dark distinctions can occur relatively early, (68 hpf), with higher-resolution form-vision beginning about 5 hours later (3.5 dpf; Easter and Nicola, 1996).

Optomotor response (OMR) measures the distance a larvae travels in the direction of a moving visual stimulus (Orger et al., 2004). This assay requires a higher level of visual sensitivity and the coordinated efforts of

both the visual and musculo-skeletal systems (Asai-Coakwell et al., 2013; Orger et al., 2004). OMR is elicited in larvae 6 dpf or older, suggesting the neural circuits responsible develop later than the ones mediating the startle response and OKR (Fleisch and Neuhauss, 2006). Projection neurons in the hindbrain that link sensory neuron processing in the brain to a motor output are required for OMR to occur (Orger et al., 2008).

Visually-impaired zebrafish larvae can also be morphologically distinguished. Visually mediated background adaptation (VBA) is a retinal ganglion cell meditated neuroendocrine response in which melanophores adjust their melanosome distribution according to ambient background light detection (Fleisch and Neuhauss, 2006; Muto et al., 2005). A direct connection from the retina to the hypothalamus stimulates the secretion of the melanin-contracting hormones required for this visual behavior (Neuhauss et al., 1999).

It is important to note that the larval retina is a functional cone-dominant retina. While rod photoreceptors are morphologically observable by 8 dpf, the first detectable electrical response from a rod photoreceptor cell does not appear until between 15 and 18 dpf (Bilotta et al., 2001), corresponding with the maturation of the rod outer segments (Branchek and Bremiller, 1984).

Visual behavior involves not only a functional visual neural circuit, but also the ability of the signal to pass through the brain and elicit a muscular response. In zebrafish, this is made possible by the simultaneous maturation of retinal image formation, signal transduction to the brain and development of extraocular muscles. These events all occur around 68-72 hpf, and it is said that this is when the visual life of the zebrafish begins (Easter and Nicola, 1996).

BMP Signaling

Bone morphogenetic proteins (BMPs) are secreted growth factors and members of the transforming growth factor-β (TGFβ) ligand superfamily, which signal through transmembrane receptors to induce or repress target gene transcription. BMPs were first discovered for their ability to induce bone and cartilage formation, and this ligand family plays important roles in embryonic patterning, axis formation and cell fate determination (Arnold and Robertson, 2009; Nohe et al., 2004; Sieber et al., 2009). BMP ligands bind to two distinct transmembrane serine/threonine kinase receptors, the BMP type I- and BMP type-II receptors (BMPR-I and BMPR-II), both of which are required for signal transduction (Sieber et al., 2009). After cleavage from a propeptide and secretion from the cell, BMP ligands dimerize and bind to BMPR-I/BMPR-II heterodimers, promoting the recruitment of a second receptor heterodimer, forming a hetero-tetrameric receptor complex. BMPR-I is transphosphorylated by BMPR-II, triggering a Smad signaling cascade (Sieber et al., 2009). There are three sub-classes of Smad proteins: [1] receptor-regulated (R-Smads), [2] inhibitory (I-Smads) and [3] common mediator Smad (co-Smad). Active BMPR-I receptors phosphorylate R-Smads (Smad1/5/8), which form complexes with the co-Smad (Smad4) and translocate into the nucleus (Massague et al., 2005; Sieber et al., 2009). Once in the nucleus, the Smad complex associates with DNA-binding co-factors and transcriptional co-effectors to bind to BMP-responsive elements (BREs) in the genome and alter expression of transcriptional targets (Figure 1.3; Massague et al., 2005).

Regulation of BMP signaling is achieved by three general methods: [1] inhibitory intracellular proteins, such as the I-Smads (Smad6/7), that prevent R-Smad/co-Smad complex formation (Hata et al., 1998), prevent
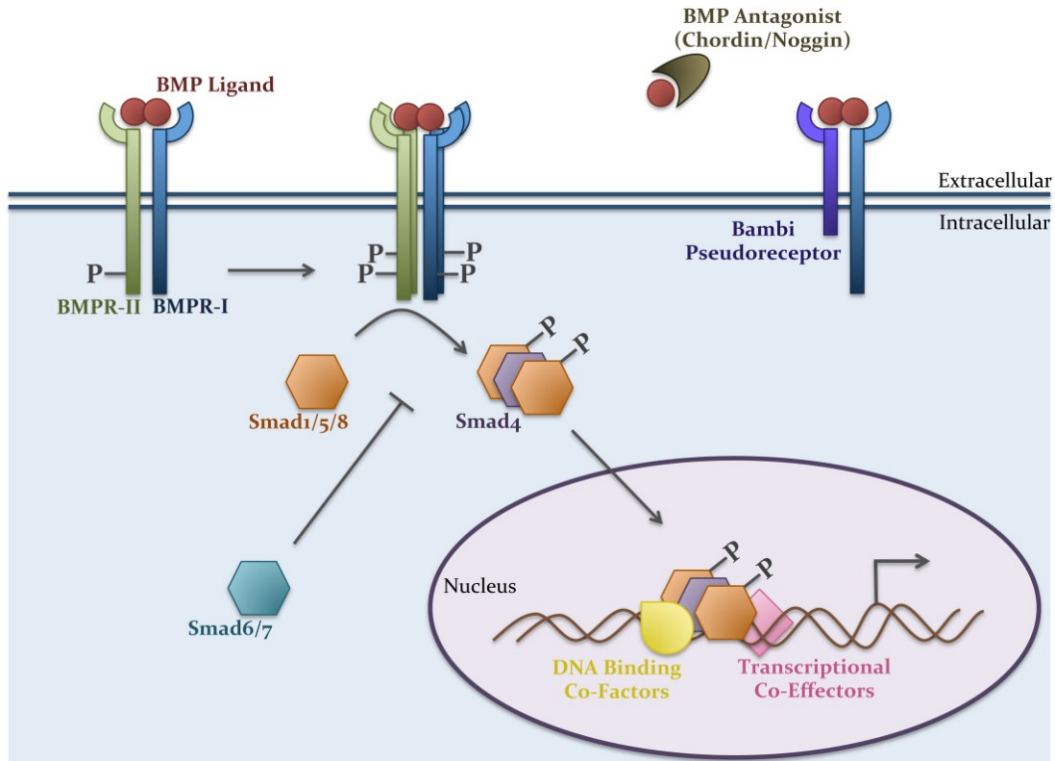
Figure 1.3: A model for BMP signaling. BMP ligand dimers bind to BMPR-I/BMPR-II heterodimers, promoting the formation of a hetero-tetrameric receptor complex. BMPR-I is transphosphorylated and activated by BMPR-II. Active BMPR-I phosphorylates and activates Smads 1/5/8, which form a complex with co-Smad4 and are translocated into the nucleus. The Smad complex associates with DNA-binding co-factors and transcriptional co-effectors to bind to BMP-responsive elements in the genome and alter expression of transcriptional targets. BMP signaling can be inhibited via ligand binding to the pseudoreceptor Bambi, which lacks the kinase domain required for BMPR-I transactivation. Intracellular inhibitory Smads 6/7 block BMP signaling by preventing the formation of an active Smad-complex. Extracellular BMP inhibitors, such as Chordin and Noggin, bind to BMP ligands preventing ligand association with the BMP receptors.

active BMPR-I receptors from phosphorylating R-Smads (Souchelnytskyi et al., 1998) and target BMPRs for degradation (Kavsak et al., 2000), [2] extracellular BMP antagonists, such as Noggin and Chordin, that bind and sequester BMP ligands, preventing ligand-receptor interactions (Liu and Niswander, 2005) and [3] pseudoreceptors, such as Bambi (BMP and activin membrane bound inhibitor), that lack an intracellular kinase domain and prevent formation of BMPR-I/II complexes (Onichtchouk et al., 1999).

Apoptosis in Retinal Development

Cell Morphology and Mechanisms of Apoptosis

The process of programmed cell death, or apoptosis, was first characterized in 1972 by Kerr and colleagues. The authors described a morphologically distinct form of cell death that aids in the balance between cell production and cell loss (Kerr et al., 1972). In this way apoptosis occurs naturally as a homeostatic method of maintaining cell populations. Apoptosis also has roles in normal embryonic development, aging and defense, such as in immune reactions and response to cell damage by disease or noxious agents (Elmore, 2007).

Cell shrinkage and pyknosis (irreversible chromatin condensation) are the most characteristic morphological features of a cell undergoing apoptosis, and the cells appear as small round or oval masses with very dense nuclear staining (Kerr et al., 1972). Next, nuclear fragmentation and "budding" of apoptotic bodies via extensive plasma membrane blebbing occurs, followed by phagocytosis and degradation of the apoptotic bodies (Elmore, 2007). These morphological characteristics of apoptosis occur due to the proteolytic activity of the executioner caspase proteases (Elmore, 2007). Additionally, extensive protein cross-linking, DNA breakdown into

180 – 200 bp fragments and expression of phagocytic recognition markers on the cell surface occurs in apoptosing cells (Elmore, 2007). Since apoptotic cells do not release their cytoplasmic contents and surrounding cells rapidly phagocytose the apoptotic bodies, there is no inflammatory reaction associated with apoptosis (Savill and Fadok, 2000).

Apoptosis typically occurs via one of two signaling cascades, the intrinsic or extrinsic pathways, both of which converge on the activation of the executioner caspases. The intrinsic pathway is activated by DNA damage or endoplasmic reticulum stress caused by environmental stimuli such as toxins, radiation or hypoxia. Initiation of the intrinsic apoptotic program results in the activation of BCL-2-associated X protein (Bax) or BCL-2 antagonist or killer protein (Bak). Upon activation, Bax and Bak relocate from the cytoplasm to the mitochondrial outer membrane to promote the formation of the mitochondrial apoptosis-induced channel (Martinez-Caballero et al., 2009). This results in mitochondrial outer membrane permeabilization (MOMP), and the release of pro-apoptotic Cytochrome c from the mitochondrial intermembrane space into the cytoplasm. Cytochrome c binds to apoptotic protease-activating factor 1 (APAF1) and induces its oligomerization, forming the apoptosome. The apoptosome recruits and activates the initiator caspase 9, which cleaves and activates the executioner caspase 3, resulting in irreversible commitment to cell death (Elmore, 2007; Tait and Green, 2010). Binding of a ligand to transmembrane death receptors initiates the extrinsic apoptosis pathway. Ligand binding recruits adaptor molecules to the death receptors that cleave and activate the initiator caspase 8. Active caspase 8 activates the executioner caspase 3, and the cell becomes committed to cell death (Figure 1.4; Elmore, 2007; Tait and Green, 2010). Active executioner caspases activate cytoplasmic endonucleases, to degrade nuclear material, and proteases, to breakdown nuclear and cytoskeletal proteins. The activity of

the executioner caspases during the demolition stage of apoptosis is what ultimately causes the morphological changes discussed above (Elmore, 2007). Caspase 3 is considered the most important executioner caspase, although other executioner caspases (caspase 6 and caspase 7) do exist (Slee et al., 2001).

Apoptosis in Normal Development and Disease

Apoptosis is critically important in a number of developmental contexts. For example, nervous system and immune system development occur through initial overproduction of cells, followed by the death of cells that fail to make synaptic connections or produce effective antigen specificities, respectively (Nijhawan et al., 2000; Opferman and Korsmeyer, 2003). Apoptosis is used to remove aged, deteriorating and pathogen-invaded cells, and is a component of wound healing (Elmore, 2007). Additionally, apoptosis is critical in shaping the limbs and digits of vertebrates (Saunders and Gasseling, 1962). Owing to its important role in development, apoptosis must be a tightly regulated process, and too little or too much cell death could lead to a number of pathologies.

Abnormalities in the regulation of apoptosis contribute to the development of diseases such as cancer, autoimmune deficiency syndrome (AIDS) and neurodegenerative diseases. Inappropriate suppression of apoptosis is thought to play a role in the development and progression of cancer (Kerr et al., 1994). Alternatively, excessive apoptosis may lead to AIDS and neurodegenerative disease. T-cells that have been infected with the human immunodeficiency virus (HIV) have increased expression of cell death receptors, resulting in excessive apoptosis of T-cells and AIDS (Li et al., 1995). Alzheimer's disease is caused by the deposition of extracellular amyloid β plaques, and amyloid β is thought to induce apoptosis via
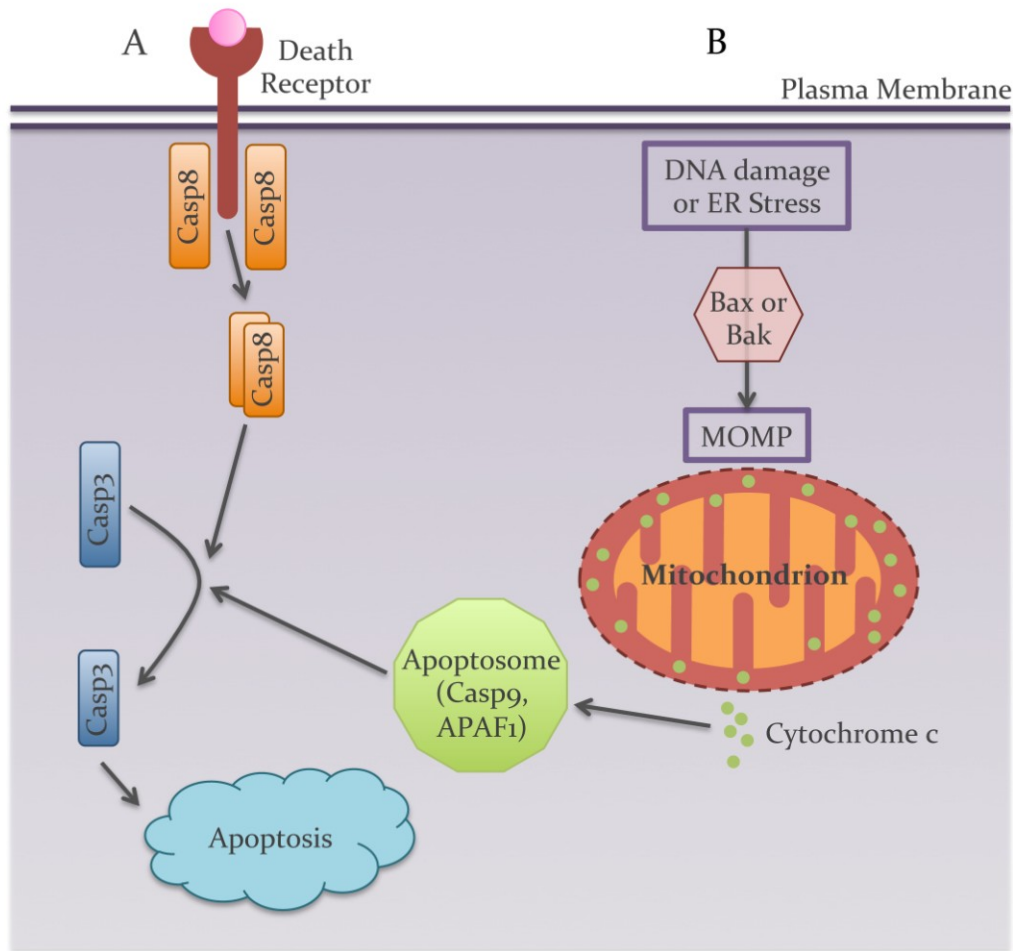
Figure 1.4: The extrinsic and intrinsic apoptotic programs. (A) The extrinsic apoptotic pathway begins with the binding of signaling ligands to death receptors on the plasma membrane. Initiator caspase 8 is dimerizes upon cleavage and becomes active. Casp8 cleaves and activates executioner caspase 3, which directly leads to apoptosis. (B) The intrinsic apoptosis pathway is activated by stimuli such as DNA damage or ER stress. These stimuli promote mitochondrial outer membrane permeabilization via the activation of Bax or Bak proteins, releasing cytochrome c from the mitochondrial intermembrane space. Cytochrome c binds to and induces oligomerization of apoptotic protease-activating factor 1 (APAF1), which recruits and activates initiator caspase 9. Casp9 cleaves and activates casp3, leading to apoptosis.

oxidative stress or activation of cell death receptors (Ethell and Buhler, 2003). Since improper regulation of apoptosis can lead to many pathological diseases, the development of anti-apoptotic strategies is an important research focus.

BMP Signaling in Apoptosis

In canonical BMP signaling, expression of downstream target genes is regulated via the action of the Smad family of proteins. Smad-independent (or non-canonical) BMP signaling can induce apoptosis via the activation of TGFβ-activated kinase 1 (Tak1). Non-canonical signaling via Bmp2 and Bmp4 activates Tak1, inducing apoptosis via the activation of the p38 MAP kinase pathway (Miyazono et al., 2010). The p38 MAP kinase pathway is also induced intrinsically via cellular stress. The exact action of p38 in promoting the apoptotic program in unclear, but there is some evidence suggesting that p38 can act both downstream of caspase activation and upstream of caspases in apoptosis (Zarubin and Han, 2005).

Apoptosis During Zebrafish Retinal Development

Apoptosis is an important process during retinal development and has been described in many species of vertebrates, including mammals and teleost fish. Apoptosis spreads across the mammalian retina in consecutive waves reminiscent of the waves of retinal neurogenesis, starting with the GCL, followed by the INL and ONL (Biehlmaier et al., 2001). Between 10% and 35% of cells in the GCL die apoptotically in a survey of various mammalian models (Potts et al., 1982; Sengelaub et al., 1986; Wong and Hughes, 1987). Waves of apoptosis also occur in the zebrafish, but the rates of apoptosis were conspicuously lower than those observed in mammalian

models (Biehlmaier et al., 2001). Retinal apoptosis peaked in the GCL and INL at 3 – 4 dpf (1.09%), followed by a second smaller wave of apoptosis in the ONL at 6 – 7 dpf (1.10%; Biehlmaier et al., 2001). During zebrafish retinal maturation (2 – 21 dpf) the waves of apoptosis were most present in the central retina, with lower rates of apoptosis occurring in the proliferative ciliary marginal zone (CMZ; Biehlmaier et al., 2001). Almost no apoptosis occurred in the adult central retina but it was still weakly present in the CMZ (Biehlmaier et al., 2001). The pattern and onset of retinal apoptosis in zebrafish is comparable to those seen in mammalian models, but the amounts of apoptosis were greatly reduced, suggesting a "fine-tuning" role for apoptosis in the zebrafish retinal network after the waves of mitosis (Biehlmaier et al., 2001).

Retinopathies

Microphthalmia, Anophthalmia and Colobomata

Coloboma refers to a hole or gap through any ocular structure and accounts for 0.6 – 1.9% of blindness in adults and 3.2 – 11.2% of blindness in children (Onwochei et al., 2000). Colobomata occur when the transient choroid fissure present during embryonic retinal development fails to close, resulting in a loss of ventral retinal tissue, and are often found in combination with microphthalmia (small eye) or anophthalmia (no eye; Taylor, 2007). Microphthalmia, anophthalmia and colobomata (MAC) are a spectrum of ocular developmental phenotypes that can be found alone or syndromically and can affect one or both eyes. Anophthalmia and microphthalmia are estimated to occur in 0.003% and 0.014% of the general population respectively, with microphthalmia reported in 3.2 – 11.2% of blind children (Verma and Fitzpatrick, 2007). Disruptions in genes implicated in early eye specification or patterning can profoundly affect eye

formation and could underlie developmental disorders such as MAC. Mutations in BMP ligand genes, such as *BMP4, GDF6* and *GDF3*, have been identified as causative mutations in MAC patients (Asai-Coakwell et al., 2009; Ye et al., 2010; Zhang et al., 2009). Additionally, mutations in a number of eye field transcription factor genes are found in MAC patients, including *SIX3, SIX6* and *OTX2* (Zhang et al., 2009).

Leber's Congenital Amaurosis

Leber's congenital amaurosis (LCA) is the most severe form of inherited blindness, with a prevalence of 1 in 30 000 – 81 000 live births and counts for ≥5% of all inherited retinopathies. LCA is commonly inherited in an autosomal recessive manner and presents very early in life, around 6 weeks of age. Clinical characteristics of LCA include severe early vision loss, nystagmus and an absent electroretinogram (ERG) response (den Hollander et al., 2008; Perrault et al., 1999). There are three observed methods of pathogenesis in LCA. Severe atrophy, dropout and gliosis of the photoreceptor layer, INL and RPE characterize retinal degeneration, the most common pathology. Retinal aplasia is observed in some cases, with the complete absence of a photoreceptor layer. Finally, biochemical dysfunction is thought to underlie some cases of LCA, because these patients appear to have fully intact and laminated retinas (den Hollander et al., 2008). A cohort of 15 genes have been identified as causative in up to 70% of all LCA cases, one of which is the transcription factor *CRX*, which plays an important role in photoreceptor differentiation (Asai-Coakwell et al., 2013; Cremers et al., 2002; den Hollander et al., 2008). Their functions include roles in retinal embryonic development (*OTX2, CRB1, CRX*), phototransduction (*AIPL1, GUCY2D*), protein trafficking (*RD3*), outer segment phagocytosis (*MERTK*), guanine synthesis (*IMPDH1*), vitamin A

metabolism (*LRAT, RDH12, RPE65*) and ciliary function (*CEP290, LCA5, RPGRIP1, TULP1*). A subset of these genes (including *CRX*) also contributes to additional later-onset retinal dystrophies such as retinitis pigmentosa and cone-rod dystrophy (Asai-Coakwell et al., 2013; Cremers et al., 2002; den Hollander et al., 2008).

Purpose of this Study

The purpose of this study is to understand the genetic basis of developmental optic abnormalities and retinal dystrophies, such as MAC and LCA, and to analyze the genetic pathways that give rise to photoreceptor cell fate. Lesions in *GDF6* have been identified in human patients with mircophthalmia (Asai-Coakwell et al., 2013). This work makes use of zebrafish *gdf6a$^{-/-}$* mutants to model microphthalmia, and to study the role that Gdf6a plays in the development of this disease. Our study reveals roles for *gdf6a* in regulating retinal apoptosis and photoreceptor morphological development, two important processes in retinal development.

Additionally, this work examines the role of the transcription factor CRX in photoreceptor cell-fate determination. Lesions in *CRX* have been identified in human LCA patients. We use a zebrafish *crx$^{-/-}$* mutant as a model for LCA. Interestingly, *crx$^{-/-}$* mutants do not have an observable retinal phenotype. Artificial knockdown of *otx5* (a zebrafish *crx* paralog) in *crx$^{-/-}$* mutants reveals a loss of photoreceptor identity. Zebrafish *otx5* mutants were generated, and these will be used in combination with *crx* mutants to create a genetic model of photoreceptor degeneration disorders in zebrafish.

Chapter 2

Materials and Methods

Zebrafish Lines and Maintenance

Embryonic and adult zebrafish were cared for as outlined in Westerfield (2007), in accordance with the Canadian Council for Animal Care guidelines and approved by the University of Alberta Animal Care and Use Committee for Biosciences. Unless otherwise noted, all experiments were performed on the AB line of wild-type fish.

The *gdf6a* mutant allele (s327) was originally identified in a forward genetic screen for visual behavior (Muto et al., 2005). The mutation is a C-to-A transition in position 164 of the *gdf6a* open reading frame with nucleotide position 1 corresponding to the A in the initiation methionine codon, producing a premature stop codon and truncated protein (Gosse and Baier, 2009). Homozygous mutants have observably smaller eyes by 48 hours-post-fertilization (hpf). When observed before 48 hpf, genotypes were determined by sequencing or high resolution melt curve analysis (HRMA).

The *crx* mutant allele (ua1005) was generated at the University of Alberta using zinc-finger nuclease (ZFN) technology (Meng et al., 2008; Pieper et al., 2010). The mutation results in a 7 base-pair deletion at position 28 of the *crx* ORF producing a frameshift mutation, a premature stop codon at the same position and is predicted to result in early truncation of the protein. Heterozygous and homozygous mutants were identified by HRMA and sequencing.

The *otx2* mutant allele (hu3652) was obtained from ZIRC (Zebrafish International Resource Center). The point mutation is an A-to-C transition at an essential splice site at the start of exon 4, the 84th amino acid residue. This results in the inclusion of an intron in the mature mRNA product and a premature stop codon.

The transgenic line *Tg(-5.5opn1sw1:EGFP)* labels UV cones with GFP was (Takechi et al., 2003). This line was bred to the *crx* mutant line to generate *crx* mutant animals that have GFP-labeled photoreceptors.

Embryo Manipulation and Care

General Embryo Maintenance

Embryos injected with morpholino oligonucleotides or mRNA were raised in embryo media (EM: 15 mM NaCl, 500 nM KCl, 1 mM $CaCl_2$, 150 nM KH_2PO_4, 1 mM $MgSO_4$, 715 nM $NaHCO_3$) with penicillin-streptomycin solution (10 000 units penicillin, 10 mg/ml streptomycin; Sigma-Aldrich, St. Louis MO, USA) diluted 1:100 in EM. Embryos were grown at the appropriate temperature (25.5°C for slow development, 28.5°C for normal development and 33°C for accelerated development) and allowed to develop to the desired stage. Embryos bred for producing a new generation were raised in fish water at 28.5°C. Stages of development were identified using developmental characteristics described by Kimmel et al. (1995). If the desired stage of development was beyond 24 hpf the EM was supplemented with 0.006% *N*-phenylthiourea (PTU) (Sigma-Aldrich, St. Louis MO, USA) to inhibit the development of melanin pigmentation. In all cases, fresh EM or fish water was provided every 24 hours.

Embryos were fixed in 4% paraformaldehyde (PFA) in phosphate buffered saline (PBS: 137 mM NaCl, 2.7 mM KCl, 10 mM Na_2HPO_4, 1.8 mM KH_2PO_4, pH 7.4) for 4 hours at room temperature or overnight at 4°C on a shaker. After fixation was complete, embryos were rinsed out of fixative by washing them in PBST (PBS + 0.1% Tween-20) five times for 5 minutes each. Fixed embryos were stored at 4°C for short-term (<1 week) or at -20°C in 100% methanol/0.1% Tween-20 for long-term. Prior to fixation, if the

desired stage was 3 days-post-fertilization (dpf) or older, the embryos were anesthetized in 0.0168% ethyl 3-aminobenzoate methanesulfonate (MS-222) (Sigma-Aldrich, St. Louis MO, USA) prior to fixation.

Embryos were dechorionated manually using fine-pointed forceps (Dumont #5) or enzymatically using Pronase E (Sigma-Aldrich, St. Louis MO, USA). Enzymatic dechorionation consisted of immersing embryos in 1 mg/ml Pronase E solution with gentle agitation for 3-5 minutes, until the first few chorions begin to deflate and crumple. This was followed by 3-5 washes in 100 ml EM in an glass beaker to remove any trace amounts of enzyme.

Embryos were photographed on the yolk using an Olympus SZX12 stereomicroscope (Olympus, Richmond Hill ON, Canada) using QCapture Suite PLUS Software v3.3.1.10 and a Micropublisher 5.0 RTV camera (QImaging, Surrey BC, Canada). For high-quality photographs, embryos were manually deyolked, successively washed in 30%, 50% and 70% glycerol in PBS and mounted on glass slides in 70% glycerol. Whole-mounted and cryosectioned samples were photographed on a Zeiss AxioImager.Z1 compound microscope using Axiovision SE64 Rel.4.8 software and an AxioCam HRm camera (Zeiss, Oberkochen, Germany) for RGB colour photos. ZEN 2010 v6.0 Software and an LSM 700 compact confocal microscope (Zeiss, Oberkochen, Germany) were used for fluorescence confocal imaging.

Morpholino Preparation and Injection

The use of MOs to knockdown gene expression in zebrafish was established over 10 years ago (Nasevicius and Ekker, 2000). Translation-blocking morpholinos were designed and ordered from Gene Tools

(Philomath OR, USA). The sequences for the MOs used in these studies are listed in Table 2.1. Stock solutions of MOs were dissolved in sterile water to a concentration of 20 mg/ml. Working solutions were diluted to the required concentration in Danieau buffer (58 mM NaCl, 0.7 mM KCl, 0.4 mM $MgSO_4$, 0.6 mM $Ca(NO_3)_2$, 5 mM HEPES [4-(2-hydroxethyl)piperazine-1-ethanesulfonic acid], pH 7.6). MO solutions were stored at 4°C. Prior to injection, MOs were heated to 65°C for 10 minutes and allowed to cool to room temperature. MOs were injected into embryos at the 1-4 cell stage at doses of 1-10 ng using a microinjection rig.

Microinjection needles were pulled from 1.2 mm thin-wall borosilicate tubing (Sutter Instruments, Novato CA, USA) using a Model P-87 Flaming/Brown Micropipette Puller (Sutter Instruments, Novato CA, USA). The sample was delivered using an ASI MPPI-2 Pressure Injector (Applied Scientific Instrumentation, Eugene OR, USA) with a pressure of 27 psi. The dose delivered was estimated by observing the bolus size formed. The pulse duration was adjusted from 0.5 – 3 ms, until the desired bolus size was injected into the embryos.

mRNA Preparation and Injection

mRNA was diluted to an appropriate working concentration in RNase-free water and stored at -80°C. Prior to injection, mRNA was thawed on ice. Embryos were injected with mRNA directly into the cell at the 1-cell stage using a microinjection rig. The dose of mRNA delivered varied from 30-200 pg. The dose was determined by testing a series of increasing doses in wild-type embryos, then the dose that gave a phenotype but was not lethal was chosen for all future injections.

Table 2.1: List of morpholino oligonucleotide sequences used in this study.

Name	Sequence (5'-3')	Type
otx5	CATGACTAAACTCTCTCTCTCTC	Translation Blocking
crx **alt ATG**	TCCATTCCTGAGGCGGACAGTGTTA	Translation Blocking

P7C3 Pharmaceutical Treatments

P7C3 is an aminopropyl carbazole that is reported to be pro-neurogenic and anti-apoptotic (Asai-Coakwell et al., 2013; Pieper et al., 2010). The P7C3 dose titration was chosen based on previous literature (Pieper et al., 2010), and doses above 0.3 μM were deemed unsuitable due to necrotic effects. Zebrafish embryos were bathed in either 0.01 μM P7C3, 0.1 μM P7C3 or DMSO vehicle control from 5-28 hpf or 5-48 hpf. 5 hpf embryos were enzymatically dechorionated and placed in agarose-coated dishes. To facilitate the dissolving of P7C3, the embryo media was supplemented with DMSO (1% final concentration). 72 hpf P7C3-treated embryos were photographed on the yolk as described above and eye area was quantified using ImageJ software (National Institutes of Health, Bethesda, MD) and student's t-tests were performed with Bonferonni correction for multiple comparisons.

Analysis of Zebrafish Visual Behavior

Visually Mediated Background Adaptation (VBA)

VBA is a retinal ganglion cell meditated neuroendocrine response in which melanophores adjust their melanosome distribution according to ambient background light detection (Fleisch and Neuhauss, 2006; Muto et al., 2005). In wild-type larvae, the melanosomes contract upon light exposure and expand on a dark background (Neuhauss et al., 1999). 7 dpf larvae were placed on a white porcelain dish in groups of 3-5 in the dark, and then moved under bright illumination under a stereomicroscope. They were allowed to acclimatize and light-adapt for 2-5 minutes, and then were scored manually into three categories: [1] normal, contracted melanosomes, [2] intermediate melanosome contraction and [3] dark, dispersed

melanophores. The score for variably dark embryos was estimated by averaging a minimum of 20 individuals.

Optomotor Response (OMR)

OMR measures the distance a larvae travels in the direction of a moving stimulus (Orger et al., 2004). This assay requires a higher level of visual sensitivity and the coordinated efforts of both the visual and musculo-skeletal systems (Asai-Coakwell et al., 2013; Orger et al., 2004). Visual stimuli (scrolling black lines) were displayed on an upward facing computer monitor (http://www.visionegg.org/). 7 dpf larvae were placed into a narrow plexiglass "racetrack"-style tank and exposed to a moving stimulus or a white screen for 2 minutes. The distance travelled along the "racetrack" (in cm) was recorded after the 2-minute stimulus exposure.

Isolation of Polymerase Chain Reaction (PCR)-ready Genomic DNA (gDNA)

This technique is based on the protocol published by Meeker et al. (2007). Zebrafish tissue was placed in a PCR tube and submerged in 20-100 µl 50 mM NaOH (enough to submerge the sample). The sample was heated at 95°C until the tissues crumbled or dissolved completely (~20 minutes for PFA-fixed or adult tissue, ~10 minutes for non-fixed embryos). Mixtures were cooled on ice and 1/10th volume of Tris-HCl (pH 8) was added to neutralize the solution. If there was a lot of tissue debris, the mixture was centrifuged (>16 000 xg) for 2-5 minutes to pellet the debris and the supernatant was removed to a new tube. Samples were stored at 4°C for short-term (1-3 days) and -20°C for long-term.

High Resolution Melt Curve Analysis (HRMA)

HRMA is a powerful and efficient method of detecting DNA sequence polymorphisms. In HRMA, the region of interest is PCR-amplified in the presence of a saturating, fluorescent dsDNA-binding dye. The PCR product is subjected to high-resolution melting where fluorescence is monitored, generating a characteristic curve (Reed et al., 2007). HRMA primers were designed to have a %GC content of ~55%, a melting temperature (T_m) of ~62°C, were designed to be ~22 nt long and to amplify a ~90 bp amplicon (Table 2.2). It was very important to match the T_m's within primer pairs. It was preferred if the primers were designed to be within one single exon around the target site, as intronic sequence has too much variation. Multiple primer sets were designed for each target site and tested before use in genotyping assays.

When using the MeltDoctor™ HRM Master Mix (Life Technologies Inc., Burlington ON, Canada) the following was combined for each 10 µl reaction: 5 µl 2X MeltDoctor HRM Master Mix, 0.6 µl each of the forward and reverse primers (5 µM), 2 µl DNA template and 1.8 µl sterile water. These HRMA reactions were run on a 7500 Fast Real-Time PCR System (Life Technologies Inc., Burlington ON, Canada). The PCR cycle conditions had three phases: [1] initial denaturation (95°C for 10 minutes), [2] 40 cycles of PCR amplification (95°C for 15 seconds, 60°C for 20 seconds) and [3] a dissociation curve (95°C for 15 seconds, 60°C for 1 minute, 95°C for 15 seconds, 60°C for 15 seconds). HRM v2.0 software (Life Technologies Inc., Burlington ON, Canada) was used to analyze melting profiles.

When using the Type-it HRM PCR Kit (Qiagen, Hilden, Germany) the following was combined for each 10 µl reaction: 5 µl 2X HRM PCR Master Mix, 0.7 µl each of the forward and reverse primers (10 µM), 2 µl DNA template and 1.6 µl sterile water. These HRMA reactions were run on

Table 2.2: List of primers used for HRMA, TALEN assembly and qPCR analysis. Blank spaces indicate data that is unknown.

Name	Sequence (5'-3")	T_m (°C)	%GC	Size (bp)	Notes
crx HRM F	GCCGTCCCAAGAATGATGTC	56.1		92	HRMA
crx HRM R	GTGTGGAGCAGGTCCATTCC	58.2			HRMA
gdf6a HRM F	GCGTTTGATGGACAAAGGTC	60.5	50	90	HRMA
gdf6a HRM R	CCGGGTCCTTAAAATCATCC	60.5	50		HRMA
otx2 HRM F1	GACACTTTGCCCTTCGGTTT	61.4	50	93	HRMA
otx2 HRM R	CCATAGTGCTGCCGTTAGTTCA	62.4	50		HRMA
otx5 HRM F	CGCCTCCTCCTCCTCATTCATC	62.2	59.1	97	HRMA
otx5 HRM R	TCAGCGGTCTGTTAGTGTGTCC	62.2	54.5		HRMA
pCR8_F1	TTGATGCCTGGCAGTTCCCT			variable	TALEN
pCR8_R1	CGAACCGAACAGGCTTATGT				TALEN
TAL_F1	TTGGCGTCGGCAAACAGTGG			variable	TALEN
TAL_R2	GGCGACGAGGTGGTCGTTG				TALEN
EF1-alpha F	CCTTCGTCCCAATTTCAGG				qPCR
EF1-alpha R	CCTTGAACCAGCCCATGT				qPCR
otx5 L #85	GGGAAGAAGTGGCTCTCAAG	59	55	75	qPCR
otx5 R #85	ATTTGGCACGACGGTTCTTA	60	45		qPCR

the Rotor-Gene Q real-time PCR cycler (Qiagen, Hilden, Germany). The PCR cycle conditions had three phases: [1] initial denaturation (95°C for 5 minutes), [2] 40 cycles of PCR amplification (95°C for 10 seconds, 60°C for 30 seconds) and [3] an HRM ramp where the temperature rose from 65°C-95°C, rising by 0.1°C per 2 second step. The melting profiles were analyzed using the Rotor-Gene Q Series Software.

PCR and Cloning Strategies

General PCR Protocol

PCR primers were deigned using the free online primer design program Primer3Plus (http://www.bioinformatics.nl/cgi-bin/primer3plus/primer3plus.cgi/) or the nucleotide-sequence editing program MacVector (www.macvector.com). Primers were designed to be 22-28 nt long, have a T_m of 57°C-65°C and have a %GC content of 40%-60%. If the desired product was an mRNA transcription insert, the primers were designed to amplify the entire CDS (coding sequence) and used cDNA (complementary DNA) as a template for the PCR reaction. These primers also contained restriction sites to allow cloning into a pCS2+ vector, and forward primers contained a Kozak sequence followed by a stuffer sequence. A typical PCR reaction contained 2 μl 10X reaction buffer, 2 μl 10X dNTP mixture, 2 μl forward primer (5 μM), 2 μl reverse primer (5 μM), 200-500 ng template, 0.25 μl *Taq* and sterile water to 20 μl. Typical PCR reaction conditions consisted of a 3 minute initial denaturing step at 94°C followed by 35-40 cycles of [1] 30 seconds at 94°C (denaturation), [2] 30 seconds at 55-65°C (annealing) and [3] 72°C for 1 min/kb (extension). The reaction was completed with a final extension step of 5 minutes at 72°C. Gel electrophoresis was performed and the PCR product was gel-extracted.

cDNA Synthesis for Cloning a CDS

cDNA synthesis reactions used the SuperScript® III First-Strand Synthesis System (Life Technologies Inc., Burlington ON, Canada). In a PCR tube, 2.5 µg total RNA, 1 µl Oligo DT, 1 µl dNTP mix, and diethylpyrocarbonate-treated water (DEPC) to 10 µl were combined and incubated at 65°C in a thermocycler for 10 minutes to denature the RNA. Following the incubation, the reactions were placed on ice for 1 minute to cool and allow primer annealing. The following was added to the reaction after cooling: 2 µl 10X Reaction Buffer, 4 µl $MgCl_2$, 1 µl RNase-Out and 1 µl SuperScript III RT Enzyme. This was incubated at 50°C for 50 minutes to synthesize the cDNA, and then moved to 85°C for 5 minutes to terminate the reaction. To remove the RNA template, 1 µl RNase H was added and the reaction was incubated at 37°C for 20 minutes. The final cDNA product was stored at -20°C until use.

Cloning and Transformation

In preparation for cloning into the pCR™4-TOPO® TA vector (Life Technologies Inc., Burlington ON, Canada), gel-extracted PCR products were incubated with ExTaq (TaKaRa, Japan) to add A's to the ends of the PCR products. This was required to allow ligation to the T overhangs present in the pCR™4-TOPO® TA vector. A mixture of 16 µl gel-extracted PCR product, 2 µl 10X ExTaq buffer, 1 µl dNTPs (10 mM) and 1 µl ExTaq (5 U/µl) was incubated in a thermocycler at 72°C for 10 minutes. This reaction was subsequently diluted with 60 µl sterile water to dilute the product for TA-ligation. The ligation reaction consisted of 4 ul diluted PCR product, 0.5 µl pCR™4-TOPO® TA vector and 1 µl Salt Solution. This was incubated at room temperature for no more than 10 minutes before continuing with the transformation procedure.

The entire ligation reaction was added to 15 µl One Shot® TOP10 chemically competent *E. coli* cells (Life Technologies Inc., Burlington ON, Canada) and incubated on ice for 10 minutes. Following a 45 second heat-shock step at 42°C, the transformations were returned to ice for an additional 2 minutes. 250 µl of super optimal broth with catabolite repression (SOC: 2% bacto tryptone, 0.5% bacto yeast extract, 10 mM NaCl, 2.5 mM KCl, 10 mM MgCl₂, 10 mM MgSO₄, 20 mM glucose) was added to the transformation, and this was incubated at 37°C for 30 minutes to 1 hour. The reaction was aseptically plated on Luria broth agar plates (LB: 1% bacto tryptone, 0.5% bacto yeast extract, 0.17 M NaCl, 1.5% bacto agar, pH 7) with 50 µg/ml carbenicillin and incubated for 12-18 hours at 37°C. Single colonies were used to inoculate liquid LB with carbenicillin (50 µg/ml) and plasmid DNA was extracted using the QIAprep Spin Miniprep Kit (Qiagen, Hilden, Germany) as per manufacturers instructions. The miniprep products were sequenced to verify insertion of the correct product.

mRNA transcription inserts needed to be subcloned from pCR™4-TOPO® into pCS2+ in preparation for in-vitro mRNA synthesis. Isolated pCR™4-TOPO® vector containing the desired insert was placed into a restriction digest (5 ul) containing 1 µl of each restriction enzyme needed (based on how the primers were designed), 2.5 µl of a compatible restriction buffer and sterile water to 25 µl. The pCS2+ vector was also treated to the same restriction digest to create compatible ends for directional cloning. The digests were allowed to continue for at least 2 hours, then electrophoresed to gel-extract the desired products for the ligation. Ligation reactions combined 5 µl vector, 10 µl insert, 2 µl 10X T4 DNA ligase buffer, 1 µl T4 DNA ligase and sterile water to 20 µl. The ligation was allowed to continue for 4 hours at room temperature or overnight at 16°C. Transformation into TOP10 cells was performed using 2.5 µl of the ligation

reaction. Plasmid DNA was isolated and the insert was verified by sequencing.

Sequencing Plasmid DNA

All sequencing reactions were performed using the BigDye Terminator v3.1 Cycle Sequencing Kit (Life Technologies Inc., Burlington ON, Canada). Reactions contained 2 µl BigDye premix, 3 µl 5X buffer, 50-400 ng template DNA, 1 µl sequencing primer (5 µM) and sterile water to 20 µl. The cycling protocol began with an initial denaturation step of 2 minutes at 96°C followed by 25 cycles of [1] 30 seconds at 96°C, [2] 15 seconds at 50°C and [3] 1.5 minutes at 60°C. This was followed by a final extension step of 5 minutes at 60°C. The sequencing reaction was cleaned-up by ethanol precipitation. First, 2 µl 1.5 M NaOAc/250 mM EDTA was added to the sequencing reaction and gently mixed. Next, 80 µl 95% ethanol was added and the mixture was vortexed and incubated at -20°C for 20 minutes. The reactions were centrifuged (>16 000 xg) at 4°C for 10 minutes and the supernatant was aspirated. Next, the pellet was washed with 500 µl 70% ethanol and centrifuged (>16 000 xg) at 4°C for 10 minutes. The supernatant was carefully aspirated and the pellet was allowed to dry. Dried sequencing reactions were submitted to the Molecular Biology Service Unit at the University of Alberta for sequencing.

In-Vitro mRNA Synthesis

All reagents used in this section were RNase-free, and the benchwork was performed in an RNase-free environment. This was also true for any work done using RNA.

Isolating Pure, Linear DNA for mRNA Synthesis

Plasmid DNA containing the CDS-of-interest was linearized using a restriction digestion. The linearization reaction used 10 µg DNA, 4 µl 10X restriction buffer, 2.5 µl restriction enzyme and DEPC to 40 µl. The digest was incubated at 37°C for at least 2 hours then topped up to 50 µl with DEPC water. To remove residual RNases and restriction enzyme, the 50 µl reaction was incubated at 50°C with 2.5 µl 10% SDS (sodium dodecyl sulfate) and 2 µl 10 mg/ml proteinase K for one hour. Next, 50 µl of DEPC and 10 µl 3M NaOAc, pH 5.2 were added and the contents were mixed. The reaction was then topped up to 200 µl with DEPC water in preparation for phenol/chloroform purification.

An equal volume of phenol:chloroform:isoamyl alcohol (25:24:1) pH 6.7 (~200 µl) was added to the reaction. The mixture was vortexed for 20 seconds, then centrifuged (>16 000 xg) for 5 minutes. The upper layer of the mixture was carefully removed to an RNase-free 1.7 ml tube (~200 µl). An equal volume of chloroform (~200 µl) was added to the transferred solution and vortexed for 20 seconds. The mixture was centrifuged (>16 000 xg) for 5 minutes and the upper layer was carefully removed to a new RNase-free 1.7 ml tube.

To precipitate the pure, linear DNA, 1/10 volume (~18-20 µl) 3M NaOAc, pH 5.2 was added to the transferred solution and mixed with 3 volumes (~600 µl) 100% ethanol. This was chilled at -20°C for 20 minutes then centrifuged (>16 000 xg) at 4°C for 10 minutes. The supernatant was carefully aspirated and the pellet was washed with 100 µl 70% ethanol in DEPC. The solution was centrifuged (>16 000 xg) at 4°C for 10 minutes, the supernatant was carefully aspirated and the pellet was allowed to dry. The DNA was then re-suspended in 15 µl DEPC and stored at -20°C.

In-vitro mRNA Synthesis and Clean-up

Capped mRNA transcription was performed using the mMessage mMachine® SP6/T7 Kit (Life Technologies Inc., Burlington ON, Canada). The mRNA synthesis reaction was assembled on ice and contained 2 µg pure, linear DNA, 10 µl 2X NTP/CAP, 2 µl 10X reaction buffer, 2 µl enzyme mix and nuclease-free water to 20 µl. The mixture was incubated at 37°C for 2 hours. To remove the template DNA, 1 µl TURBO™ DNase was added and the reaction was incubated at 37°C for 10 minutes.

The mRNA was cleaned-up using Amicon Ultra-0.5 ml Centrifugal Filters (Millipore, Billerica MA, USA). The reaction volume was topped up to 500 µl with DEPC and placed into a column and collection tube (supplied with kit). This was centrifuged (14 000 xg) for ~2 minutes or until ~400 µl of flow-through was collected. The column was inverted into a new collection tube and centrifuged (1000 xg) for 2 minutes to recover the solute. The recovered solute was topped up to 500 µl once more and the previous steps were repeated (using the same column). The remaining recovered solute should contain the concentrated mRNA transcripts. The concentration of the mRNA was measured and the mRNA was diluted with RNase-free water for microinjection. All mRNA was stored at -80°C.

RNA Extraction and Quantitative Real-Time PCR (qPCR)

Whole RNA Extraction

RNA was isolated from pools of 30-50 dechorionated embryos using the RNaqueous®-4PCR Kit (Life Technologies Inc., Burlington ON, Canada). Dechorionated embryos were immersed in 350 µl lysis/binding solution in 1.7 ml tubes and completely homogenized by vortexing. An equal volume of 64% ethanol (from kit) was added and the solution was gently mixed. The

mixture was transferred to a supplied column and centrifuged (>16 000 xg) for 1 minute. The flow-through was discarded. The column was washed once with 700 µl wash solution #1 and twice with 500 µl wash solution #2/#3, using 1 minute spins at >16 000 xg. The column was removed to a new RNase-free collection tube and the RNA was eluted in 60 µl pre-heated (to 70°C) elution buffer. One-half the desired volume of pre-heated elution buffer (30 µl) was applied to the column and spun (full speed) for 30 seconds. This step was repeated in the same collection tube, giving a final volume of 60 µl.

The RNA sample was next treated with DNase I to remove remaining DNA. 1/10 volume (6 µl) of 10X DNase I buffer (from kit) was added to the RNA with 1 µl DNase I and gently mixed. This was incubated at 37°C for 30 minutes. Following the incubation, 1/10 volume (6 µl) of DNase inactivating reagent was added and gently mixed. This was incubated at room temperature for 2 minutes then the whole mixture was centrifuged (>16 000 xg) for 2 minutes to pellet the precipitated DNase inactivating reagent. The supernatant (containing the RNA) was removed to a new RNase-free 1.7 ml tube and stored at -80°C.

cDNA Synthesis for qPCR

cDNA synthesis was performed using the AffinityScript QPCR cDNA Synthesis Kit (Agilent Technologies, Santa Clara CA, USA). In a PCR tube, 10 µl 2X cDNA Synthesis Master Mix, 3 µl random primers, 1 µl AffinityScript RT/RNase Block Enzyme Mixture, ~3 µg RNA and RNase-free water to 20 µl was mixed together. The mixture was placed in a thermocycler and incubated at [1] 25°C for 5 minutes (primer annealing), [2] 42°C for 30 minutes (cDNA synthesis) and [3] 95°C for 5 minutes (reaction termination). cDNA was stored at -20°C.

Quantitative Real-Time PCR (qPCR)

Primers were designed by the Universal ProbeLibrary website from Roche Applied Sciences (http://www.roche-applied-science.com/shop/ CategoryDisplay?catalogId=10001&tab=&identifier=Universal+Probe+Librar y) (Table 2.2). qPCR primer sets were validated by running qPCR reactions on a 2-fold cDNA dilution series from 1/8 to 1/256 prior to qPCR analysis. All qPCR reactions and primer validations were performed on the Rotor-Gene Q real-time PCR cycler from Qiagen (Qiagen, Hilden, Germany). The qPCR reactions used the Qiagen Rotor-Gene SYBR® Green PCR Kit (Qiagen, Hilden, Germany). In a single tube, 7.5 µl 2X Rotor-Gene SYBR Green PCR Master Mix, 0.75 µl forward primer (20 µM), 0.75 µl reverse primer (20 µM), 2 µl template cDNA and 4 µl RNase-free water were combined. The reactions were incubated at 95°C for 5 minutes, then exposed to 45 cycles of [1] 95°C for 5 seconds, [2] 55°C for 20 seconds and [3] 60°C for 20 seconds, acquiring data on the 60°C step. Data was analyzed using the Rotor-Gene Q Series Software v2.1.0 to validate primers and analyze the qPCR data. All primer sets used conformed to the following parameters: R^2 value close to 1 (0.97-1.00), percent efficiency over 95% and a standard curve slope of −3.3±0.1. The endogenous control primer set used was for the housekeeping gene *elongation factor 1 alpha (ef1a;* Table 2.2). The Rotor-Gene Q Series Software was used to identify the following values: Ct (threshold cycle) of the reference (ref) and the gene-of-interest (GOI), the relative concentration (RC) and the standard deviation of the Ct ($SD_{ref/GOI}$) for the reference and the GOI samples.

qPCR data was submitted to statistical analysis (Comparative or ΔΔCt Method) according to methods previously described (Bookout et al., 2006). Average Ct values were calculated across multiple replicates, and the ΔCt was calculated by subtracting the average Ct_{ref} from the average Ct_{GOI}.

The standard deviation of each ΔCt ($SD_{\Delta Ct}$) was calculated using the following formula: $SD_{\Delta Ct}=\sqrt{[(SD_{ref})^2+(SD_{GOI})^2]}$. This was calculated for each sample (wild type and mutant), and then averaged to collect the $avgSD_{\Delta Ct}$. The calibrated Ct ($\Delta\Delta$Ct) was calculated for each sample using the following formula: $\Delta\Delta Ct=\Delta Ct_{mutant}-\Delta Ct_{AB}$. The fold-change (FC) was calculated using the following formula: $FC_{mutant}=2^{(-\Delta\Delta Ct)}$. The FC_{AB} is always 1. The standard deviation of the FC (SD_{FC}) was calculated to measure the variability of individual values. This was calculated for each sample using the following formula: $SD_{FC}=(\ln 2)(avgSD_{\Delta Ct})(FC)$. The standard error of the mean (SEM) was calculated to measure the accuracy of the sample mean. This was calculated for each sample using the following formula: $SEM_{sample}=(avgSD_{\Delta Ct})/(\sqrt{N})$ where N=number of biological repeats. The FC was graphed using Microsoft Excel using SD_{FC} or SEM as the values for error bars. Fold changes in gene expression were compared using an unpaired t-test, which requires the input of the SEM, FC, and number of biological replicates for each sample (AB and mutant). These were placed into the online statistics calculator GraphPad (http://www.graphpad.com/quickcalcs/) to generate a p-value for the experiment.

Whole Mount mRNA In Situ Hybridization (WISH)

PCR-based Riboprobe Synthesis

Digoxigenin (DIG)-labeled riboprobes were synthesized directly from a PCR product. This was made possible by adding a T3 RNA polymerase binding site (5'-CATTAACCCTCACTAAAGGGAA-3') to the reverse PCR primer (Table 2.3; Thisse and Thisse, 2008). Primers were designed to create a product 800-1200 nt long. The unique 3'UTR of the desired transcript was targeted to increase specificity of the riboprobe. PCR products were obtained using the SuperScript® III One-Step RT-PCR System

Table 2.3: List of primers used for PCR-based riboprobe synthesis. The T3 RNA polymerase site was added to the 5' part of the reverse primer in all cases (*italics* indicate the T3 site).

Gene	Forward Primer (5'-3')	Reverse Primer (5'-3')	T_m (°C)	Size (bp)
crx	TCCAGGTGCTGTAGAAAAGAAAGTG	*CATTAACCCTCACTAAAGGG*ATGCCATAATCAACAAGAAGCGAG	55.8	1083
nr2e3	ACATACCAGGAGGAGGTGACAAAC	*CATTAACCCTCACTAAAGGG*AGGACTGTTGGAGTGTTGGCTACC	55.1	813
nrl	GCCACCTGCCTCTACCCTAAAG	*CATTAACCCTCACTAAAGGG*ACGTCTTCATTCAGTGTCCGTTCAAG	58.8	1154
opn1lw1	TTCTGCTGGGGTCCTTACAC	*CATTAACCCTCACTAAAGGG*ATGTACATGGGCAGGCATCTA	60.1	718
opn1mw1	CCCGTCACCACAATTTTCTT	*CATTAACCCTCACTAAAGGG*ATTCCATTGCCTCCACCTAAC	59.8	632
opn1sw1	ATTCCGATGAGCCAAACAAG	*CATTAACCCTCACTAAAGGG*ATTGGACAGGAGCAGACAGTG	60	753
opn1sw2	TGCTCTTGTGGACCTGACTG	*CATTAACCCTCACTAAAGGG*AATGTTCAGCAAGCCAAGACC	60	646
otx5	CGCTCCAGCTATCCTATGACCTACA	*CATTAACCCTCACTAAAGGG*ATGCTGTCGTTCTATTGGAGTTTTCA	64.2	938
rho	TGCACTTCTTCATCCCACTG	*CATTAACCCTCACTAAAGGG*ACTGCTGCGTTTTAGGAGGAG	59.8	723

45

with Platinum® *Taq* (Life Technologies Inc., Burlington ON, Canada). Per single reaction, 12.5 µl 2X Reaction Mix, 2 µl forward primer (5 µM), 2 µl reverse primer (5 µM), 1 µl SuperScript® III RT/Platinum® *Taq* Mix, ~1 µg whole RNA extract and sterile water to 25 µl were combined in a PCR tube. In a thermocyler, the reaction was first incubated at 54°C for 30 minutes for cDNA synthesis, followed by a typical PCR cycling program using an extension temperature of 68°C. The RT-PCR product was gel-extracted in preparation for probe synthesis.

Each DIG-labeled probe synthesis reaction contained 2 µl 10X Transcription Buffer (Roche Applied Science, Penzberg, Germany), 2 µl 10X DIG RNA Labeling Mix (Roche Applied Science, Penzberg, Germany), 1 µl T3 RNA Polymerase (Roche Applied Science, Penzberg, Germany), 1 µl RNase-OUT™ Recombinant Ribonuclease Inhibitor (Life Technologies Inc., Burlington ON, Canada), 200-400 ng cDNA template and DEPC water to 20 µl. This reaction was incubated at 37°C for 2 hours, with 1 µl additional T3 RNA Polymerase added halfway through the incubation. Following a 10 minute incubation at 37°C with 1 µl TURBO™ DNase (Life Technologies Inc., Burlington ON, Canada), the reaction was stopped by the addition of 2 µl RNase-free 0.2 M EDTA (pH 8.0). The probe synthesis reaction was cleaned-up using SigmaSpin™ Post-Reaction Clean-Up Columns (Sigma-Aldrich, St. Louis MO, USA). The column was placed in an RNase-free 2 ml tube and centrifuged for 30 seconds (425 xg) in a tabletop centrifuge. The bottom of the column was broken off and the column was spun again for 2 minutes (425 xg). The column was moved into a new, RNase-free 1.7 ml tube and the entire probe synthesis reaction was pipetted directly onto the resin. This was spun for 4 minutes (425 xg). 0.5 µl RNase-OUT was added to the purified probe product, and this was stored at -80°C for long-term storage.

Whole Mount mRNA In Situ Hybridization (WISH) Protocol

This protocol is based on a protocol published by Thisse and Thisse (2008). All washes are performed at room temperature on a shaker unless stated otherwise. Dechorionated embryos were rehydrated out of methanol using successive 5-minute washes of 70% methanol in PBST, 50% methanol in PBST and 30% methanol in PBST, followed by four 5-minute PBST washes. Embryos were permeabilized in 10 μg/ml proteinase K for the following lengths of time: 28 hpf (7 minutes), 48-52 hpf (40 minutes), 3-4 dpf (1 hour 15 minutes). Embryos were re-fixed in 4% PFA for 20 minutes followed by four 5-minute washes in PBST. Embryos were pre-hybridized for a minimum of 2 hours in hybridization solution (hyb: 50% formamide, 5X SSC [saline sodium citrate buffer], 50 μg/ml heparin, 0.1% Tween-20, 0.092 M citric acid in sterile water) with 500 μg/ml tRNA (hyb+tRNA). Working stocks of riboprobes were made by diluting probe in hyb+tRNA from 1:200 to 1:500 and stored at -20°C. Embryos were hybridized overnight at 65°C in pre-warmed probe in hyb+tRNA.

Embryos were washed for 5 minutes each at 65°C in [1] 66% hyb (no tRNA)/33% 2X SSC, [2] 33% hyb (no tRNA)/66% 2X SSC and [3] 2X SSC. Embryos were washed for 20 minutes in 0.2X SSC/0.1% Tween-20 followed by two consecutive 20 minute washes in 0.1X SSC/0.1% Tween-20, still at 65°C. Next, embryos were washed for 5 minutes each in [1] 66% 0.2X SSC/33% PBST, [2] 33% 0.2X SSC/66% PBST and [3] PBST at room temperature. Embryos were blocked for a minimum of 1 hour in blocking solution (2% sheep serum and 2 mg/ml bovine serum albumin [BSA] in PBST) then incubated in Anti-Digoxigenin-AP, Fab fragments (Roche Applied Science, Penzberg, Germany) diluted 1:5000 in blocking solution. Antibody binding was allowed to continue for a minimum of 2 hours at

room temperature or overnight at 4°C on a shaker. Antibody was rinsed from the embryos with five 15-minute washes in PBST.

To begin the staining reaction, embryos were washed four times for 5 minutes each in colouration buffer (100 mM Tris-HCl pH 9.5, 50 mM MgCl$_2$, 100 mM NaCl and 0.1% Tween-20 in sterile water). Embryos were incubated in the dark at room temperature in colouration solution (0.45 mg/ml 4-nitro blue tetrazolium chloride [NBT], 0.175 mg/ml 5-bromo-4-chloro-3-indolyl-phosphate [BCIP] in colouration buffer) with periodic monitoring until sufficiently stained. Colouration solution was rinsed from the embryos with five 5-minute washes in stop solution (PBST, pH 5.5) and stored at 4°C in the dark in stop solution. If the embryos were to be photographed on the yolk, they were rinsed twice with 100% methanol/0.1% Tween-20 for 10 minutes each to whiten the yolk.

Whole Mount Immunofluorescence

All washes were performed at room temperature on a shaker/nutator unless otherwise stated.

Anti-active Caspase 3 Immunofluorescence

Embryos were rinsed out of 4% PFA with three 20-minute washes in PBST then washed once in water + 0.1% Tween-20. Embryos were permeabilized with one 7-minute wash in ice-cold acetone and rinsed out of acetone with one 5-minute wash in water + 0.1% Tween-20. Embryos were blocked for 30-90 minutes in PBSDTT (1X PBS, 1% DMSO [dimethyl sulfoxide], 0.1% Tween-20, 0.1% Triton X-100) with 5% goat serum then incubated in anti-active caspase 3 antibody (1:400 in blocking solution; BD

Biosciences, Mississauga ON, Canada) overnight at 4°C or for 2 hours at room temperature. Diluted antibody was saved and reused 2-3 times. Next, embryos were quickly rinsed twice in PBSDTT, and then washed 2 times for 20 minutes each in PBSDTT. The rest of the washes in this protocol were performed in the dark. Embryos were incubated in Alexa Fluor® 488/555 goat anti-rabbit secondary antibody (1:1000 in blocking solution; Life Technologies Inc. Burlington ON, Canada) overnight at 4°C or for 2 hours at room temperature. Diluted secondary antibody was saved and reused 2-3 times. Next, embryos were quickly rinsed twice in PBSDTT then washed 4 times for 15 minutes each in PBSDTT. Embryos were co-stained with the nuclear dyes Hoechst or TOPRO®-3 (Life Technologies Inc., Burlington ON, Canada). After the final PBSDTT wash, the embryos were incubated in 3 μg/ml Hoechst in PBSDTT for 15 minutes in the dark then rinsed 4 times for 5 minutes each in PBSDTT. TOPRO-3 was simply added to the secondary antibody incubation at a concentration of 1:1000.

To count the number of apoptotic foci in each eye, Z-stacks for each eye were combined into maximum projections using ImageJ software (National Institutes of Health, Bethesda, MD) and foci were counted manually.

Zpr-1 Antibody Staining

Embryos were rinsed out of 4% PFA with four 5-minute washes in PBST and permeabilized in 10 μg/ml Proteinase K for the appropriate amount of time (see WISH protocol). Embryos were re-fixed in 4% PFA for 20 minutes then washed 4 times for 5 minutes each in PBSDTT. Embryos were blocked in 2.5% goat serum + 2 mg/ml BSA in PBSDTT for 1 hour. Embryos were incubated overnight at 4°C in primary Zpr-1 antibody (1:200 in PBSDTT). After overnight incubation, embryos were rinsed out of

primary antibody with five 5-minute washes in PBSDTT. Embryos were re-blocked as described above, and incubated in Alexa Fluor® 488/555 goat anti-mouse secondary antibody (1:1000 in blocking solution) overnight at 4°C. Secondary antibody was rinsed from the embryos with four 10-minute washes in PBSDTT. Embryos were co-stained with the nuclear dyes Hoechst or TOPRO®-3, as described above.

Phalloidin F-Actin Staining

Embryos were washed out of 4% PFA with four 5-minute washes in PBST and two 5-minute washes in tris buffered saline + Tween-20 (TBST: 50 mM Tris, 150 mM NaCl, 0.1% Tween-20, pH 7.6). Embryos were permeabilized in 4% Triton X-100 in TBST for 45 minutes (3 dpf) or 1 hour 15 minutes (4 dpf). Next, embryos were washed twice in TBST for 5 minutes each and incubated in Alexa Fluor® 488 Phalloidin 1:100 in TBST + 50 mg/ml BSA overnight at 4°C. Lastly, embryos were rinsed out of phalloidin with six 5-minute washes in TBST.

Immunofluorescence on Cryosectioned Samples

Cryosectioning Sample Preparation

Zebrafish embryos were fixed in 4% PFA overnight at 4°C then rinsed out of fix in 4 consecutive 5-minute washes of PBST. Embryos were allowed to sink through two sucrose/PBS solutions: 25% sucrose in PBS and 35% sucrose in PBS. Sucrose solutions were always made fresh. Embedding molds were filled with Tissue Freezing Media (TFM: Triangle Biomedical Sciences, Durham NC, USA) and embryos were suspended in the medium. The molds were then placed on dry ice and allowed to freeze completely

and were wrapped in parafilm and stored at -80°C until sectioning. TFM-embedded embryos were sectioned using a Leica CM1900 UV cryostat (Leica, Concord ON, Canada).

Immunofluorescence Protocols

Immunofluorescence protocols for labeling with anti-active caspase 3, Zpr-1 and phalloidin were performed as described above with the following alterations: a permeabilization step was not required and all washes were performed by pipetting ~1 ml solution onto a slide that was placed in a humid chamber to prevent evaporation. Samples were outlined with a hydrophobic pen before beginning the protocol.

Labeling with the crx antibody requires a citrate buffer epitope retrieval step. Samples were rehydrated in washing buffer (1X PBS and 1% goat serum) for 5 minutes then placed in boiling hot sodium citrate buffer (10 mM tri-sodium citrate dehydrate, 0.05% Tween-20, pH 6) for 5 minutes. Samples were washed twice for 5 minutes each in washing buffer then placed in blocking reagent (1X PBS, 20% goat serum, 0.5% triton X-100) for 1 hour. Embryos were incubated in crx primary antibody (1:5000) in diluting reagent (1X PBS, 1% goat serum, 0.5% triton X-100) overnight at 4°C. Primary antibody was removed and kept (can be used up to 3 times) and the samples were washed 5 times for 5 minutes each in washing buffer. Slides were incubated in Alexa Fluor® 488/555 goat anti-mouse secondary antibody (1:1000 in diluting reagent) for 2 hours. Secondary antibody was rinsed off with five 5-minute washes in washing buffer. TOPRO-3 nuclear stain may be added to the secondary antibody incubation (1:5000). Excess buffer was gently blotted off with paper towel, and samples were mounted in Aqua Poly/Mount (Polysciences Inc., Warrington PA, USA). The crx

antibody was graciously provided by Pamela Raymond (Shen and Raymond, 2004).

Transcription Activator-like Effector Nucleases (TALENs)

TALENs are highly efficient molecular tools for directed gene mutagenesis that fuse modified DNA sequence-specific TAL effectors (originally from *Xanthomonas spp.* plants) to the FokI nuclease catalytic domain (Cermak et al., 2011). TALENs can be designed for virtually any DNA sequence desired. The TAL effector domain is made up of a series of amino acid modules that contain variable residues at positions 12 and 13, the repeat-variable di-residues (RVDs). Each RVD can bind one specific nucleotide (NG=T, HD=C, NI=A, NN=G), such that a desired DNA sequence can be easily targeted by engineering the TAL effector domain to contain the corresponding sequence of RVD modules (Cermak et al., 2011).

The following protocol was based closely on a protocol published by Cermak et al. (2011). The Golden Gate TALEN and TAL Effector Kit 2.0 was designed by Daniel Voytas' group (Cermak et al., 2011) and purchased from the non-profit organization AddGene (www.addgene.org). All plasmids used in this protocol were provided in this kit except for the GoldyTALEN modified scaffold, which was designed by Stephen Ekker's group (Bedell et al., 2012; Ma et al., 2013) and acquired from AddGene separately. TALENs were designed using the TAL Effector Nucleotide Targeter 2.0 online tool (https://tale-nt.cac.cornell.edu/), using the preset architecture by Cermak et al. (2011; 15-20 RVD modules, 15-24 bp spacer; Table 2.4). Before assembly, RVD module vectors were tested with a BsaI restriction digest. The digest was run on a gel, and a ~100 bp product was observed in working plasmids. RVDs were first assembled into intermediate arrays of 1-10 repeats (Golden Gate reaction #1), and then these intermediate arrays were joined into the

Table 2.4: Sequence of the *otx5* TALEN RVD arrays. This TALEN targets exon 1 of the *otx5* CDS. Lowercase letters in the Plus Strand Sequence indicate the spacer area between TAL binding sites.

	RVD Array Sequence	Plus Strand Sequence
TAL 1	NG HD NI NG HD NG HD NI HD NG NH NG HD NI HD	TTCATCTCACTGTCACcgggagaccgagacaCGCGCACCGAGCGCTCA
TAL 2	NH NI NH HD NH HD NG HD NH NH NG NH HD NH HD NH	

GoldyTALEN backbone to make the final construct (Golden Gate reaction #2).

Golden Gate Reaction #1 (GG#1)

Consider the one of the *otx5* RVD arrays NG HD NI NG HD NG HD NI HD NG NN NG HD NI HD, targeting the sequence 5'-TCATCTCACTGTCAC-3' (15 RVD modules in total). RVD module plasmids 1-10 were selected using the plasmids numbered in the order the RVDs were required. For example, the first RVD module was pNG1, the second pHD2, the third pNI3, etc. Module plasmids for RVDs 11-14 were also selected this way (ex. pNN1, pNG2, etc.). RVDs 1-10 were fused into the array plasmid pFUS_A and RVDs 11-14 were fused into the array plasmid pFUS_B(x-1) where x was the total number of RVD repeats minus 10 (in this case, pFUS_B4). 5 μg of each desired pFUS plasmid was linearized with BsaI restriction enzyme in the presence of BSA and the ~2000 bp linearized plasmid was gel-extracted.

For each GG#1 reaction, the following was combined in a PCR tube: 150 ng of each RVD module plasmid, 150 ng pFUS plasmid, 1.5 μl BSA (100X), 1.5 μl BsaI, 1.5 μl T4 DNA ligase, 1 μl dATP (25 mM), 2 μl 10X T4 DNA ligase buffer and sterile water to 20 μl. In a thermocycler, the reaction was exposed to 10 cycles of [1] 37°C for 5 minutes and [2] 16°C for 10 minutes, then heated to 50°C for 5 minutes and then 80°C for 5 minutes. After the thermocycler incubation, 1 μl dATP (25 mM) and 1 μl Plasmid-Safe DNase was added and the entire mixture was incubated at 37°C for 1 hour. 5 μl of this reaction was used to transform One Shot TOP10 cells and the cells were plated on LB agar plates containing 50 μg/ml spectinomycin, with XGAL and IPTG for blue/white screening.

The next morning, 6 white colonies from each GG#1 transformation were picked, re-streaked and used in a colony PCR reaction. A typical PCR reaction was prepared using pCR8_F1 (forward) and pCR8_R1 (reverse) primers (Table 2.2) and, after re-streaking, the picked colony was suspended in the PCR reaction (template) and gently mixed. The PCR program used an annealing temperature of 55°C, an extension time of 1 minute 45 seconds and had 30-35 cycles. Correct clones had a ~1200 bp band (corresponds with 10 RVDs) with laddering every ~100 bp between 200-500 bp (Figure 2.1). Incorrect clones had a single band at ~500 bp. Overnight cultures of correct clones were set up and miniprepped the following morning. GG#1 minipreps were validated by restriction digest with Esp3I in the presence of 5 mM DTT (dithiothreitol). Correct plasmids had a ~1000 bp band for pFUS_A constructs and pFUS_B constructs had ~100 bp per RVD repeat (ex. a pFUS_B4 would have a 400-500 bp band; Figure 2.1).

Golden Gate Reaction #2 (GG#2)

Prior to setting up the GG#2 reaction, 5 μg of the GoldyTALEN backbone plasmid was linearized by digesting with Esp3I (with 5 mM DTT) and the ~2000 bp linearized plasmid was gel-extracted. For each GG#2 reaction, the following was combined in a PCR tube: 150 ng of each pFUS plasmid (A and B) containing the intermediate arrays, 150 ng GoldyTALEN plasmid, 150 ng of the last repeat RVD module plasmid (in the above example, pLR-HD), 1 μl Esp3I, 1 μl T4 DNA ligase, 2 μl 10X Tango Buffer (Thermo Scientific, Ottawa ON, Canada), 1 μl dATP (25 mM) and sterile water to 20 μl. In a thermocycler, the reaction was exposed to 10 cycles of [1] 37°C for 5 minutes and [2] 16°C for 10 minutes, then heated to 37°C for 15 minutes and then 80°C for 5 minutes. After the thermocycler incubation, 5 μl of this reaction was transformed into One Shot TOP10 cells and the cells
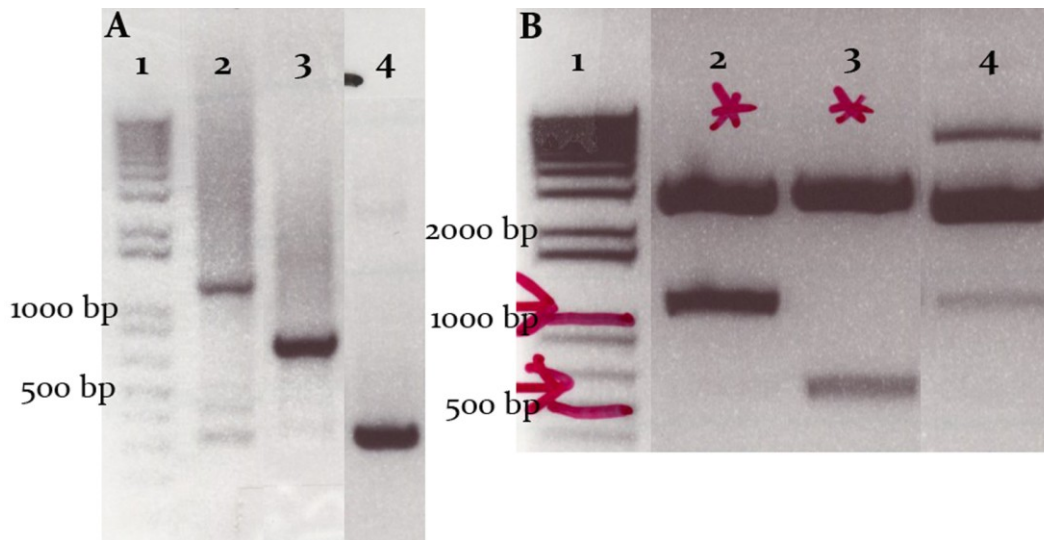
Figure 2.1: Examples of the Golden Gate #1 colony PCR and verification digest. (A) Colony PCR of Golden Gate #1 pFUS clones. A positive result for a pFUS assembly that contains 10 RVD repeats should display a band at ~1200 bp with laddering every ~100 bp below (A, lane 2). A positive result for a pFUS array that contains 5 RVD repeats should have a band at ~500 bp and laddering every ~100 bp below (A, lane 4). Lane 3 shows a negative (empty) pFUS clone. (B) Esp3i restriction digest of isolated Golden Gate #1 pFUS plasmids. A positive results for a pFUS assembly that contains 10 RVD repeats should display a ~1000 bp insert (B, lane 3). A positive results for a pFUS array that contains 5 RVD repeats should display a ~500 bp insert (B, lane 4). An example of a negative verification digest is shown in lane 2.

were plated on LB agar plates containing 50 μg/ml carbenicillin, with XGAL and IPTG for blue/white screening.

Colony PCR was performed as described for GG#1 using TAL_F1 (forward) and TAL_R2 (reverse) primers (Table 2.2) and an extension time of 3 minutes. Correct GG#2 clones result in a large smear, with the brightest spot at ~3000-5000 bp, with ~1600 bp band and some laddering from ~1000 bp and below (Figure 2.2). Overnight cultures were set up for positive clones and miniprepped the following morning. GG#2 minipreps were validated using a restriction digest with BamHI and SphI (in the presence of BSA) and ran on a 0.6% agarose gel. Correct plasmids had two bands at ~3000 bp (Figure 2.2).

Test TALENs In Vivo

To synthesize TALEN mRNA, fully assembled GoldyTALENs were linearized with SalI and mRNA was synthesized using T3 RNA polymerase. 200 pg of TALEN mRNA was injected into 1-cell stage embryos. After 24 hours of development, a portion of the embryos was pooled, gDNA was isolated and the region of interest was PCR-amplified and TOPO-cloned. The remainder of the embryos was raised to adulthood for germline mutation analysis. Individual colonies were picked and suspended in 25 μl sterile water and 2 μl of this suspension was used for HRMA. 2 μl of the suspension was also spotted on LB agar (with carbenicillin) for setting up future liquid cultures. Colonies that were identified as "variant" were miniprepped and sequenced to identify the nature of the mutation.
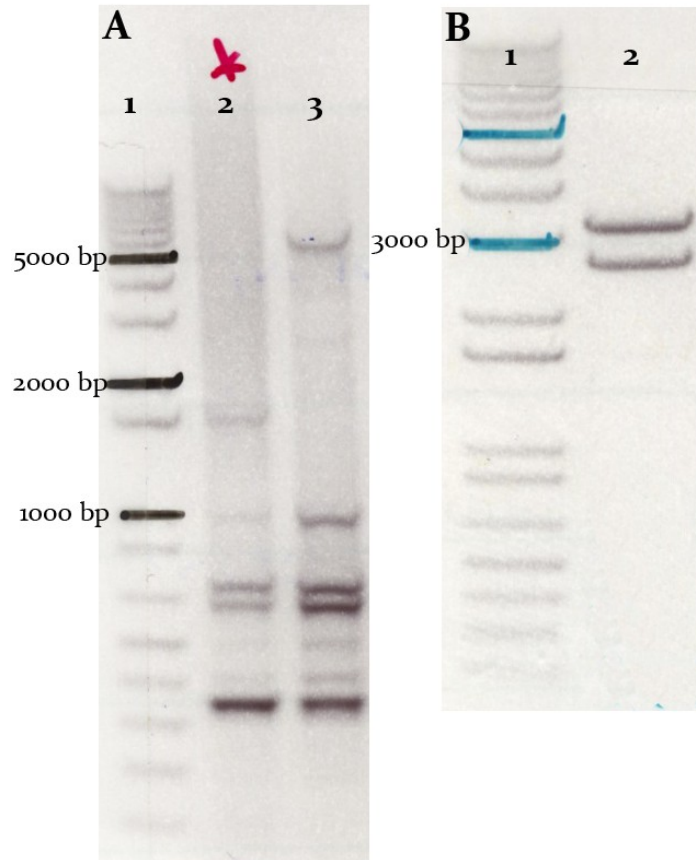
Figure 2.2: Examples of the Golden Gate #2 colony PCR and verification digest. (A) Colony PCR of Golden Gate #2 GoldyTALEN clones. A positive result for a fully assembled GoldyTALEN should display a large smear with the brightest spot at ~3000-5000 bp, a ~1600 bp band and some laddering from ~1000 bp and below (A, lane 2). Lane 3 is an example of an incorrect clone. (B) Esp3I restriction digest of isolated GoldyTALEN plasmids containing a fully assembled TALEN. A positive clone should display two bands around ~3000 bp (B, lane 2).

Identifying Heterozygous Founders

Pairs of P_o (TALEN mRNA-injected) adults were bred and the offspring were allowed to develop to 24 hpf. Genomic DNA from five pools of 10 embryos each was isolated and used for HRMA. Any remaining embryos were raised to adulthood for somatic mutation analysis and to identify heterozygous founders. Genomic DNA pools that were identified as "variant" by HRMA were used as templates to PCR amplify and clone the mutational target site. HRMA was performed on individual colonies (as described above) and colonies identified as "variant" were miniprepped and sequenced to identify the nature of the mutations that were passed through the germline. If the mutations were desirable (insertions/deletions that cause frameshifts and premature stop codons) the progeny of that cross were fin-clipped and genotyped to identify heterozygous F_1 founders (See Figure 2.3 for schematic).
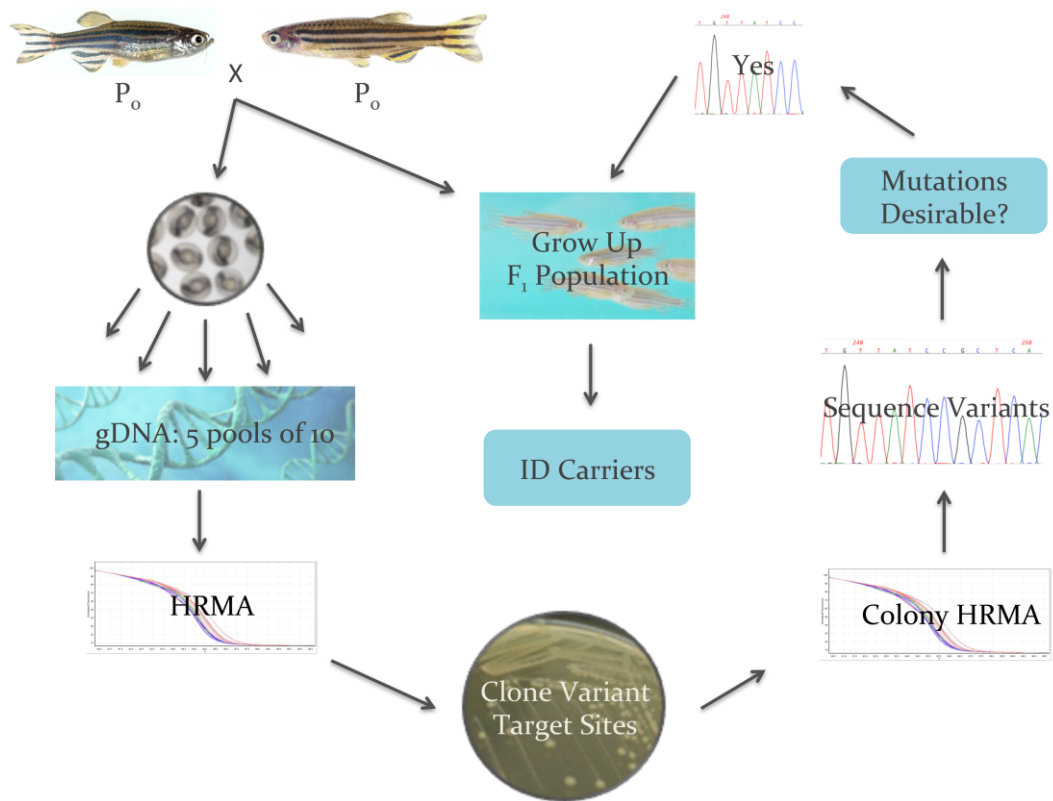
Figure 2.3: Identifying heterozygous founders from the TALEN mRNA-injected population. Pairs of P_0 (TALEN mRNA-injected) adults were bred and genomic DNA from five pools of 10 embryos each was isolated and used for HRMA. Any remaining embryos were raised to adulthood for somatic mutation analysis and to identify heterozygous founders. Genomic DNA pools identified as "variant" by HRMA were used as templates to PCR amplify and clone the mutational target site. Colonies identified as "variant" by HRMA were sequenced to identify the nature of the mutations that were passed through the germline. If the mutations were desirable, (insertions/deletions that cause frameshifts and premature stop codons) the progeny of that cross were genotyped to identify heterozygous F_1 founders.

Chapter 3

A novel role for Gdf6a in retinal dystrophies

Introduction

Microphthalmia (small eye), anophthalmia (no eye) and colobomata (failure of optic fissure closure) are phenotypic features of a spectrum of eye abnormalities (known collectively as MAC) that are present in up to 11% of blind children (Verma and Fitzpatrick, 2007). MAC is a form of congenital blindness with variable patterns of inheritance (Zhang et al., 2009). Mutations in BMP ligands, such as *BMP4*, *GDF6* and *GDF3*, have been identified as causative in MAC patients (Asai-Coakwell et al., 2009; Ye et al., 2010; Zhang et al., 2009). Additionally, mutations in a number of eye field transcription factors are found in MAC patients, including *SIX3*, *SIX6* and *OTX2* (Zhang et al., 2009).

Leber's congenital amaurosis (LCA) is an early-onset retinal degeneration disorder and is the most severe form of inherited blindness. LCA has a prevalence of 1 in 30 000 – 81 000 live births and accounts for ≥5% of all inherited retinopathies (Koenekoop, 2004). Mouse models of this disorder display retinal cell degeneration and death (Furukawa et al., 1999). Mutations in genes involved in visual processes [including: embryonic retinal development, phototransduction, protein trafficking, outer segment phagocytosis, guanine synthesis, retinoid cycling and ciliary function] have been identified in ~70% of all LCA cases. A subset of these genes also contributes to additional later-onset retinal dystrophies such as retinitis pigmentosa and cone-rod dystrophy (Asai-Coakwell et al., 2013; Cremers et al., 2002; den Hollander et al., 2008).

Bone morphogenetic proteins (BMPs) are members of the transforming growth factor-β (TGFβ) ligand superfamily, which signal through transmembrane receptors to induce or repress target gene transcription. This ligand family has diverse roles, including regulation of cellular differentiation, proliferation and cell survival (Arnold and

Robertson, 2009; Nohe et al., 2004; Sieber et al., 2009). Mutations in BMP ligands including *BMP4, BMP7, GDF3,* and *GDF6* result in a spectrum of ocular abnormalities in human patients (Asai-Coakwell et al., 2007; Asai-Coakwell et al., 2009; Bakrania et al., 2008; Wyatt et al., 2010; Ye et al., 2010) and aberrant apoptosis has been observed in retinas of animal models deficient in *Bmp7* and *Gdf6* (den Hollander et al., 2010; Gosse and Baier, 2009; Luo et al., 1995).

Growth differentiation factor 6 (Gdf6) is a BMP ligand that signals through BMP-responsive transmembrane receptors in a dose-dependent manner. Gdf6 dimers bind to heteromeric complexes of transmembrane Type I and Type II serine-threonine kinase receptors. Ligand binding induces phosphorylation and activation of the Type I receptor. Downstream signaling is activated by phosphorylation of Smad proteins by active Type I receptors. Active Smad proteins enter the nucleus and promote transcription of target genes (Sieber et al., 2009). Zebrafish Gdf6a is required for the initiation of dorsal retinal identity, for correct retinotectal mapping, and is necessary to initiate expression of dorsal retinal markers (*bmp4, tbx5, tbx2b, efnb2a, aldh1a2, bambi)* and to suppress ventral markers (*vax2, aldh1a3, ephb2, ephb3).* Conversely, eye-specific overexpression of *gdf6a* results in increased expression of dorsal markers and reduced expression of ventral markers (French et al., 2009; Gosse and Baier, 2009). Additionally, Gdf6a appears to protect retinal cells from apoptosis, based on increased levels of TUNEL and active caspase 3 immunolabeling in multiple Gdf6-deficient models (Asai-Coakwell et al., 2013; Gosse and Baier, 2009; Hanel and Hensey, 2006; Pant et al., 2013).

Zebrafish *gdf6a* retinal expression is first detected at 11 hpf, adjacent to the developing eye field (French et al., 2009). By 14 hpf, expression of *gdf6a* is restricted to the presumptive dorsal retina. Expression remains in

the dorsal retina at 28 hpf, and by 48 – 96 hpf the expression of *gdf6a* is restricted to the dorsal ciliary marginal zone (CMZ), the proliferative zone of the retina (French et al., 2009; French et al., 2013). The late-embryo expression pattern of *gdf6a* in the proliferative region of the retina is consistent with the model that Gdf6a regulates retinal progenitor cell number and later cell proliferation within the CMZ of the zebrafish larvae (French et al., 2013).

A segmental deletion on human chromosome 8 (46, XX, del 8 q21.2q22.1) was identified in a patient who presented with bilateral coloboma. This deletion covered an 10.37 Mb region, encompassing the human *GDF6* gene (Asai-Coakwell et al., 2007). Similarly, mouse *Tcm* (total cataract with microphthalmia) mutants are born with microphthalmia and coloboma. This mutation has been characterized as a 1.3 Mb deletion of a region that includes the murine *Gdf6* gene (Wang et al., 2005). Due to its role in early retinal patterning, and regulation of retinal proliferation, we hypothesized that mutations in *GDF6* could underlie the phenotypes observed in retinal disease such as MAC and LCA. Indeed, *GDF6* mutations have been found in MAC patients, with 1.4% (7/489) of ocular patients presenting with MAC having a mutation in human *GDF6* (0/366 control patients; Asai-Coakwell et al., 2009). Additionally, 4/279 patients from an LCA and juvenile retinitis pigmentosa cohort have been identified with heterozygous mutations in *GDF6,* one of which is a compound heterozygote (Asai-Coakwell et al., 2013). We used a zebrafish line with a recessive mutation in the *gdf6a* gene (the zebrafish ortholog to human *GDF6*) to study the contribution of *gdf6a* to the development of these retinal diseases. These mutants display microphthalmia and early retinal apoptosis that can be rescued by pharmaceutical treatment with an anti-apoptotic compound. Interestingly, the rescue of retinal apoptosis in the early mutant retina does not rescue the eye size, but does partially rescue the visual function of these

fish. These studies show a novel role for TGFβ signaling in the development of retinal dystrophies.

Results

Examining the ocular phenotype of gdf6a$^{-/-}$ mutants.

To examine the role of *gdf6a* in the development of retinopathies and to study the nature of long-term *gdf6a* mutations, we utilized the *gdf6a^{s327}* zebrafish line. This fish line has a C to A transversion early in the ORF, resulting in a p.S55X truncation in the predicted polypeptide. This mutation results in a truncated Gdf6a pro-protein that lacks the C-terminal signaling peptide characteristic of BMP ligands (Gosse and Baier, 2009). *gdf6a$^{s327/s327}$* mutants (hereafter referred to as *gdf6a$^{-/-}$*) display microphthalmia, which can be first observed at 48 hpf (Figure 3.1 A-B, E-F). To observe the effects of long-term *gdf6a* loss on retinal and photoreceptor structure, histological analyses were performed. Homozygous mutants and non-mutant siblings were analyzed at 2-weeks of age for photoreceptor morphology and retinal laminar structure. Cryosections were immunolabeled using the zpr-1 monoclonal antibody, which labels the Arrestin 3a protein in red- and green-cones in zebrafish. *gdf6a$^{-/-}$* mutants displayed dysmorphic red/green photoreceptors, with shortened, misshaped cone inner segments (Figure 3.1 C-D). Immunolabeling with phalloidin, which binds and labels F-actin microfilaments, reveals that the general retinal lamination remains relatively unchanged (Figure 3.1 E-H). All retinal layers appear to develop, although the width of the layers appear narrower in the mutant (Figure 3.1 E-F) and the length of the photoreceptor cells are shorter (Figure 3.1 G-H).
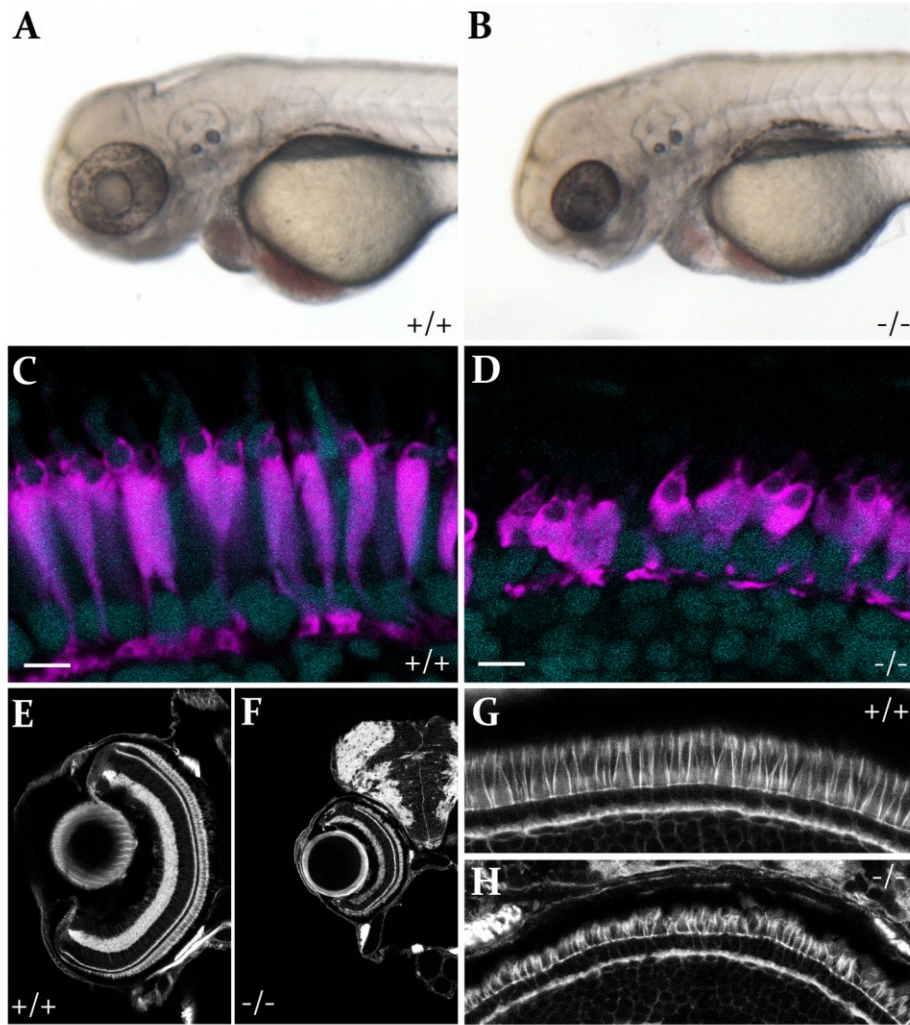
Figure 3.1: *gdf6a*^{-/-} mutants display microphthalmia, colobomata and dysmorphic cone photoreceptors. Microphthalmia was first observed in *gdf6a*^{-/-} mutants at 48 hpf, and was more distinguishable by 72 hpf (A-B). Immunolabeling for Arrestin3a at 2 weeks of age demonstrated that red/green cone photoreceptor morphology (magenta) in the *gdf6a*^{-/-} mutant was profoundly altered compared to non-mutant siblings, with shortening of the inner segment (C-D). This was also observed in phalloidin labeled (actin microfilaments) 2-week-old retinas (G-H). In contrast, the overall retinal lamination appeared relatively normal (phalloidin) with minor narrowing of the layers (E-F). Scale bars 5 µm.

gdf6a^{-/-} mutants display retinal apoptosis, which is reduced by treatment with
the anti-apoptotic compound P7C3.

Since retinal cell death is observed in human retinal dystrophies and animal models of retinal dystrophies (French et al., 2013; Garcia-Valenzuela et al., 1995; Genini et al., 2013; Portera-Cailliau et al., 1994; Sancho-Pelluz et al., 2008) we analyzed the amount of apoptosis present in the differentiating retina of *gdf6a^{-/-}* mutants and their non-mutant siblings. Previous studies have demonstrated that Gdf6-deficient zebrafish and *Xenopus* models have increased retinal apoptosis (Asai-Coakwell et al., 2013; Gosse and Baier, 2009; Hanel and Hensey, 2006). To determine the developmental time period where this apoptosis is occurring in zebrafish, we analyzed retinas at 6 different time points during retinal differentiation (24, 28, 30, 32, 48 and 96 hpf) and quantified the average number of apoptotic foci at each stage of retinal development. Apoptosis was observed by immunolabeling for active-caspase 3, a key executioner caspase in the apoptosis signaling pathway (Fernandes-Alnemri et al., 1994; Nicholson et al., 1995; Tewari et al., 1995). Compared to non-mutant siblings (Figure 3.2 A-F), *gdf6a^{-/-}* mutants displayed increased apoptosis from 24 – 32 hpf, with very few foci observed at 48 hpf, and no foci observed at 96 hpf (Figure 3.2 A'-F'). The time point with the highest level of apoptosis observed in *gdf6a^{-/-}* mutants was 28 hpf, with an average of 102.9 cells undergoing apoptosis (n= 22, Figure 3.2 G).

We next evaluated whether the apoptotic effect observed in *gdf6a^{-/-}* mutants could be improved by treatment with a novel anti-apoptotic compound, P7C3, an aminopropyl carbazole that protects newborn neurons from apoptotic cell death (Pieper et al., 2010). Zebrafish *gdf6a^{-/-}* mutants and non-mutant siblings were immersed in 0.01 µM or 0.1 µM P7C3 from 5
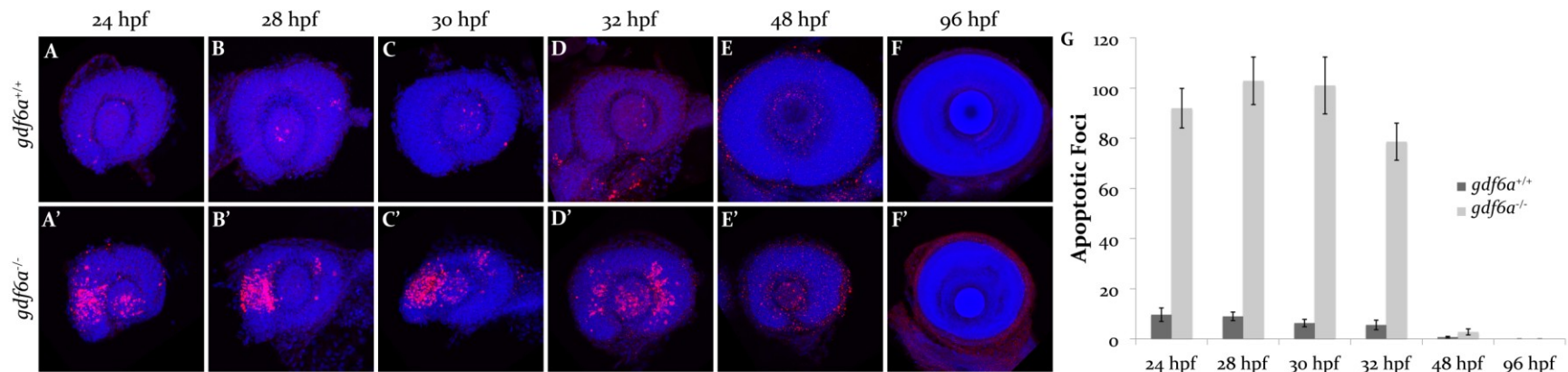
Figure 3.2: Analysis of amounts of apoptosis in the *gdf6a*^{-/-} developing retina. (A-F') Immunolabeling of active caspase 3 (red) in *gdf6a*^{+/+} (A-F) and *gdf6a*^{-/-} (A'-F') zebrafish counterstained with the nuclear dye Hoechst (blue). (G) Quantification of the numbers of apoptotic foci at each time point (*gdf6a*^{+/+}: 24 hpf n=9, 28 hpf n=13, 30 hpf n=15, 32 hpf n=19, 48 hpf n=15, 96 hpf n=18; *gdf6a*^{-/-}: 24 hpf n=14, 28 hpf n=22, 30 hpf n=19, 32 hpf n=27, 48 hpf n=20, 96 hpf n=18). Error bars, SEM.

hpf – 28 hpf and retinal apoptosis was analyzed with immunolabeling for active-caspase 3 and the number of apoptosing cells per retina was quantified. P7C3-treatment significantly reduced the number of caspase 3-positive cells in 28 hpf mutant retinas compared to DMSO control-treated mutant siblings [70% and 79% reductions at 0.01 μM and 0.1 μM P7C3 respectively, $p < 0.0001$, ANOVA (Figure 3.3 D-G)]. P7C3-treatment did not have an effect on cell survival in retinas of *gdf6a* non-mutant siblings (Figure 3.3 A-C, G).

P7C3-treatment does not rescue eye size in gdf6a^{-/-} mutants, but does partially recover visual function.

While the role of *Gdf6* in the initiation of dorsal retinal identity early in development is well established (French et al., 2009; Gosse and Baier, 2009), mechanisms behind the microphthalmic phenotype observed in *Gdf6^{-/-}* mutant models remain unclear. To determine if the high rates of apoptosis observed in the zebrafish *gdf6a^{-/-}* mutant retina contribute to the microphthalmic phenotype observed later in development, we analyzed the relative eye size of *gdf6a^{-/-}* mutants after long-term P7C3 treatment. *gdf6a^{-/-}* mutants and non-mutant siblings were treated with 0.1 μM P7C3 (or DMSO control) from 5 hpf – 48 hpf (the time period of maximum retinal apoptosis) then switched to embryo media and allowed to develop to 72 hpf. Upon phenotypic examination, the P7C3-treatment did not rescue the eye size of *gdf6a^{-/-}* mutants (Figure 3.4 A-D). Relative eye area was quantified, with the mean eye size of DMSO-treated non-mutant siblings set to 1. Consistent with the phenotypic observation, no significant rescue of eye size was apparent in P7C3-treated *gdf6a^{-/-}* mutant larvae. The P7C3-treated *gdf6a^{-/-}* mutant eyes remain significantly smaller than those of their non-mutant siblings ($p < 0.05$ [DMSO], $p < 0.001$ [P7C3], Figure 3.4 E).

Figure 3.3: P7C3-treatment reduces retinal apoptosis in *gdf6a*^{-/-} mutants. (A-F) Immunofluorescence for active caspase 3 (red) co-stained with Hoechst (blue) on 28 hpf dissected retinas. (G) Quantification of the number of active caspase 3 positive cells in the retina. Non-mutant siblings treated with DMSO, 0.01 μM P7C3 and 0.1 μM P7C3 had a mean of 3.34 (n=44), 2.07 (n=58) and 1.32 (n=112) apoptosing cells per eye respectively. *gdf6a*^{-/-} mutants treated as above had a mean of 76.41 (n=34), 23.13 (n=18) and 16.09 (n=35) apoptosing cells per eye respectively. All embryos included in statistics were genotyped via sequencing as being *gdf6a*^{-/-} mutants or non-mutant siblings. Error bars, SEM; * $p < 0.00001$, ANOVA.

Figure 3.4: P7C3-treatment does not rescue the microphthalmic phenotype in *gdf6a*$^{-/-}$ mutants. (A-D) Lateral images of 72 hpf *gdf6a*$^{-/-}$ mutants and non-mutant siblings treated with DMSO solvent control (A-B) or 0.1 μM P7C3 (C-D). *gdf6a*$^{-/-}$ mutants retain the microphthalmic phenotype after P7C3-treatment (D) when compared to DMSO-treated mutant siblings (B). (E) Quantification of eye area in DMSO- and P7C3-treated *gdf6a*$^{-/-}$ mutants and non-mutant siblings (*gdf6a*$^{+/+}$: DMSO n=13, P7C3 n=16; *gdf6a*$^{-/-}$: DMSO n=15, P7C3 n=12). The data is displayed as a relative size compared to DMSO-treated non-mutant siblings (A). * p<0.001; ** p<0.05; student's t-test with Bonferroni correction for multiple comparisons.

To assess whether P7C3-treatment rescued functional visual ability in $gdf6a^{-/-}$ mutants we utilized two distinct visual behavior assays: visually mediated background adaptation (VBA) and optomotor response (OMR). VBA is a retinal ganglion cell-meditated neuroendocrine response in which melanophores adjust their melanosome distribution according to ambient background light detection (Fleisch and Neuhauss, 2006; Muto et al., 2005). Control-treated $gdf6a^{-/-}$ mutants displayed increased pigmentation when placed on a light background for 2-5 minutes compared to similarly-treated non-mutant siblings, indicating a non-responsive VBA in the mutants. After P7C3-treatment, 50% of the $gdf6a^{-/-}$ mutants assayed displayed at least a partial VBA response ($gdfa6^{-/-}$: DMSO 1/22 were VBA-responsive; P7C3 11/22 were VBA-responsive; Figure 3.5 C-E). All of the $gdf6a^{+/+}$ siblings assayed were VBA-responsive ($gdfa6^{+/+}$: DMSO 25/25; P7C3 24/24; Figure 3.5 A-B, E).

OMR measures the distance a larva travels in the direction of a moving visual stimulus (Orger et al., 2004). This assay requires a higher level of visual sensitivity and the coordinated efforts of both the visual and musculo-skeletal systems (Asai-Coakwell et al., 2013; Orger et al., 2004). Zebrafish larvae were placed into a narrow plexiglass "racetrack"-style tank on top of an upturned computer monitor and exposed to a moving stimulus (scrolling black lines) or a white screen (no stimulus negative control). The distance that the larvae swam along the track was measured in cm. Wild-type larvae swam in the direction of the scrolling bars and did not swim in any particular direction when exposed to a white screen (Figure 3.6 A). $gdf6a^{-/-}$ mutant larvae did not follow a moving visual stimulus, and their behavior was similar to a wild-type larvae not exposed to a visual stimulus (Figure 3.6 A). This indicates that $gdf6a^{-/-}$ mutant larvae do not have higher visual function. In contrast to the VBA results, P7C3-treated $gdf6a^{-/-}$ mutant larvae did not show any significant improvement in OMR response (Figure 3.6 B). In both of the visual function assays, $gdf6a^{-/-}$ mutant and non-mutant
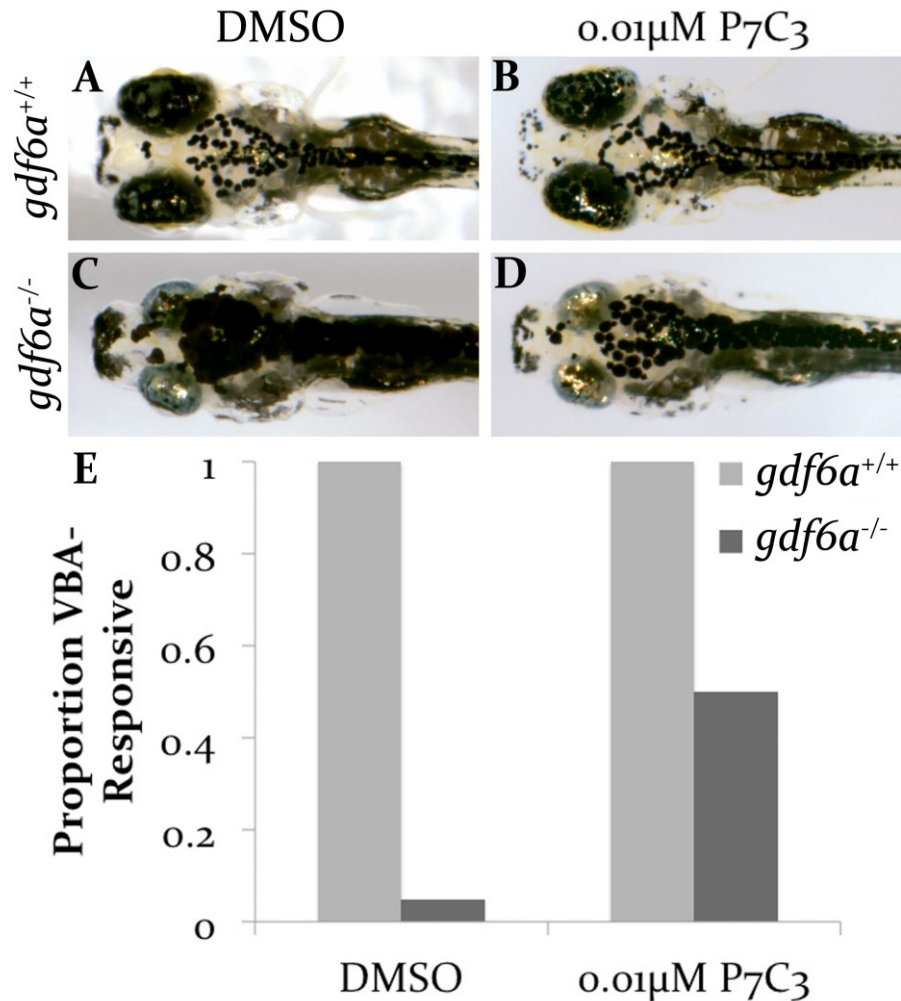
Figure 3.5: P7C3 treatment recovers VBA activity in *gdf6a*^{-/-} mutants. (A-D) dorsal images of *gdf6a*^{-/-} mutant and non-mutant siblings treated with a control dose of DMSO (A, C) or 0.01 μM P7C3 (B, D) at 8 dpf. DMSO-treated and P7C3-treated non-mutant siblings have normal melanophore contraction (A, 100% VBA, n=25; B, 100% VBA, n=24; E) while DMSO-treated *gdf6a*^{-/-} mutants have unresponsive VBA and widely distributed melanophores (C, 5% VBA, n=21; E). Treatment of *gdf6a*^{-/-} mutants with P7C3 partially recovers VBA and melanophores appear partially contracted (D, 50% VBA, n=22; E). (E) Graph of the proportion of embryos that present fully or partially responsive VBA under the indicated conditions.
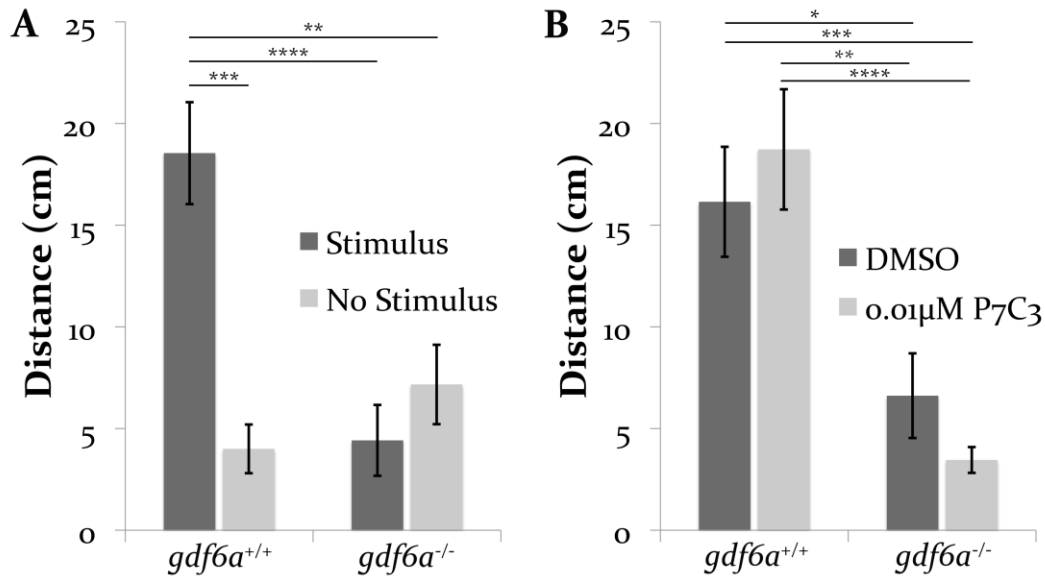
Figure 3.6: P7C3 treatment does not rescue OMR in 7 dpf $gdf6a^{-/-}$ mutant larvae. (A) Measurements of the distance the larvae will swim when exposed to a stimulus (scrolling black lines) vs. no stimulus (white screen). Wild-type zebrafish larvae will follow a visual stimulus at 7 dpf. $gdf6a^{-/-}$ larvae do not display this response ($gdf6a^{+/+}$: stimulus n=38, no stimulus n=26; $gdf6a^{-/-}$: stimulus n=38, no stimulus n=26). (B) Measurements of the distance the larvae will follow a stimulus when exposed to P7C3 or a solvent control ($gdf6a^{+/+}$: DMSO n=30, P7C3 n=30; $gdf6a^{-/-}$: DMSO n=34, P7C3 n=31). P7C3 treatment does not interfere with the OMR in $gdf6a$ non-mutant siblings and does not rescue OMR in $gdf6a^{-/-}$ mutant larvae. * $p<0.05$, ** $p<0.01$, *** $p<0.001$, **** $p<0.0001$ (ANOVA).

siblings were treated with 0.01 μM P7C3 as described above, and allowed to develop to 7 dpf.

Discussion and Conclusions

Summary

We found that *gdf6a*$^{-/-}$ mutant larvae have microphthalmia, but relatively normal retinal lamination (Figure 3.1). The mutants display aberrant retinal apoptosis at a time at which the retinal progenitor cells are differentiating, with the maximal level of apoptosis occurring at 28 hpf (Figure 3.2). This aberrant apoptosis is rescued by treatment with the anti-apoptotic compound P7C3 (Figure 3.3). Rescuing retinal apoptosis in the *gdf6a*$^{-/-}$ mutant retina did not rescue the microphthalmic phenotype in the larvae (Figure 3.4). P7C3-treatment partially recovered a RGC-mediated neuroendocrine response (Figure 3.5), but these larvae did not regain higher-level visual processing (Figure 3.6).

gdf6a$^{-/-}$ mutants display increased retinal apoptosis.

Our study shows a novel, early-onset role for *gdf6a* in regulating retinal degeneration in disease development. *gdf6a*$^{-/-}$ mutants display an early peak of apoptosis that is rescued by pharmaceutical treatment with the anti-apoptotic compound P7C3 (Figure 3.3). This finding may lead to new treatment strategies for patients with retinal degenerative disorders, such a LCA. While the timing of the retinal cell loss in zebrafish *gdf6a*$^{-/-}$ mutants does not match that of human patient retinal degeneration (pre- vs. post-natal), the apoptotic defect in the zebrafish mutants is still of interest because retinal apoptosis has been shown to be a major contributor

to other degenerative blinding disorders (French et al., 2013; Garcia-Valenzuela et al., 1995; Genini et al., 2013; Portera-Cailliau et al., 1994; Sancho-Pelluz et al., 2008). Additionally, previous studies of zebrafish retinal dystrophy models (including models for retinitis pigmentosa, cone-rod dystrophy and achromatopsia) have also revealed the presence of ectopic apoptosis, but these studies looked at apoptosis during later development, from 48 hpf – 7 dpf (Daly and Sandell, 2000; Riera et al., 2013; Shu et al., 2011; Viringipurampeer et al., 2014). These retinal dystrophy models display a late-onset increase in apoptosis, consistent with retinal degeneration disorders in humans. Because of the early-onset timing of apoptosis in the $gdf6a^{-/-}$ mutants, we predict that $gdf6a$ is playing an early-onset role in the development of retinal dystrophies.

The molecular mechanisms that regulate retinal apoptosis in $gdf6a^{-/-}$ mutant embryos have begun to be elucidated. The p38 MAPK pathway can be induced by cellular stress and by non-canonical BMP-signaling via the activation of TGFβ-activated kinase 1 (Tak1; Miyazono et al., 2010). A Tak1-independent intrinsic apoptotic program is induced in the $gdf6a^{-/-}$ mutants via p38 MAPK activation, indicating a role for Gdf6a in mediating the regulation of the intrinsic apoptotic pathway (Pant et al., 2013).

Functional roles for P7C3 in regulating apoptosis

P7C3 is an aminopropyl carbazole that was discovered using an *in-vivo* screen in living mice. Mice deficient in the neuronal PAS domain protein 3 (Npas3) lack hippocampal neurogenesis and have increased levels of hippocampal apoptosis. Administration of P7C3 to $npas3^{-/-}$ mice normalized the levels of apoptosis and increased neurogenesis in the hippocampus (Pieper et al., 2010). P7C3, or structural variants of P7C3, have also been observed to protect dopaminergic neuron cell death in a

Parkinson's disease murine model (De Jesus-Cortes et al., 2012), protect spinal cord neurons from death in an amyotropic lateral sclerosis murine model (Tesla et al., 2012) and facilitate neural recovery after traumatic brain injury in mice (Blaya et al., 2014). The determination of how this biologically active molecule functions molecularly may reveal previously unknown proteins or biochemical pathways that are relevant to disease (Pieper et al., 2014).

Since P7C3 prevents cell death in multiple different disease settings, it is likely acting at a late and common stage of the apoptotic program. One such stage is the depolarization and permeabilization of the mitochondrial outer membrane followed by the release of Cytochrome c. Several piperazines, with similar structural characteristics as P7C3, inhibit the release of Cytochrome c by inhibiting the formation of the mitochondrial apoptosis-induced channel (Bombrun et al., 2003; Peixoto et al., 2009). While a specific binding partner for the piperazines was not identified, it was hypothesized that they inhibit channel formation by inhibiting the ability of the pro-apoptotic Bax protein to form these channels (Pieper et al., 2014).

A synthetic chemistry approach to discover the binding partner for P7C3 concluded that the P7C3 class of chemicals most likely interacts with a specific biological molecule instead of acting within a cell membrane or as a general antioxidant (Pieper et al., 2014). Additionally, the authors concluded that some regions of the P7C3 molecule could tolerate substitution without reducing biological activity (Pieper et al., 2014). This allows the potential for the addition of a biotin moiety to use with affinity chromatography, and could help to identify the P7C3 receptor.

gdf6a$^{-/-}$ mutants have microphthalmia that is not caused by ectopic retinal apoptosis.

Mutations in the BMP ligand *GDF6* have been observed in human patients that present with congenital blindness and retinal degeneration due to MAC and LCA (Asai-Coakwell et al., 2009; Asai-Coakwell et al., 2013). Zebrafish *gdf6a$^{-/-}$* mutants have microphthalmia, colobomata and dysmorphic photoreceptors, but interestingly the overall retinal lamination is relatively normal (Figure 3.1). Some of these phenotypes reflect those presented by MAC patients (microphthalmia, colobomata). The zebrafish neural retina is formed as retinal progenitor cells differentiate into different types of retinal neurons and exit the cell cycle. Eye-size determination is dependent on the precise control of progenitor cell proliferation and survival. Throughout the zebrafish lifecycle a population of self-renewing cells remains as the CMZ, allowing new neurons to be added to the eye their entire lives (Raymond et al., 2006). *gdf6a$^{-/-}$* mutants display increased retinal cell death during retinal cell differentiation (Figure 3.2). While the apoptotic phenotype of *gdf6a$^{-/-}$* mutants can be rescued with pharmaceutical treatment, the microphthalmic phenotype cannot (Figures 3.3 and 3.4). These data indicate that *gdf6a$^{-/-}$*-induced microphthalmia is not a result of the inability of differentiating cells to survive.

Our results are consistent with previous studies that indicate that the microphthalmic phenotype is more likely due to dysregulation of retinal progenitor cell number and proliferation (French et al., 2013). In these studies, *gdf6a$^{-/-}$* mutants display reduced number of retinal progenitor cells at 24 hpf, but normal proliferation. At 48 hpf there is reduced expression of cell-cycle regulators (*myca, mycb, mcm3, pcna* and others*)* and a reduced number of proliferating cells in the inner neural layers (48 hpf) and CMZ (96 hpf) which is attributed to the dysregulation of the forkhead box

transcription factors *foxi1* and *foxi2* in the CMZ (French et al., 2013). This suggests that regulation of retinal progenitor cell number and proliferation of retinal progenitor cells, in combination with the apoptotic defect, could be the underlying cause of microphthalmia in these mutants. P7C3 may have been able to rescue the ectopic apoptotis, but not the retinal progenitor cell number or proliferation, resulting in the continued small eye phenotype. To verify this, the effect of P7C3 on the retinal progenitor cell number and the regulation of proliferation in $gdf6a^{-/-}$ mutants should be performed.

Zebrafish have endogenous apoptosis during normal retinal development.

Biehlmaier and colleagues discovered that during normal zebrafish development there are waves of apoptosis, reminiscent of the waves of retinal development (2001). These apoptotic waves occur first in the GCL at 72 hpf, followed by a peak in the INL at 96 hpf and a late-onset wave of apoptosis in the ONL that peaks at 7 dpf (Biehlmaier et al., 2001). These waves of apoptosis align somewhat to the maturation stages of retinal cell differentiation. For example, the first retinal RGCs are observed in the GCL at 28 hpf (Easter and Nicola, 1996), they begin to mature and form axonal projections at 48 hpf (Burrill and Easter, 1994). The first wave of apoptosis does not occur until 72 hpf (the time at which the RGCs begin innervating their targets in the tectum), suggesting that the wave of apoptosis functions as a fine-tuning mechanism that occurs after the mitotic waves of development, but in the same order (Biehlmaier et al., 2001). Similarly, cone photoreceptors are born from 48 – 72 hpf (Hu and Easter, 1999), with outer segments first observed at 55 hpf (Schmitt and Dowling, 1999) and functional synapses first observed at 65 hpf (Gestri et al., 2012). The second wave of apoptosis does not peak in the ONL until 7 dpf (Biehlmaier et al.,

2001). An important thing to note about the Biehlmaier study is that they did not look for apoptosis any stage earlier than 48 hpf. It would be interesting to investigate the levels of apoptosis in recently differentiated retinal cells shortly after they are born. Our data suggests that low levels of apoptosis are observed in wild-type retinas from 24 – 32 hpf, the time in which the RGCs are differentiating. Perhaps this indicates an even earlier, first round of apoptosis that helps fine-tune the retina very shortly after neuronal cells are born. This investigation would require a more detailed look at the retina at these times.

P7C3 treatment partially rescues vision in gdf6a$^{-/-}$ mutants.

P7C3-treated mutant embryos display a partial VBA response, indicative of restored visual function (Figure 3.5). Directly contradicting this result is that fact that P7C3-treatment does not rescue OMR response (Figure 3.6). The difference between these results might be explained by the differences in the visual assays performed. VBA is a retinal ganglion cell-meditated neuroendocrine response in which melanophores adjust their melanosome distribution according to ambient background light detection (Fleisch and Neuhauss, 2006; Muto et al., 2005). OMR requires a higher level of visual sensitivity and the coordinated efforts of both the visual and musculo-skeletal systems (Asai-Coakwell et al., 2013; Orger et al., 2004). Visual mutants have been identified in previous studies with functional VBA and impaired OMR, indicating that the assays analyze two separate processes (Muto et al., 2005). OMR is mediated by red/green double cones at 7 dpf, the stage at which we were testing vision (Orger and Baier, 2005). The differences in required cell-type alone could explain the behavioural differences we observe (RGC [VBA] vs. cone photoreceptor [OMR]). Indeed, by 2-weeks of age the *gdf6a$^{-/-}$* mutants display dysmorphic double cones

which may not be rescued by P7C3-treatment as indicated by the maintained microphthalmic phenotype (this remains to be tested). In addition to the differences in cell-type required, OMR also requires higher-level processing to be elicited. This includes the ability of the sensory neurons to relay the message to the brain, and from the brain to the motor neurons in the body. Firstly, *gdf6a$^{-/-}$* mutants have lenticular and skeletal defects that may impede the ability to respond to visual stimuli, even if the brain has the ability to receive the visual signal (Asai-Coakwell et al., 2009; French et al., 2009). Secondly, small groups of 12 cells that are located on either side of the hindbrain are required to link the sensory neuron processing in the brain to a motor output in OMR (Orger et al., 2008). These processing neurons have not been analyzed in *gdf6a$^{-/-}$* mutants, but the retino-tectal mapping of the optic nerve to the optic tectum of the brain is defective (Gosse and Baier, 2009).

It is important to note that the visual behavior we have documented on non-treated *gdf6a$^{-/-}$* mutants does not match that observed in the original forward genetic screen that discovered the *gdf6a* mutants (Muto et al., 2005). In this study, mutants were identified by analyzing different visual behaviours, including VBA and OMR. On a scale of 0 – 1 (with 1 = wild-type response) the *gdf6a$^{-/-}$* mutants scored 0.7 for VBA and 0.8 for OMR, indicating a milder, close to wild-type response (Muto et al., 2005). These differences could be attributed to the way the visual assays were utilized. Muto and colleagues investigated the ability of visually impaired mutants to respond to long-term light adaptation (2005). They allowed larvae to light-adapt for 20+ minutes before scoring for a VBA response. We analyzed a short-term response to light adaptation, giving the larvae 5 minutes to adapt before scoring for VBA. We found that 5 minutes was enough time to get a wild-type response (contraction of melanophores) in the control larvae. This could indicate that the neuroendocrine response in

gdf6a^{-/-} mutants is slower to respond. Additionally, Muto *et al.* analyzed OMR using pools of 25 – 40 larvae at once, and it was used as a method of detecting mutants in a group of F2 family clutches (2005). We used individual embryos and manually recorded the distance travelled per larvae. Previous studies have found that OMR is better suited for sorting mutant larvae from a population, as opposed to measuring vision with the specificity we were trying to achieve (Muto et al., 2005). The optokinetic response (OKR) would better suit our needs. This assay measures the tracking eye movements of individual embryos elicited by surrounding motion (Fleisch and Neuhauss, 2006), and this assay can be adapted to quantitatively measure visual performance (Muto et al., 2005; Rinner et al., 2005).

Previously, phenotypes due to mutations in BMP ligands have been predominantly restricted to large morphological changes in eye size and morphogenesis (Asai-Coakwell et al., 2009; Ye et al., 2010; Zhang et al., 2009). This study sheds light on alternative roles of BMP ligands in retinal dystrophies as well as MAC. Furthermore, it implicates for the first time the role of a growth factor in the development of LCA, a disease that has been historically characterized by defects in photoreceptor-specific genes (den Hollander et al., 2008).

Chapter 4

Studies of *crx*-dependent photoreceptor differentiation in zebrafish

Introduction

      All neuronal retinal cells are derived from a population of common multi-potent retinal progenitor cells. The vertebrate retina is a highly organized laminar tissue that contains seven cell types (six neuronal and one glial cell) that are born in a stereotypical order conserved throughout vertebrates. Photoreceptors in the retina are central in our ability to convert light into the neural messages that result in a visual experience. The specification of cell type from a multi-potent progenitor depends on intrinsic genetic programs and the expression of specific combinations of transcription factors. *Cone-rod homeobox (Crx)* is a member of the highly conserved *orthodenticle*-related (*otx*) gene family of paired-class homeobox proteins that bind DNA and function as transcription factors (Furukawa et al., 1997). *Crx* is the earliest expressed photoreceptor marker in the retina, expressed in newly differentiated photoreceptors of mice (Furukawa et al., 1997). Interestingly, *crx* mRNA is first observed at 24 hpf in the zebrafish retina in a few cells in the ventronasal region, before the development of photoreceptors. These cells are still thought to be mitotically active, multi-potent retinal progenitors (Liu et al., 2001). The first post-mitotic differentiated retinal neurons, the retinal ganglion cells, appear a few hours later. The first photoreceptors are not post-mitotic until 48 hpf (Hu and Easter, 1999). The differences in timing of expression between mammalian and teleost models suggest that zebrafish *crx* may have additional roles not present in the mammalian orthologue. Mammalian and teleost *crx* is also expressed in the pineal gland and plays roles in circadian entrainment in mice (Furukawa et al., 1999; Liu et al., 2001).

      The absence of functional Crx protein in $Crx^{-/-}$ knockout mice results in photoreceptors that initially develop, but lack an outer segment, resulting in defective phototransduction and a non-responsive ERG. These

photoreceptors eventually degenerate later in life (Furukawa et al., 1999). Crx-deficient mice also display perturbed synaptogenesis in the outer plexiform layer, providing further evidence of the essential role *Crx* plays in photoreceptor development (Morrow et al., 2005). Knocking-down the translation of Crx protein in zebrafish using morpholino technology results in ectopic retinal apoptosis, delayed cell-cycle withdrawal and reduced photoreceptor gene expression (Shen and Raymond, 2004). These data suggest a role for *crx* in promoting photoreceptor cell fate during retinal development.

The mammalian photoreceptor lineage is specified by expression of the *Otx*-family gene *Otx2* in retinal progenitor cells (Swaroop et al., 2010). Otx2 promotes the transcription of *Crx* in early post-mitotic photoreceptor precursors (Koike et al., 2007; Nishida et al., 2003) and directly activates *Nrl* expression, promoting a rod-photoreceptor cell fate (Roger et al., 2014). Crx protein binds to the promoters of several rod and cone photoreceptor-specific genes to promote photoreceptor cell fate (Chen et al., 1997; Furukawa et al., 1997; Mitton et al., 2000). Crx alone has only moderate transcriptional activity, and often interacts synergistically with a transcriptional regulator. One such protein is the basic leucine zipper transcription factor Nrl (neural leucine zipper; Mitton et al., 2000). Crx is also thought to activate transcription by promoting chromatin remodeling by the recruitment of co-activators with histone-acetyl-transferase activity to its target genes. This chromatin remodeling allows binding of additional transcription factors (such as Nrl) and RNA Polymerase II (Peng and Chen, 2007).

In humans, patients with photoreceptor degeneration disorders such as Leber's congenital amaurosis (LCA), retinitis pigmentosa and cone-rod dystrophy experience ongoing sight deterioration, usually resulting in

blindness. LCA is the most severe form of congenital blindness, usually diagnosed shortly after birth, and accounts for >5% of all inherited retinopathies (Perrault et al., 1999). Mutations in *CRX* have been identified in a number of de-novo (autosomal dominant) and inherited (autosomal recessive) forms of LCA (Freund et al., 1998; Silva et al., 2000; Sohocki et al., 1998; Swaroop et al., 1999). Our goal was to create a zebrafish model of photoreceptor degeneration and to use this photoreceptor-less zebrafish model to study the development retinal degeneration diseases such as LCA, as well as to identify novel components of the transcriptional networks that give photoreceptors their identity.

Results

Identification of a ZFN-generated crx mutant.

To analyze the role of *crx* in photoreceptor development and the progression of retinopathies such as LCA, a *crx* mutant was created. Zinc finger nucleases (ZFNs) are synthetic target endonucleases that selectively bind and cleave specific gene sequences. Repair of this lesion by non-homologous end joining can result in insertions or deletions at the ZFN target site (Porteus and Carroll, 2005). A ZFN was designed to target the early part of the first exon of the zebrafish *crx* gene (Figure 4.1). The *Sharkey* FokI nuclease domain variant was used to enhance catalytic activity. This variant increased in-vivo cutting of the *crx* ZFN 26-fold (Pillay et al., 2013). *Sharkey* ZFN mRNA was injected into wild-type (AB) embryos and raised to adulthood (P_0). To identify carriers of germline mutations, the P_0 fish were incrossed and the offspring were screened for mutations in *crx*. The carriers were outcrossed to AB fish and the offspring were raised to adulthood (F_1). F_1 fish were screened for somatic mutations by genomic DNA extraction (from fin clips), PCR-amplification and high-resolution melt-curve analysis

GATTAGCTGCTCGGTCTCTTATTGCTCATAGTGTCCCGCT
CCTGTCCGGTCTTACCCAAGGGACACGCGCCTTTACCAAC
GCCAAAACTCTTGACCAAGAGCCAGCAACTTTTGTGCATA
TAGACATTTATTTGTTCTTTAACTCACATTAAGGGTCTAT
TATTGGATATTTAGAGCGATAGTAATGGTAGATTGGTAGT
TAAACTTGGGCAAAAGTGTAAGCTTATTGAAGACAGCGAG
TAGCGCGCGCGCGAGCATCTACAGGTGTTTGAGGAGCACA
GACACGCGCCAGGCGCGAGCACAGACACGCGACCCCCGAC
CCGTAAAACAGCGTCGCAGAGAAAAAGAGAGTGAGAGAG
GGGTGAGAGAGGGAGGGAGAGAGAGAGCAATAGAGAGAGT
GTGCGAGAGACGCG<mark>GCCGTCCCAAGA**ATG**ATGTC</mark>CTACAT
AAAGCA<mark>GCCCCATTA**TGCTGT**GAACGGGTT</mark>AACACTGTCC
GCCTCA<mark>GGAATGGACCTGCTCCACAC</mark>CGCCGTCGGCTACC
CAG

Figure 4.1: The *crx* ZFN binds DNA early in exon 1, after the start codon. The sequence of the first exon of the *crx* gene with important features highlighted. [ZFN binding site (blue); ZFN spacer region (bold); *crx* HRM primers (yellow); ATG start codon (green)].

(HRMA). 6/111 (5.4%) of the screened F$_1$ fish had variations identified by HRMA. Two individuals had a 2 bp deletion and two individuals had a 4 bp insertion at the ZFN target site. Both resulted in a frameshift mutation that would produce a protein with 11 amino acids of normal sequence followed by 74 amino acids of scrambled sequence and a premature stop codon. The F$_1$ screen also identified 2 fish with a 7 bp deletion that occurs at position 28 of the coding sequence (Figure 4.2 A-B). This results in a premature stop codon at the position of the deletion, and truncation of the protein 10 amino acids into the protein sequence (Figure 4.2 C). This mutation was predicted to be a strong hypomorph because the premature stop codon occurs before any known conserved functional domains (Figure 4.2 C). For these reasons we chose to do future studies on the 7 bp deletion allele, which was designated *crx*^{ua1005} (hereafter referred to as *crx*$^{-/-}$).

Because preliminary analysis of this mutant allele revealed an outwardly wild-type phenotype, we verified that the ua1005 allele was transmitted through the germline of the F$_1$ founders and was not simply found in somatic tissue. We outcrossed individual F$_1$ *crx*$^{+/-}$ heterozygotes to AB fish and genotyped the individual offspring from the cross. If the mutation was passed through the germline of these founders, a 50:50 ratio of heterozygous:wild-type offspring would be expected. 43% (13/30) of the offspring were heterozygous for the ua1005 allele and 57% (17/30) were wild-type. We concluded that the allele is transmissible through the F$_1$ founder germline.

crx$^{-/-}$ *mutants have normal retinal morphology and crx target gene expression.*

crx mRNA is normally expressed in the ONL, the bipolar cells in the outer part of the INL of the retina (Figure 4.3 A) and the pineal gland. Crx

88
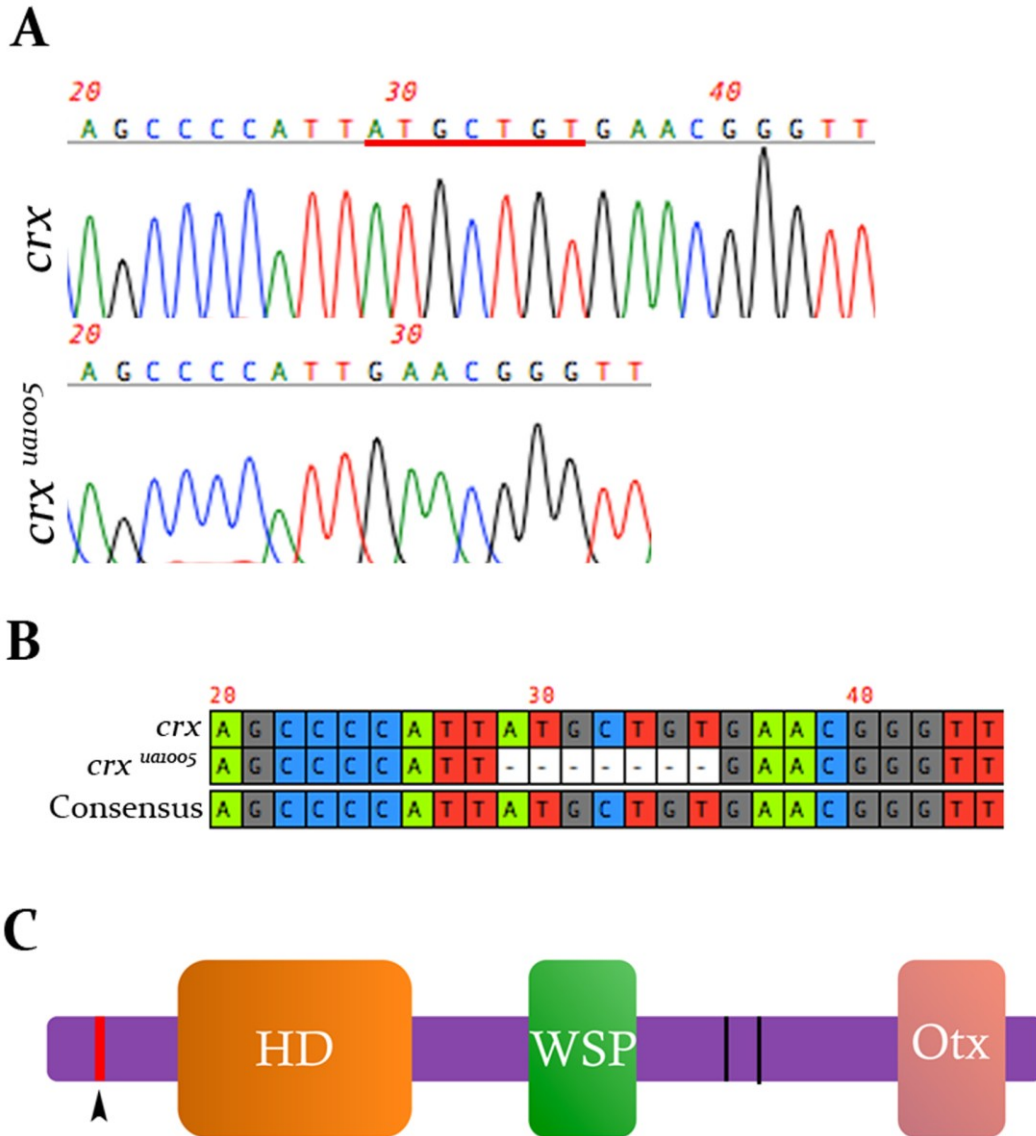
Figure 4.2: Identification of a ZFN-generated mutation in the *crx* gene. (A) Sequencing chromatograms of wild-type (*crx*) and mutant (*crx^ua1005^*) alleles (deletion underlined in red). (B) The ua1005 allele has a 7 bp deletion at position 28 of the coding sequence. This results in a premature stop codon (red) at the position of the deletion, 10 amino acids into the protein (C; arrowhead). (C) Diagram of the Crx protein with known conserved and functional domains indicated [homeodomain (HD); *wolbachia* surface protein motif (WSP); Otx-tail (Otx); transcriptional transactivation domains (black)].
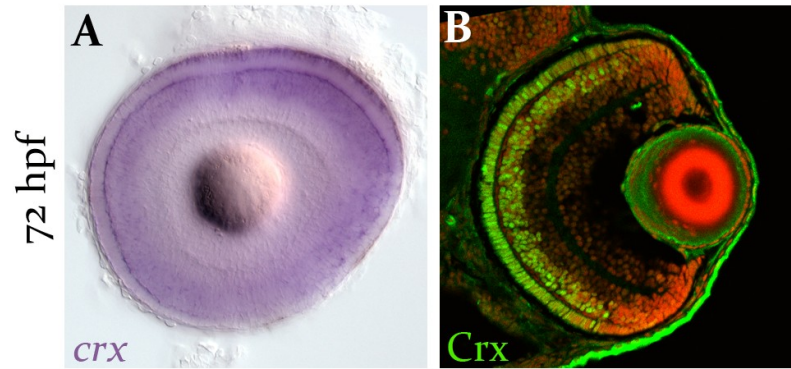
Figure 4.3: Expression pattern of *crx* mRNA and localization of Crx protein. (A) *crx* mRNA is expressed in the ONL and the outer part of the INL of the retina. (B) Crx protein localizes to the same regions as the mRNA is expressed.

protein is localized to the same areas as its transcription (Figure 4.3 B). We wanted to analyze the retinal and photoreceptor integrity of the $crx^{-/-}$ mutants to see if the phenotypes recapitulate those previously observed in mouse models of LCA and human LCA patients. Contrary to our prediction that the $crx^{-/-}$ mutant would be a strong hypomorph, the $crx^{-/-}$ mutants displayed no outward phenotypes expected of a *crx* mutant and appeared overtly normal. Additionally, these mutants were viable and fertile. Phalloidin staining revealed that the overall retinal lamination was normal in the mutants at 4 dpf (Figure 4.4 A-B). $crx^{-/-}$ mutants that carry a transgene [*Tg(-5.5opsin1sw1:EGFP)*], which fluorescently labels UV cones with GFP, display normal cone organization at 4 dpf (Figure 4.4 C-D). To see if there may be a later-onset phenotype such as those observed in mouse $Crx^{-/-}$ mutants, we analyzed the retina at 4 weeks of age. Immunofluorescence for Arrestin3a reveals normal red/green cone morphology in the $crx^{-/-}$ mutants (Figure 4.4 E-F).

To test if the mutant Crx protein is able to promote transcription of target genes in the retina, we performed whole-mount in-situ hybridizations for known *crx*-dependent gene transcripts. Expression of *rho* (rod opsin), *opn1mw1* (green opsin), *opn1sw1* (UV opsin) and *opn2sw2* (blue opsin) mRNA in $crx^{-/-}$ mutant retinas is comparable to wild-type (Figure 4.5). This suggests that $crx^{-/-}$ mutants are still able to regulate these transcripts, either by compensatory changes in the mutant fish or through the function of the truncated Crx protein.

During normal retinal development, Crx protein interacts with the orphan nuclear receptor Nr2e3 and the neural leucine zipper transcription factor Nrl to facilitate target gene expression and promote rod photoreceptor cell identity (Peng et al., 2005). The mRNA expression of *nrl* and *nr2e3* in $crx^{-/-}$ mutants is comparable to wild-type at 52 hpf and 4 dpf
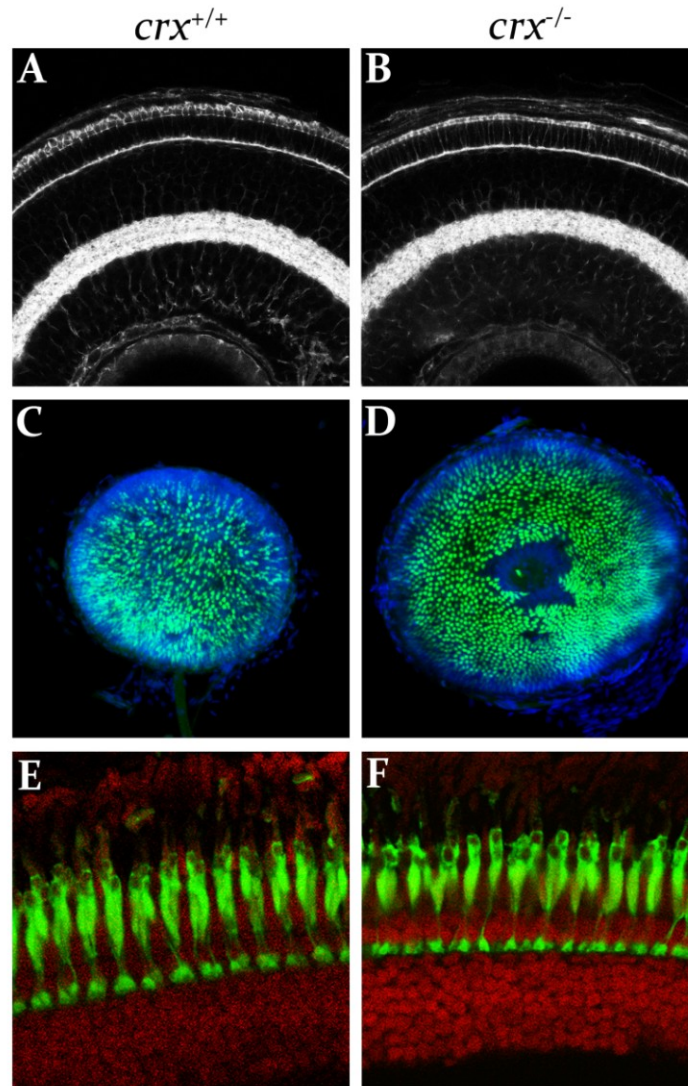
Figure 4.4: Homozygous *crx*$^{-/-}$ mutants have normal retinal histology. (A-B) Whole-mount 4 dpf retinas labeled with phalloidin reveal normal retinal lamination in *crx*$^{-/-}$ mutants. (C-D) Whole-mount 4 dpf retinas from a *Tg(-5.5opn1sw1:EGFP)* line that has GFP-labeled UV-cones (green) counter-stained with To-Pro3 (blue) show a normal UV-cone array in *crx*$^{-/-}$ mutants. The area of cone absence in the *crx*$^{-/-}$ (D) is due to a tear in the retina as a result of whole-mounting. (E-F) Sections through 4-week-old retinas immunolabeled for Arrestin3a, which labels red/green double cones (green) counter-stained with propidium iodide (red) show normal morphology of mature cones in *crx*$^{-/-}$ mutants.
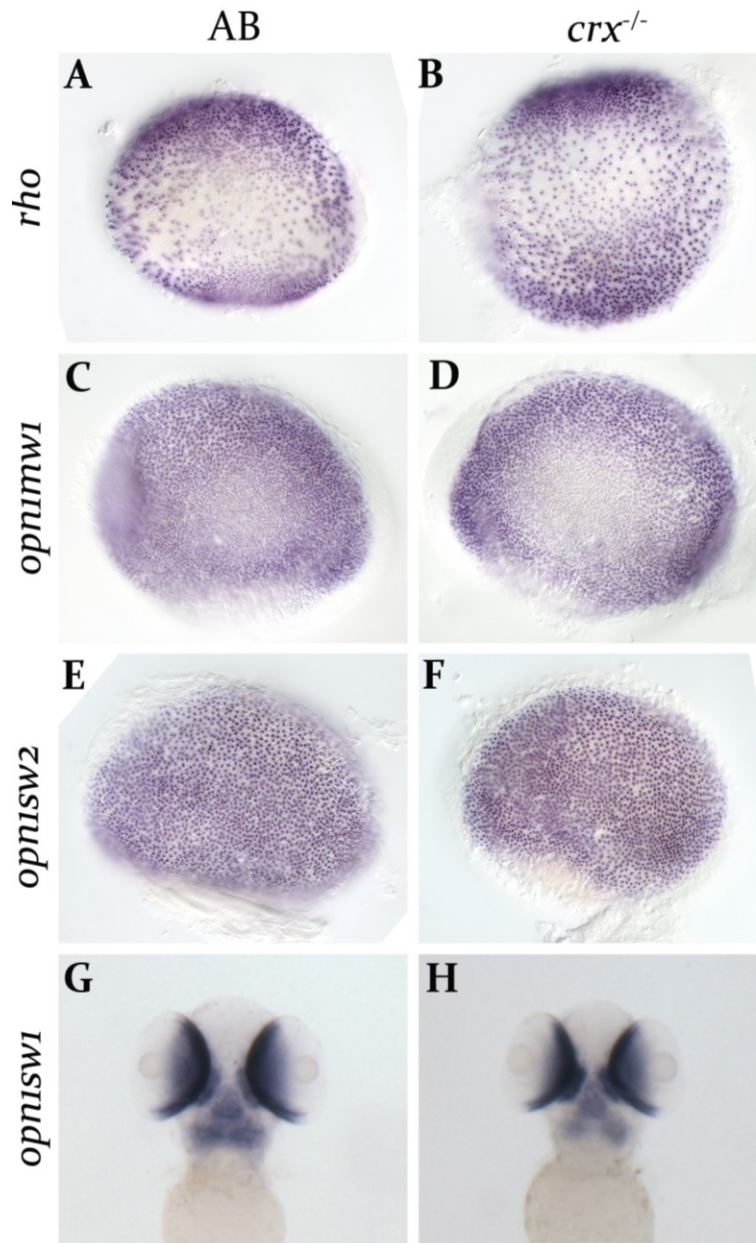
Figure 4.5: *crx*^{-/-} mutants have normal levels of target-gene expression in the retina. Whole-mount in situ hybridizations for *rho* (A-B, rod), *opn1mw1* (C-D, green cone), *opn1sw2* (E-F, blue cone) and *opn1sw1* (G-H, UV cone) transcripts. *crx*^{-/-} mutants have levels of opsin gene transcription that are comparable to wild-type (AB). [Whole-mount retina 4 dpf (A-F); ventral view 3 dpf larvae (G-H)].
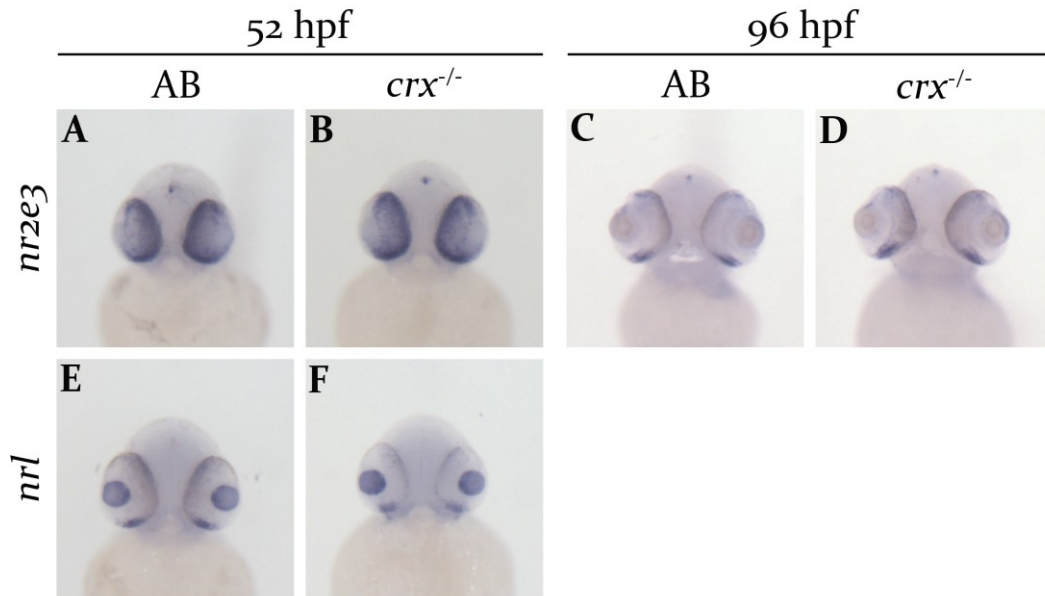
Figure 4.6: Expression of retinal transcription factors that interact with Crx is unchanged in *crx*^(-/-) mutants. Expression of *nr2e3* mRNA at 52 hpf (A-B) and 4 dpf (C-D) is unchanged in *crx*^(-/-) mutants. (E-F) Expression of *nrl* mRNA at 52 hpf is unchanged in *crx*^(-/-) mutants at 52 hpf.

(Figure 4.6). This suggests that a compensatory up-regulation of these genes does not explain the wild-type expression of Crx target genes in the $crx^{-/-}$ mutants.

An alternative, in-frame start codon could produce a functional Crx protein.

Since $crx^{-/-}$ mutants do not have nonsense-mediated decay, we wondered if there was any Crx protein being translated in the $crx^{-/-}$ mutants. We used an antibody that targets the C-terminal domain of the protein (Figure 4.10; Shen and Raymond, 2004) and found that Crx protein is translated in $crx^{-/-}$ mutants in the ONL and the outer part of the INL in the bipolar cells (Figure 4.7). An analysis of the DNA sequence led us to an explanation for this unexpected result. We found a second, in-frame start codon that occurs after the 7 bp deletion in the $crx^{-/-}$ mutant, but before any known functional domain. This start codon occurs at position 64 of the coding sequence of *crx* (Figure 4.8 A). The resulting protein would lack the N-terminal domain, but all known functional domains would be intact (Figure 4.8 B). Since the C-terminal domain of this alternative Crx protein would be intact, it is reasonable to assume that the Crx antibody can bind to Crx protein that results from the endogenous start codon as well as the alternative start codon in the mutants. There are 4 additional in-frame start codons located in the *crx* transcript after the 7 bp deletion, but these are all located within or after the known functional domains of *crx* (Figure 4.8 A, bold).

We hypothesized that the alternative Crx protein may be functional, and this is why we see no retinal phenotype in the $crx^{-/-}$ mutants. To test this hypothesis, we used a morpholino oligonucleotide (MO) that blocks translation from the alternative start codon in the *crx* transcript (*crx* alt
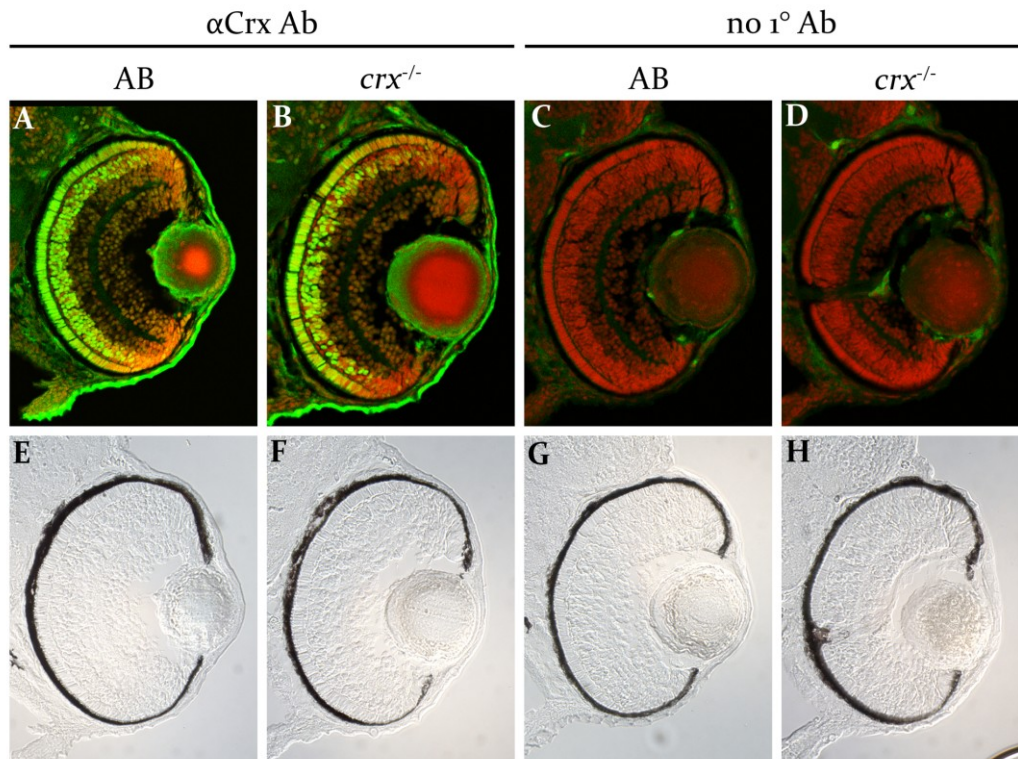
Figure 4.7: Crx protein is translated in *crx*$^{-/-}$ mutants at 3 dpf. (A-D) Immunofluorescence for Crx using Crx primary antibody (A, B) or no primary antibody (green; C, D), counterstained with ToPro3 (red). Crx protein levels in *crx*$^{-/-}$ mutants are comparable to wild-type. (E-F) Brightfield images of the corresponding immunofluorescence image show the structural integrity of the retina sections.

A

```
ATG ATG TCC TAC ATA AAG CAG CCC CAT TAT GCT GTG AAC GGG TTA
ACA CTG TCC GCC TCA GGA ATG GAC CTG CTC CAC ACC GCC GTC GGC
TAC CCA GCC ACT CCG AGG AAG CAG CGT CGA GAG CGC ACC ACC TTC
ACT CGC ACC CAG CTG GAC ATT CTG GAA GCT TTG TTC ACC AAA ACA
CGC TAT CCA GAC ATA TTT ATG AGA GAA GAG GTA GCT CTG AAA ATC
AAC CTT CCC GAG TCC AGA GTT CAG GTG TGG TTT AAG AAC CGT CGT
GCT AAA TGC CGC CAG CAG CAG CAG CAG ACC AGC GGT CAG CCC AAG
CCC CGT CCC CCC AAA AAG AAG TCC TCC CCT CCC CCT GAT CTG ACC
TCT GAC CCT GGC ACT AGC TCC TCG GTG GTG GCT GCC CCG ACC CCG
ACC GTG CCC CCT AGT GTG AGC GCA GGC ACA GCA CCA GTT TCT GTA
TGG AGT CCC ACT TCT CTT TCC CCC CTC CCT GAT CCA CTG TGT GGT
TCA GGC ACC CCC TGC GTG CAG CGT CCT GCT CCA TAT CCC ATG AGC
TAC GGT CAG CCC TCT TCC TAC AGC CAG GGC TAT GGC TCT TCT CCT
TAC TTC AGC GGA TTG GAT TGC AGC CCG TAC CTT TCT CCC ATG ACC
ACC CAG CTG TCA GCA AGT GGA GGC GCC CTC TCC CCC CTC ACC GTG
CCC TCC ATG GGC GGC TCG CTC AGC CAG TCG CCC TCT CTC TCC TCC
CAG GGA TAC AGC ACT GCG TCG TTG GGC TTC AGT TCG GTA GAC TGC
CTT GAC TAC AAG GAC CAG CAG GCC TGG AAG CTC AAC TTC AGC ACT
GTG GAC TGC CTC GAC CAC AAA TTC CAG GTG CTG TAG
```

B
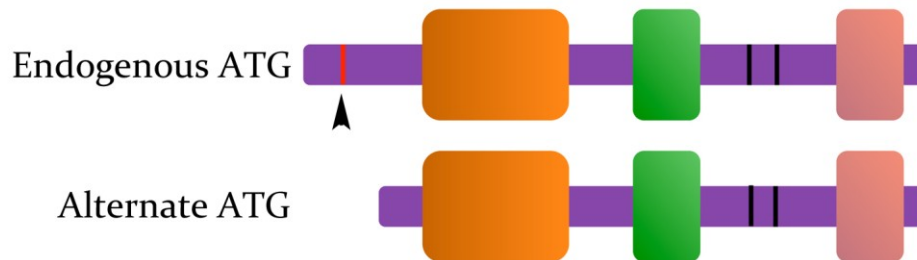
Figure 4.8: An alternate, in-frame start codon in the *crx*^{−/−} transcript may result in a functional protein. (A) The *crx* transcript has an in-frame start codon that occurs after the pre-mature mutant stop codon and before any known functional domains [start codon (green); stop codon (red); 7 bp deletion (grey); homeodomain (yellow); *crx* alt ATG MO binding site (underlined)]. (B) Diagram of the Crx proteins that would result in translation from the endogenous or alternate start codon [homeodomain (orange); WSP motif (green); transcriptional transactivation domains (black); Otx tail (pink)].

ATG MO; Figure 4.8 A). The MO was injected into transgenic animals that have GFP-labeled UV cones [*Tg(-5.5opsin1sw1:EGFP)*] that were either homozygous for the mutant *crx* allele or wild-type. The UV cones in *crx*^{-/-} mutants (Figure 4.9 F-J) remain comparable to wild-type (Figure 4.9 A-E) when injected with 1 – 10 ng of MO. Although this is negative data and we cannot be sure that this morpholino is effective, these results suggest that the alternative Crx protein may be non-functional. If the alternative Crx protein were compensating for the loss of wild-type Crx protein in *crx*^{-/-} mutants you would expect a phenotype to be revealed in the MO-injected *crx*^{-/-} mutants because these embryos would have no Crx protein translated.

otx5, an otx-family paralog of crx, may compensate in the crx^{-/-} *mutant retinas.*

As mentioned above, *crx* is a member of the conserved *otx*-family of genes (Chen et al., 1997; Furukawa et al., 1997). It has evolutionarily conserved function to the *Drosophila* gene *orthodenticle* (*otd*), which is required for brain and photoreceptor neuron development (Ranade et al., 2008). Due to a whole-genome duplication event that occurred in the teleost lineage approximately 270 million years ago (Postlethwait et al., 1998), zebrafish have, in many cases, two copies of genes present as single copies in mammalian genomes. The zebrafish genome contains five *otx*-family genes: *otx1a, otx1b, otx2, otx5* and *crx*. Amino acid alignment of these five proteins, along with the *Drosophila melanogaster* Otd, was performed and these proteins display a high degree of sequence similarity in the conserved functional domains (homeodomain, WSP motif, Crx transcriptional transactivation domains, and the Otx-tail; Figure 4.10). Since the known functional domains are so highly conserved, we hypothesized
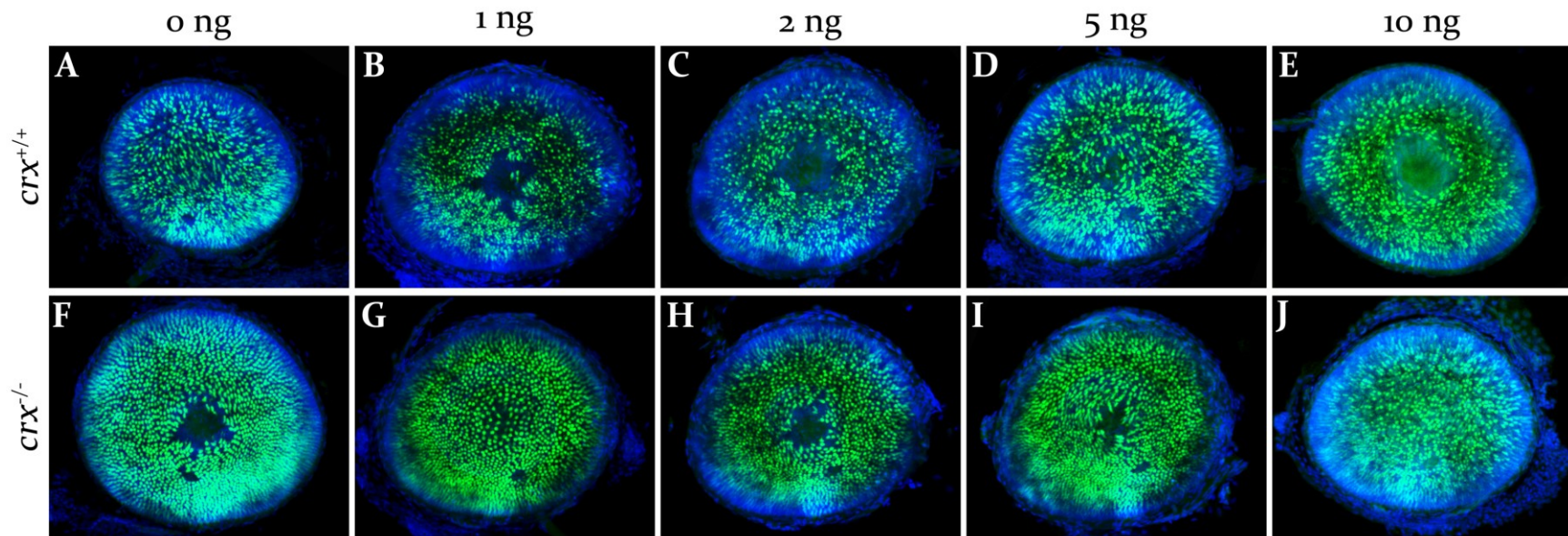
Figure 4.9: Blocking translation from the putative alternate start codon does not reveal a phenotype in *crx*$^{-/-}$ mutants. 1-10 ng of translation-blocking MO against the alternative start codon was injected into *Tg(-5.5opn1sw1:EGFP)* transgenic embryos that are homozygous for the ua1005 *crx* allele (F-J) or homozygous for the wild-type *crx* allele (A-E). Even with large doses of MO, UV-cones retain their integrity. Areas of cone absence are due to tears in the retina from the mounting process. UV-cones (green); ToPro3 (blue).

Multiple sequence alignment of otd, otx1a, otx1b, otx2, otx5, and crx.

Positions 1–60

```
otd    MAAGFLKSGDLGPHPHSYGGPHPHHSVPHGPLPPGMPMPSLGPFGLPHGLEAVGFSQGMW
otx1a  -MMSYLK---------------QAPYAM-NGLGLGGATMDLLHP-------SVGYP----
otx1b  -MMSYLK---------------QPPYAM-NGLGLSGAAMDLLHP-------SVGYP----
otx2   -MMSYLK---------------QPPYTV-NGLSLTTSGMDLLHP-------SVGYP----
otx5   -MMSYMK---------------QPHYSV-NGLTLSGTGMDLLHS-------AVGYP----
crx    -MMSYIK---------------QPHYAV-NGLTLSASGMDLLHT-------AVGYP----
       MMSYLKSGDLGPHPHSYGGPQP Y VPNGL.L.G MDLLHPFGLPHGLE VGYPQGMW
```

Positions 70–120

```
otd    GDLCYPGVNTRKQRRERTTFTRAQLDVLEALFGKTRYPDIFMREEVALKINLPESRVQVW
otx1a  ------TNPRKQRRERTTFTRTQLDILESLFAKTRYPDIFMREEVALKINLPESRVQVW
otx1b  ------ATPRKQRRERTTFTRSQLDILEALFAKTRYPDIFMREEVALKINLPESRVQVW
otx2   ------ATPRKQRRERTTFTRAQLDVLEALFAKTRYPDIFMREEVALKINLPESRVQVW
otx5   ------NTPRKQRRERTTFTRAQLDVLEALFSKTRYPDIFMREEVALKINLPESRVQVW
crx    ------ATPRKQRRERTTFTRTQLDILEALFTKTRYPDIFMREEVALKINLPESRVQVW
       GDLCYPG.TPRKQRRERTTFTR QLD.LEALF KTRYPDIFMREEVALKINLPESRVQVW
```

Positions 130–180

```
otd    FKNRRAKCRQQLQQQQQSNSLSSSKNASGGGSGNSCSSSSANSRSNSNNNGSSSNNNTQS
otx1a  FKNRRAKCRQQQQQS-----------ST--NSKIRPAKKKPSPSRESP----GSES
otx1b  FKNRRAKCR-QQQQS-----------GS--STKTRPAKKKSSPTREST----GSES
otx2   FKNRRAKCRQQQQQS-----------QNGGQNKVRAREAS----SESGA
otx5   FKNRRAKCRQQQQQQ-----------TS-GQTKPRPPKKKSSPARDSSASEPSAST
crx    FKNRRAKCRQQQQQT-----------SG--QPKPRPPKKKSSPPPDLT-SDPGTSS
       FKNRRAKCRQQQQQ.QQSNSLSSSKNASGG..GG..K.RPAKKKSSP R... S ...S
```

Positions 190–240

```
otd    SGGNNSNKSSQKQGNSQSSQQGGGSSGGNNSNNNSAAAAASAAAAVAAAQSIKTHHSSFL
otx1a  SG-------------HFTPPAVSSSSSSSSSSSGSNPSALSGVGLISSSSSGTPVPSIW
otx1b  SG-------------QFTPPAVSSAGSSSSSSSTNNT-----GISSTSTSISTVSSIW
otx2   SG-------------QFTPPSSTSVPAI---STTTAPV------SIW
otx5   SG-------------PYSPPP-PPPGTAITPSSSSATV------SIW
crx    SV-------------VAAPTP-TVPPSV---SAGTAPV------SVW
       SGGNNSNKSSQKQGNS ..PP. .S... S S...A. .A G S SSS T VSSIW
```

Positions 250–300

```
otd    SAAAAASGGTNQSANNNSNNNQGNSTPNSSSSGGGGGSQAGGHLSAAAAAAALNVTAA
otx1a  SPAP----------------------------------VSPV
otx1b  SPA-----------------------------------ISPG
otx2   SPAS----------------------------------ISP-
otx5   SPAS----------------------------------ISP-
crx    SPTS----------------------------------LSP-
       SPASAAASGGTNQSANNNSNNNQGNSTPNSSSSGGGGGSQAGGHLSAAAAAAALN.SP
```

Positions 310–360

```
otd    HQNSSPLLPTPATSVSPVSIVCKKEHLSGGYGSSVGGGGGGGGASSGGLNLGVGVGVGVG
otx1a  PAPPS--LPDI---SPPASASCMQRAMSGGGTT--------
otx1b  SAPPSVSLPEP---VAPSNTSCMQRSVSGTASST--------
otx2   ------LSDP---LSTSSS-CMQRS--------
otx5   ------LPDP---LSAPSTACLQRSS--------
crx    ------LPDP---LCGSGTPCVQRPAP--------
       APPS LPDPATS... S C.QR .SGG GSTVGGGGGGGGASSGGLNLGVGVGVGVG
```

Positions 370–420

```
otd    VGVGVSQDLLRSPYDQLKDAGGDIGAGVHHHHSIYGSAAGSNPRLLQPGGNITPM--DSS
otx1a  ----GVPSYPMPYNQ-APSYAQGYPTSNAASYFGG-------MDCGSYLAPMTGHAH
otx1b  ----YPMPYNQ-TTGYSQGYPTP-SGSYFSG-------VDCGSYLAPM--HSH
otx2   ----YPMTYTQ-ASGYSQGYAG--STSYFGG-------MDCGSYLTPM--H
otx5   ----YPMTYSQ-APAYGQSYAA--SSSYFTG-------LDCSSYLSPM--H
crx    ----YPMSYGQ-PSSYSQGYG--SSPYFSG-------LDCSPYLSPM--T
       VGVGV YPM Y.QLK. .Y.QGY. S.YF.GAAGSNPRL.DCGSYL.PMTGHSH
```

Positions 430–480

```
otd    SSITTPSPPITPMSPQSAAAAAHAAQSAQSAHHSAAHSAAYMSNHDSYNFWHNQYQQYPN
otx1a  HHPHAHHSQLSTAAAVSGHHHP-HHIGQSSGH-HPHHQGYGG
otx1b  HHPH----QLSPMTASSMPTHPHHHISQSSGHHHHHHHQAYSG
otx2   HQLTGPGSTLSPMSSNAVT----SHLNQSPA---SLPTQGYGA
otx5   PQLSASGGALSPMS-----GALSQSPA---SLSSQGYTA
crx    TQLSASGGALSPLTVPSMG----GSLSQSP---SLSSQGYST
       ...A G. LSPM. S. HPH .SQS AHH . .QGY. NHDSYNFWHNQYQQYPN
```

Positions 490–540

```
otd    NYAQAPSYYSQMEYFSNQNQVNYNMGHSGYTASNFGLSPSPSFTGTVSAQAFSQNSLDYM
otx1a  ---------TALPF-SSSDCLDYKEQVASSWKLNF----------SSAAADCLDYK
otx1b  ---------TGLAF-NSSDCLDYKEQTASSWKLNF----------NT--TDCLDYK
otx2   ---------SGLGFNSTADCLDYKDQ-ASSWKLNF----------NA--DCLDYK
otx5   ---------ASLGF-GAVDCLDYKDQ-TSAWKLNF----------ST--VDCLDYK
crx    ---------ASLGF-SSVDCLDYKDQ-QAWKLNF----------NA--PDCLDYK
       NYAQAPSYY..LF S. DCLDYK.Q AS.WKLNFGLSPSPSFTGTVSA. DCLDYK
```

Position 550

```
otd    SPQDKYANMV-
otx1a  DQ-AAWRFQVL
otx1b  DQ-ASWRFQVL
otx2   DQTSSWKFQVL
otx5   DQ-NSWKFQVL
crx    -------FQVL
       DQ SW.FQVL
```

Legend:
- Conserved domain
- Homeodomain
- WSP motif
- Transcriptional transactivation domains
- Otx-tail
- Crx antibody antigen

Figure 4.10: Amino acid alignments of *Drosophila melanogaster* Otd, and *Danio rerio* Otx1a, Otx1b, Otx2, Otx5 and Crx. Conserved functional domains are highlighted in orange (homeodomain), green (WSP motif), brown (transcriptional transactivation domains) and pink (Otx-tail). The portion of the Crx protein that is skipped if translation begins from the alternate ATG start codon in the *crx*$^{-/-}$ is also conserved (blue). The C-terminal portion of the Crx protein is the antigen for the Crx antibody utilized (red).

that one or more of these paralogs is compensating for a loss of wild-type Crx in the $crx^{-/-}$ mutants.

In-situ hybridization for *otx2* and *otx5* was performed on wild-type and $crx^{-/-}$ mutants. At 52 hpf *otx2* is expressed in the retina (overlapping with expression of *crx*) and the midbrain. By 96 hpf *otx2* expression is restricted to the ciliary marginal zone of the retina and the midbrain. *otx2* mRNA expression in $crx^{-/-}$ mutants is comparable to wildtype at 52 hpf and 96 hpf (Figure 4.11 I-L). The expression pattern of *otx5* is identical to that of *crx* at both 52 hpf and 96 hpf. *otx5* is expressed in the retina and the pineal gland at both stages (Figure 4.11 A-H). Additionally, *crx* mRNA expression is retained in the $crx^{-/-}$ retina (Figure 4.11 A-D), indicating that nonsense-mediated decay of the mutant transcript is not present.

The *otx5* gene is not found in mammals and has been described as a mammalian *crx*-paralog (Ranade et al., 2008). For this reason, and because the mRNA expression pattern of *otx5* is identical to that of *crx,* we hypothesized that *otx5* is taking up the function of *crx* in its absence. In-situ hybridization shows that *otx5* transcript is mildly up regulated in $crx^{-/-}$ mutants at 52 hpf, the period of photoreceptor differentiation (Figure 4.11 E-F). To quantify this result, we performed real-time quantitative PCR (qPCR) to detect *otx5* transcripts in $crx^{-/-}$ mutants at 52 hpf. Compared to wild-type controls (AB), $crx^{-/-}$ mutants have a 38.5% increase in *otx5* expression (student's t-test: t=4.286, $p<0.05$, df=4; Figure 4.11 M). At 96 hpf the expression of *otx5* in $crx^{-/-}$ mutants is comparable to wild-type (Figure 4.11 G-H). Conversely, knock-down of *otx5* using morpholino oligonucleotides results in a reciprocal up-regulation of *crx* mRNA expression at 96 hpf (Figure 4.11 N-O). These results suggest that *otx5* and *crx* may be able to compensate for one another and that their expression is regulated by each other.
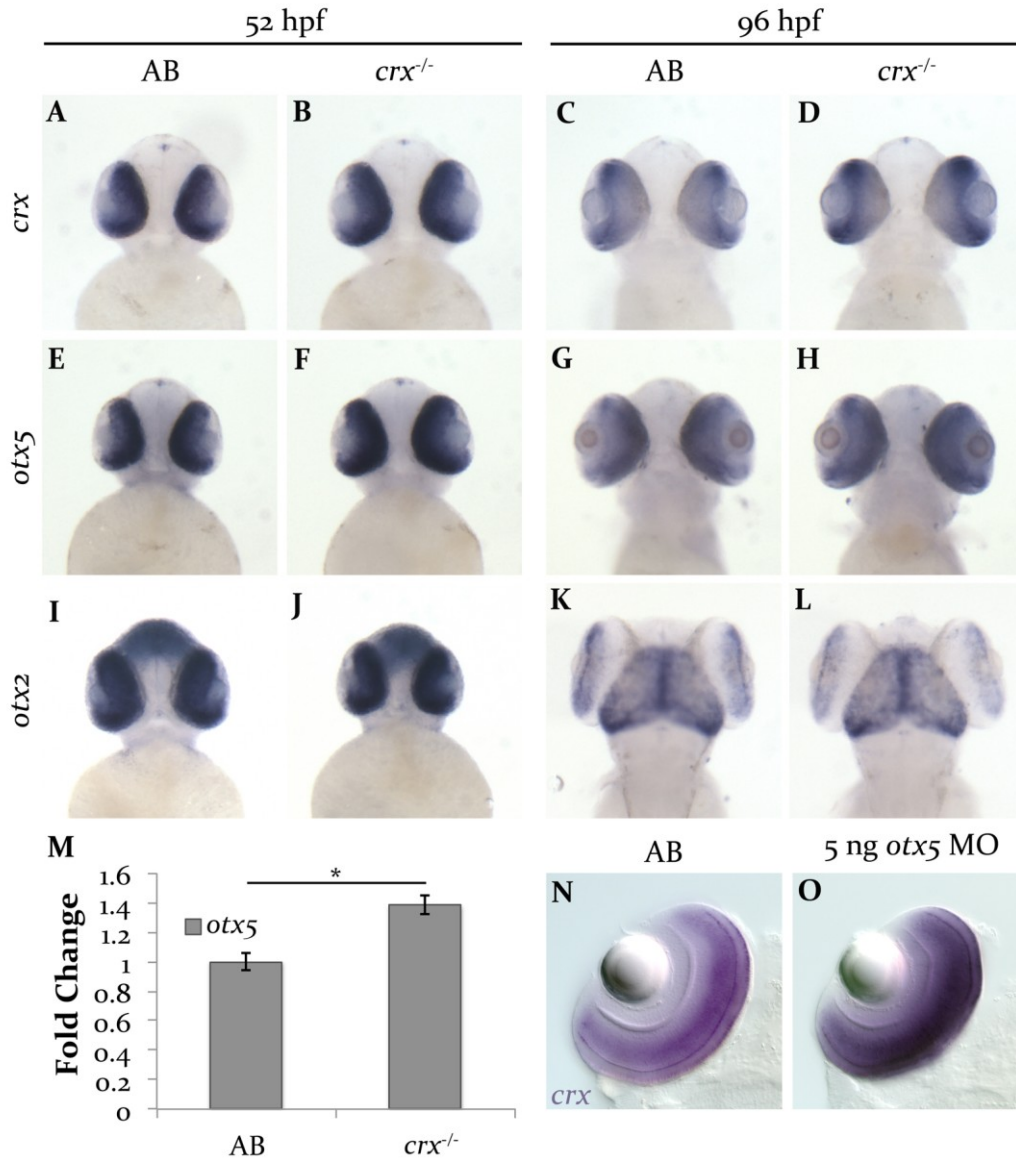
Figure 4.11: mRNA expression of *otx*-family genes in *crx*^{-/-} mutants and *otx5* morphants. Whole-mount in-situ hybridization of *crx* (A-D), *otx5* (E-H) and *otx2* (I-L) mRNA at 52 hpf and 96 hpf in wild-type (AB) and *crx*^{-/-} mutant embryos. (M) qPCR showing the significantly increased expression of *otx5* transcript in *crx*^{-/-} mutants at 52 hpf (error bars, SEM; * $p<0.05$, student's t-test, t=4.286, df=4). Whole-mount in-situ hybridization of *crx* transcript at 96 hpf in AB (N) and *otx5* morphant (O) retinas. [Ventral view (A-J); Dorsal view (K-L, N-O)].

To test the hypothesis that Otx5 and Crx transcription factors have overlapping functions in photoreceptor specification, we used *otx5* MO to block the translation of Otx5 in *crx*$^{-/-}$ mutants. Injection of 5 ng *otx5* MO alone resulted in the expansion of *otx2* mRNA expression from the ciliary marginal zone throughout the GCL and INL of the retina in 54% (21/39) of the offspring. When *otx5* MO is injected into the *crx*$^{-/-}$ mutant background 90% (44/49) of the offspring have expanded *otx2* expression (Fisher's exact test: p<0.001; Figure 4.12 A-D, M). We also investigated whether *otx5* MO reveals a phenotype in the photoreceptors of *crx*$^{-/-}$ mutants by examining the expression of *opn1sw2* transcript in blue cones and the localization of Arr3a protein in red/green double cones. Injection of 5 ng *otx5* MO alone resulted in reduction of *opn1sw2* expression in blue cones in 40% (14/43) of the offspring. The expression of *opn1sw2* is reduced in 87% (40/46) of the morpho-mutants (Fisher's exact test: p<0.0001; Figure 4.12 E-H). Additionally, there are areas lacking red/green cone photoreceptors in the *otx5* morphant retinas. The phenotype is exacerbated in the morpho-mutants, with very few red/green cone photoreceptors present (Figure 4.12 I-L).

The same results were observed when a smaller dose of *otx5* MO was used, but to a lesser extent. Expression of *opn1sw2* in blue cones was reduced in 14% (2/14) of wild-type embryos injected with 2.5 ng *otx5* MO. When the same dose of MO was injected into a *crx*$^{-/-}$ mutant background, the prevalence of the phenotype increased to 35% (7/20; Figure 4.13 A-D, I). Similarly, the expression of *opn1mw1* in green cones was reduced in 50% of 2.5 ng MO-injected embryos (9/18). This phenotype was observed in 61% (8/13) of the morpho-mutant embryos (Figure 4.13 E-F, I). These results suggest that there is a synergistic effect when both *otx5* and *crx* are knocked-down, and that Otx5 could be compensating in the *crx*$^{-/-}$ mutants.
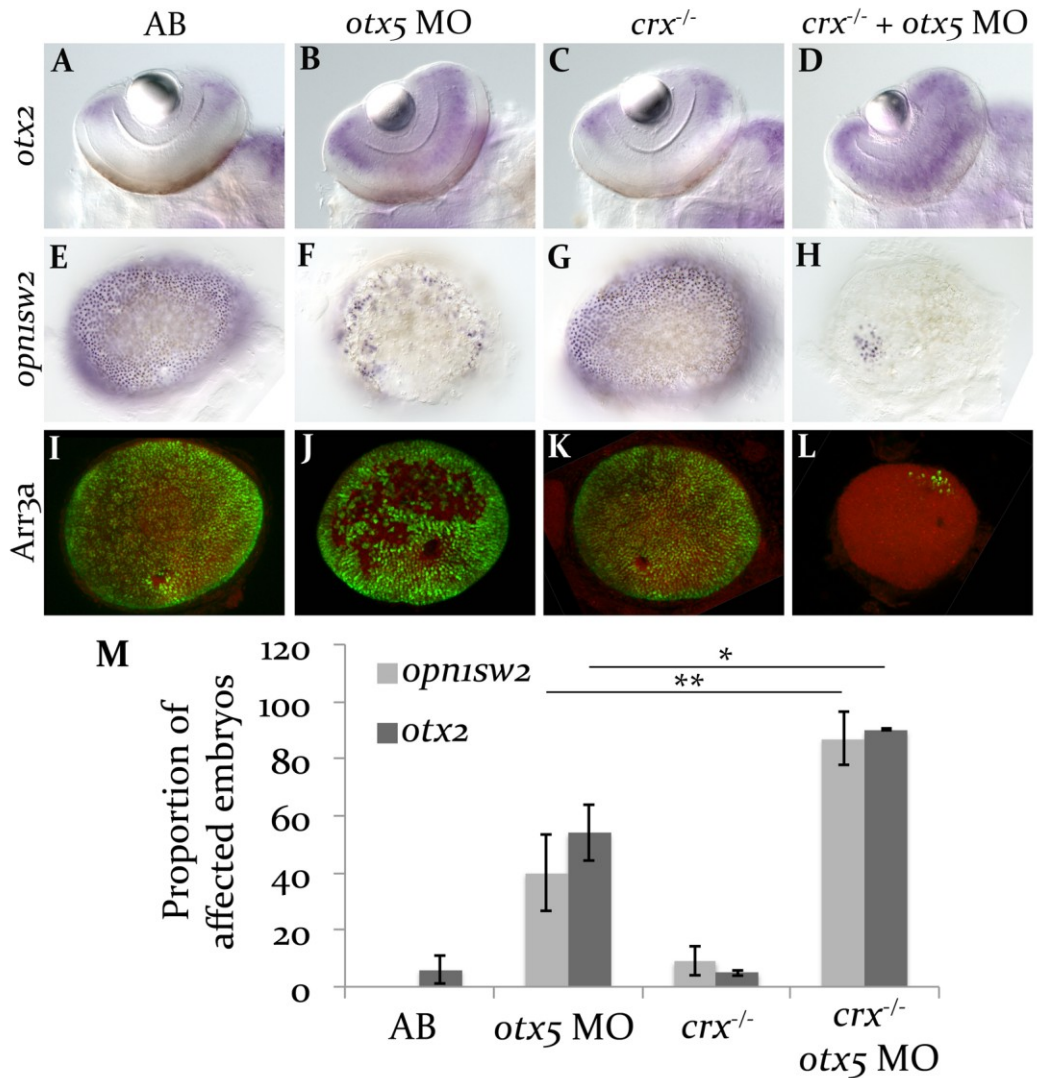
Figure 4.12: Knock-down of *crx* and *otx5*, but not *crx* alone, results in a loss of photoreceptor identity. Whole-mount in-situ hybridization for *otx2* (A-D) and *opn1sw2* (E-H) mRNA at 4 dpf. Wild-type (A-B, E-F, I-J) and *crx*^{-/-} mutant (C-D, G-H, K-L) embryos were injected with 5 ng *otx5* MO. (I-L) Immunofluorescence for Arrestin3a in red/green double cones (green) counter-stained with propidium iodide (red). (M) Graph displaying the proportions of embryos with expanded *otx2* mRNA expression or reduced *opn1sw2* mRNA expression [*otx2*: AB 3/51, *otx5* MO 21/39, *crx*^{-/-} 2/41, *crx*^{-/-}+ *otx5* MO 44/49; *opn1sw2*: AB 0/51, *otx5* MO 17/43, *crx*^{-/-} 4/43, *crx*^{-/-}+ *otx5* MO 40/46; Fisher's exact test, * p<0.001, ** p<0.0001].
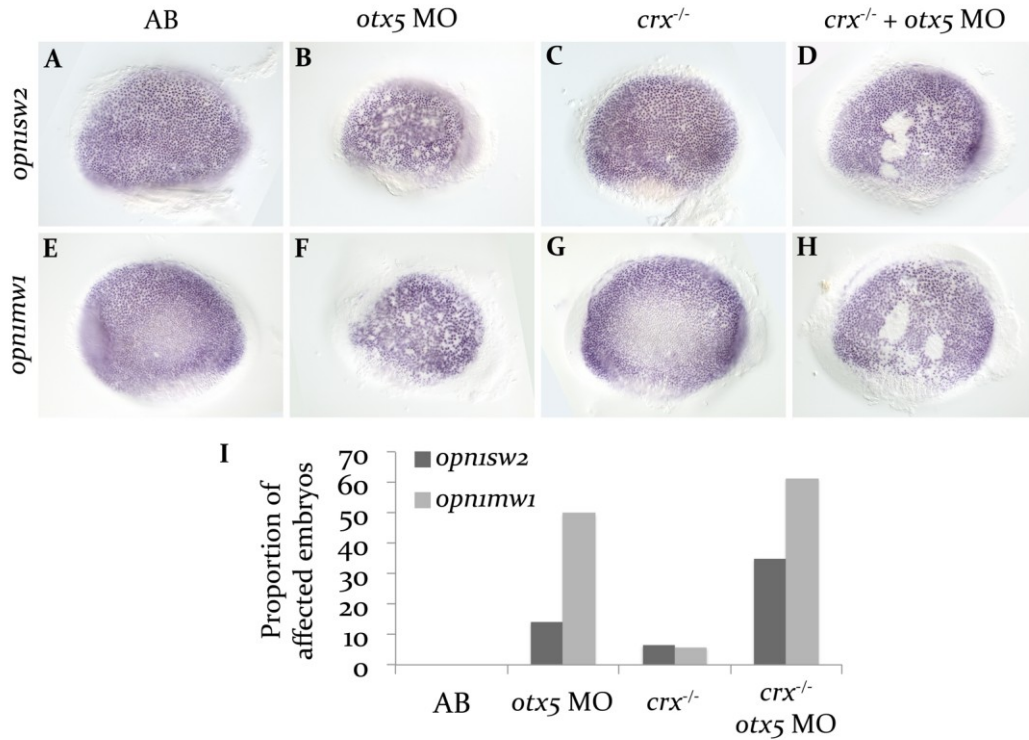
Figure 4.13: Low doses of *otx5* MO also reveal a phenotype in *crx*^{-/-} mutants. Whole-mount in-situ hybridization of *opn1sw2* (A-D) and *opn1mw1* (E-H) mRNA at 4 dpf. Wild-type (A-B, E-F) and *crx*^{-/-} mutant (C-D, G-H) embryos were injected with 2.5 ng *otx5* MO. (I) Graph displaying the proportions of embryos with reduced *opn1sw2* and *opn1mw1* mRNA expression [*opn1sw2*: AB 0/18, *otx5* MO 2/14, *crx*^{-/-} 1/15, *crx*^{-/-} + *otx5* MO 7/20; *opn1mw1*: AB 0/19, *otx5* MO 9/18, *crx*^{-/-} 1/17, *crx*^{-/-} + *otx5* MO 8/13].

Generation of an otx5 mutant using TALEN mutagenesis.

Morpholinos have been known to exhibit non-specific toxicity in the developing embryo (Ekker and Larson, 2001; Robu et al., 2007). Additionally, morpholino activity only persists for the first 48 - 72 hpf, after which the effectiveness of the MO has worn off (Nasevicius and Ekker, 2000; van der Sar et al., 2002). These pitfalls of using morpholino technology, especially when the developmental stage we are interested in is past the point of full morpholino activity, prompted us to obtain a genetic *otx5* mutant. Transcription activator-like effector nucleases (TALENs) are highly efficient molecular tools for directed gene mutagenesis that fuse modified DNA sequence-specific TAL effectors (originally from *Xanthomonas spp.* plants) to the FokI nuclease catalytic domain (Cermak et al., 2011). TALENs can be designed for virtually any DNA sequence desired. We designed a TALEN to target the promoter region of the *otx5* gene (Figure 4.14). We predicted that by disrupting the promoter sequences of the gene we would effectively prevent the transcriptional machinery from binding the DNA and prevent all mRNA transcription.

otx5 TALEN mRNA was injected into wild-type (AB) embryos and raised to adulthood (P_o). The offspring of P_o fish incrosses were screened via HRMA to identify carriers of germline mutations. The carriers were in-crossed to other P_o carriers and the offspring was raised to adulthood (F_1). F_1 fish were screened for somatic mutations by genomic DNA extraction (from fin-clips), PCR-amplification and restriction fragment length polymorphism (RFLP) analysis. 14/45 (31.1%) of the screened F_1 fish had homozygous mutations in *otx5* and 27/45 (60%) had heterozygous mutations. One of the mutations identified was a 161 bp deletion in the promoter region of *otx5* (Figure 4.15). This allele was designated *otx5*^{ua1012} (hereafter referred to as *otx5*$^{-/-}$). The phenotypic analysis of this mutation is yet to be determined.

```
CATTGGTCTTTCTGGTATATTACTGTAGCTGTTGTGTTACCATAGCAACTGTAGAAT
CACCACAACAGATCAATTACGAAAGTTGTTTTGTTACCATAGCAACTGTAGAATCGC
CACAACAGATCAATTACGAAAGTTGTTTTGTCACCATAGCAACTGTAGAATCACCAT
AATATATTACTTTAAATGCTTTGTTATAGATCAAAAACACTGCAGTCTAAAAATACT
GGCCTTTTGTAACCCAGCATTGGGTCAAACATGGAATGCTGGGTTCTTCAGTTCGGT
CATACCAAACATTGGGTAAAATCTGGTCCAAGAAATTTAGATAAAAAAATTAACCCA
GCAGTTGGTTTAGTCCGCATTACACCCAGAATTGGGTTGAAAT AACCCAGCATTTTT
AAGCGCAT ATAATATTTGCCATAACAAAATAAAATTTTAGAGATTTTAAAATTTAAG
ATAAAAGAGAGTGTGACGTGCGCGCGCGCGTGTGTGTGTGAGAGAGAGAGAAAGAGA
GAGAGAGAGAGAGAGAGAGAGAGAGAGAGATGAAGGAGGGGTTTATTGAGGTCTTGT
CGGTCTGTAATTAGC CGCCTCCTCCTCCTC A TTCATCT CACTGTCAC CGGGAGACCG
AGACA CGCGCACCGAGCGCTCA GCCGCAGCACC GGACACACTAACAGACCGCTGAT G
AGCTCACACACACACACGATCAACACATACACACACTCGAGCTCGTCT ACACGCTGC
TGACTGATAGAAA AAGTCCATCAGAGACAGAAACACACAGAAAGAGAGAGAGAGGAG
GAGAGAGAAAGAGAGAGAGAGAGAGTTTAGTC ATG ATGTCCTACATGAAACAGCCTC
ATTACTCCGTTAACGGGTTGACTCTGTCCGGTACCGGGATGGATCTCCTGCACTCCG
CCGTCGGTTACCCTA
```

Figure 4.14: The *otx5* TALEN binds DNA in the promoter region of the gene. The sequence of the first intron and exon of the *otx5* gene with important features highlighted. [TALEN binding site (purple); *otx5* HRM primers (orange); *otx5* PCR primers (blue); intron (grey); exon (black); ATG start codon (green)].

Figure 4.15: Identification of a TALEN-generated mutation in the *otx5* gene. (A) Sequencing chromatograms of wild-type (*otx5*) and mutant (*otx5^ua1012^*) alleles. The ua1012 allele has a 161 bp deletion (underlined in red) in the promoter region of the *otx5* gene. (B) Sequence alignments showcasing the 161 bp deletion in the *otx5^ua1012^* allele.

Discussion and Conclusions

Morpholino-generated phenotypes do not always phenocopy those of the mutants.

Morpholino-mediated gene knock-down has been a popular strategy for studying loss-of-function phenotypes in zebrafish for the last 14 years. Morpholinos have reliably phenocopied the phenotypes observed in zebrafish mutants such as *one-eyed-pinhead, chordin, no tail, bmp7, smad5, wnt5* and more (Heasman, 2002; Lele et al., 2001; Nasevicius and Ekker, 2000). A recent project undertaken by the Wellcome Trust Sanger Institute to create a mutant zebrafish line for every annotated protein-coding gene has greatly increased our resources for studying loss-of-function phenotypes (Kettleborough et al., 2013). At the time of publication, Kettleborough et al. (2013) had produced potentially disruptive mutations in more than 38% of all known protein-coding genes in zebrafish. In addition to the Sanger Institute's mutagenesis project, the relative ease of using TALENs or ZFNs for directed gene mutagenesis has allowed zebrafish researchers the ability to study genes with mutations in virtually any part of the gene sequence they desire (Cermak et al., 2011; Pillay et al., 2013). These advances have allowed researchers to study genes that have previously only been studied with morpholino technology. As a result, a number of studies have revealed that the MO-induced phenotypes for a particular gene knock-down do not match those observed in the mutant lines.

Examples of this phenomenon are observed in the case of zebrafish *gdf6a, aldh1a3, gbx1, gbx2* and *crx* mutants. *gdf6a* morphant zebrafish display a severe mirophthalmic or anophthalmic phenotype that has variable penetrance and can occur uni- or bilaterally. They also display a loss of retinal lamination (Asai-Coakwell et al., 2007). Studies performed on *gdf6a*$^{-/-}$ mutant fish revealed less-severe, bilateral microphthalmia with

100% penetrance (French et al., 2013). Additionally, the $gdf6a^{-/-}$ mutants have relatively normal retinal lamination (this work). *aldh1a3* morphant fish display microphthalmia, colobomata and reduced tectal innervation (Yahyavi et al., 2013), but $aldh1a3^{-/-}$ mutant fish are phenotypically wild-type (Jennifer Weekes, personal communication). Embryos injected with *gbx1* MO have a posteriorly-shifted midbrain-hindbrain boundary (Rhinn et al., 2009) and *gbx2* morphants lose midbrain-hindbrain boundary marker gene expression (Kikuta et al., 2003). Mutants in *gbx1* or *gbx2* alone have normal brain patterning (Su et al., 2014). Finally, this work has described the wild-type like phenotype of $crx^{-/-}$ mutants. The results observed in this work directly contradict that of published morpholino data. Zebrafish *crx* morphants display defects in optic cup patterning, retinal neuron differentiation and lack expression of photoreceptor-specific genes such as opsins (Shen and Raymond, 2004).

There are a number of explanations for this phenomenon: [1] Strain-specific penetrance of a phenotype could allow some morphant or mutant phenotypes to be observed only in a particular wild-type strain. This is a common occurrence in mouse. For example, penetrance of neural tube defects in mouse is highly dependent on the genetic background of mouse *Men1* and *Cecr2* mutants (Kooistra et al., 2012; Lemos et al., 2009). [2] Non-specific effects of the morpholinos, in combination with knocking-down your gene of interest, could reveal phenotypes in the morphants but not the mutants. Even the earliest publications based on morpholino technology describe the presence of a non-specific toxicity in 15-20% of morpholinos (Ekker and Larson, 2001; Heasman, 2002; Nasevicius and Ekker, 2000). The non-specific effects are attributed to activation of the tumor suppressor gene *p53*, leading to increased levels of apoptosis (Gerety and Wilkinson, 2011; Robu et al., 2007). As a result, a common practice when using morpholino technology is to combine your morpholino of interest with one

that blocks translation from *p53* transcript. One of the phenotypes observed in the *crx* morphants is ectopic retinal apoptosis (Shen and Raymond, 2004). It is possible that *crx* morpholino activated the *p53*-driven apoptosis pathway, leading to apoptosis in the morphants, who do not have the protective *p53* MO. Additionally, *crx* morphants have defects in cell-cycle exit (Shen and Raymond, 2004). The *crx* MO may cross-react with unknown transcripts whose knock-down, in combination with the knock-down of *crx*, results in cell survival and proliferation defects. [3] A paralogous protein is taking up the function of the protein lost in the mutant, resulting in a wild-type phenotype. This hypothesis will be discussed in detail below.

Compensation by otx5 is likely occurring in crx$^{-/-}$ mutants.

An interesting observation in the *crx*$^{-/-}$ mutants is the presence of Crx protein. The premature stop codon in the mutant transcript should prevent the production of full-length protein. It is unlikely that the Crx protein being made in the mutants is functional. The protein observed is hypothesized to be a result of utilizing a secondary in-frame start codon in the *crx* mutant transcript that occurs after the premature stop codon (Figure 4.8). If this protein were functional, we would expect that by blocking its translation in the *crx*$^{-/-}$ mutants we would reveal a phenotype. We did not observe any retinal phenotype at any MO dose used (Figure 4.9). It is possible that in our mutant there is a functional Crx protein being produced, and the reason a phenotype is not revealed in the *crx* alt ATG morphants is that *otx5* is still compensating for the loss of *crx*. The amino acid sequence prior to the secondary start codon is relatively conserved and the functional properties of this domain have not been tested. It is also possible that this domain is important for wild-type function.

We hypothesized that the *crx* paralog, *otx5*, is taking up the function of Crx protein in its absence. Phylogenetic reconstructions of DNA and protein sequences have led to the hypothesis that the *Crx* genes are the mammalian representative of the *Otx5* class of genes found in chondrichthyans (cartilaginous fishes, including the dogfish shark), actinopterygians (ray-finned fishes, including zebrafish) and amphibians (such as *Xenopus laevis*; Plouhinec et al., 2003; Sauka-Spengler et al., 2001). It is thought that these two classes of genes have conserved roles in the specification of photoreceptors (Plouhinec et al., 2003; Sauka-Spengler et al., 2001). The hypothesis of a single *Otx5*/*Crx* class is contradicted by the fact that zebrafish (and pufferfish, another teleost) have both *crx* and *otx5* genes (Gamse et al., 2002; Liu et al., 2001; Plouhinec et al., 2003). Phylogenetic analysis of the *Otx5* and *Crx* genes across a range of mammals, reptiles, amphibians and fish resulted in the hypothesis that *otx5* and *crx* are both present in zebrafish and pufferfish due to an independent duplication event in that lineage. Additionally, the evolutionary constraints on the *Otx5* class of genes in mammals was relaxed due to the evolution of multiple *Otx* orthologous classes, and was referred to as *Crx* (Plouhinec et al., 2003).

Functional redundancy is not an uncommon situation in zebrafish. A whole-genome duplication event that occurred in the teleost lineage resulted, in many cases, two copies of genes present as single copies in mammals (Postlethwait et al., 1998). Examples of functional redundancy are also found in the literature. As was described above, mutations in *gbx1* and *gbx2* alone do not reveal a phenotype in the hindbrain of zebrafish. But when the mutations are combined, the *gbx1*$^{-/-}$;*gbx2*$^{-/-}$ double mutant loses midbrain-hindbrain identity, a phenotype similar to that observed in *gbx1* or *gbx2* morphants (Kikuta et al., 2003; Rhinn et al., 2009; Su et al., 2014). These studies revealed a functional redundancy between *gbx1* and *gbx2* in

cerebellar development in zebrafish (Su et al., 2014). It is reasonable to hypothesize that a similar situation may be occurring in the $crx^{-/-}$ mutants with *crx* and *otx5*.

In conclusion, we found that the phenotype of a $crx^{-/-}$ mutant does not match that found in morphant studies, and that this is likely due to the functional redundancy of the *otx*-family paralogs, *crx* and *otx5*. We gave an example of the relative ease of ZFN- and TALEN-mediated mutagenesis, and discussed the merits of mutant studies. These studies reveal pitfalls in the use of morpholinos, and continuing research on multiple-mutant strains will help us reach our goal of producing a photoreceptor-less zebrafish line that can be used in future studies to identify novel factors that are central to photoreceptor development in zebrafish.

Chapter 5

Future Directions

A novel role for Gdf6a in retinal dystrophies

Summary of results

Correct retinal patterning during early eye-field development and the regulation of retinal cell proliferation later in development are crucial for the formation of a functional eye. Defects in these pathways can result in the development of blinding disorders such as microphthalmia (small eye), anophthalmia (no eye) and colobomata (known collectively as MAC) and retinal degeneration disorders such as Leber's congenital amaurosis (LCA). BMP ligands have diverse roles, including regulation of cellular differentiation, proliferation and cell survival. The BMP ligand Gdf6 plays important roles in early retinal patterning and proliferation. A segmental deletion on human chromosome 8 (46, XX, del 8 q21.2q22.1) was identified in a patient that presented with bilateral coloboma. This deletion covered an 10.37 Mb region, encompassing the human *GDF6* gene (Asai-Coakwell et al., 2007). Similarly, mouse *Tcm* (total cataract with microphthalmia) mutants are born with microphthalmia and coloboma. This mutation has been characterized as a 1.3 Mb deletion of a region that includes the murine *Gdf6* gene (Wang et al., 2005). Additionally, 4/279 patients from an LCA and juvenile retinitis pigmentosa cohort have been identified with heterozygous mutations in *GDF6,* one of which is a compound heterozygote (Asai-Coakwell et al., 2013). We hypothesized that mutations in *GDF6* could underlie the phenotypes observed in MAC and LCA. To study the development of these disorders, we used a zebrafish *gdf6a*$^{-/-}$ mutant line. These fish exhibited microphthalmia that was evident by 48 hpf. They had relatively normal retinal lamination, but by 2 weeks of age these fish had dysmorphic red/green cone photoreceptors (Figure 3.1). Before the onset of microphthalmia, the mutant retinas displayed increased levels of apoptosis, which peaked at 28 hpf (Figure 3.2). This ectopic apoptosis was diminished

by treatment with the anti-apoptotic compound P7C3 (Figure 3.3). Interestingly, treatment with P7C3 did not rescue the microphthalmic phenotype (Figure 3.4), but did partially recover visual responsiveness (Figure 3.5). Mutants treated with P7C3 had partially responsive visually-mediated background adaptation (VBA) but did not display any higher levels of visual acuity (Figure 3.6).

Will P7C3 improve the phenotypes observed in other retinal dystrophy models?

P7C3 has been found to improve the neural phenotypes of a number of neurodegenerative disease models in mice, including Parkinson's disease (De Jesus-Cortes et al., 2012), amyotrophic lateral sclerosis (Tesla et al., 2012) and traumatic brain injury (Blaya et al., 2014). In all cases, P7C3 acted as a neuroprotective agent, protecting newborn neurons from aberrant apoptosis. Additionally, P7C3 is orally bioavailable, can cross the blood-brain barrier, and is non-toxic at the appropriate dose (Pieper et al., 2014). Our studies expanded the role of P7C3 to being protective in retinal degeneration disease, demonstrating the use of P7C3-class compounds as general neuroprotective agents that can act in multiple disease settings. Previous studies of zebrafish retinal dystrophy models (including models for retinitis pigmentosa, cone-rod dystrophy and achromatopsia) have also revealed the presence of ectopic apoptosis (Daly and Sandell, 2000; Riera et al., 2013; Shu et al., 2011; Viringipurampeer et al., 2014). The use of P7C3-class compounds in these models of retinal dystrophy could further broaden the scope of P7C3 activity. We predict that P7C3 will be able to rescue the apoptotic defect observed in these zebrafish retinal dystrophy models.

What is the role of gdf6a in the maturation of photoreceptors?

While the genetic pathways required for the establishment of photoreceptor cells during embryonic development is relatively well-characterized, the factors required for the maturation of photoreceptor cells into adulthood are not well understood. In *gdf6a*$^{-/-}$ mutant zebrafish, cone photoreceptors are initially able to form properly, but by 2 weeks of age they display shortened, dysmorphic inner segments (Figure 3.1). Interestingly, this phenotype persists into adulthood, with no photoreceptor degeneration. At 28 dpf, UV-cones are present but the apical domain of the inner and outer segments are shortened. Additionally, red/green double cones remain present up to 20 months of age, but they also retain an apically-shortened phenotype (Jennifer Hocking, personal communication). RNA-seq analysis on wild-type and *gdf6a*$^{-/-}$ mutant eyes at a late stage of photoreceptor development may reveal Gdf6a-dependent transcriptional networks that are required for the proper maturation of photoreceptor cells. This work is currently being performed by Jennifer Hocking, under the supervision of Andrew Waskiewicz at the University of Alberta. At 5 dpf, she found a general decrease in the expression of cone-specific transcripts. Candidate gene analysis from this RNA-seq data set may reveal previously unknown factors in the maturation of photoreceptor cells.

Does nasal apoptosis in the gdf6a$^{-/-}$ *mutant retina indicate a role for gdf6a in nasal retinal development?*

Retinal apoptosis in *gdf6a*$^{-/-}$ mutants is often, but not always, focused in the nasal retina. Not surprisingly, little is known of a role for *gdf6a* in the nasal retina, most likely due to the fact that *gdf6a* is not expressed in the nasal retina. The few nasal-temporal patterning genes that

have been studied in *gdf6a* knockdown models show contradicting results. The retinal expression of the nasal marker *hmx1,* a gene that is required for nasal-temporal retinal patterning in chickens, is lost in *gdf6a*$^{-/-}$ mutants (French, 2010). Conversely, expression of the nasal marker *foxg1* is expanded dorsally in *gdf6a* morphants (Asai-Coakwell et al., 2007). Finally, the temporal expression of the guidance molecule *ephA4b* remains unchanged in *gdf6a*$^{-/-}$ mutants (Gosse and Baier, 2009). It would be interesting to know if the nasal-heavy apoptosis in the retina results in long-term defects in nasal-temporal identity. This could be achieved by injection of the nasal retina with lipophilic dyes (DiI or DiO) that label the retinal ganglion cell axonal projections to the optic tectum.

Why do P7C3-rescued gdf6a$^{-/-}$ *mutants have recovered VBA, but not OMR?*

A striking finding of our studies was the observation that P7C3-mediated rescue of retinal apoptosis also partially rescues the VBA response, but not OMR. As discussed in Chapter 3, this difference may be simply due to the nature of the assay used to analyze visual behavior. VBA is a retinal ganglion cell-mediated neuroendocrine response, while OMR requires functional cone photoreceptors and the coordinated efforts of the visual and musculo-skeletal systems (Asai-Coakwell et al., 2013; Fleisch and Neuhauss, 2006; Muto et al., 2005; Orger et al., 2004). Additionally, the VBA response requires both the retinal and pineal pathways to function (Zhang et al., 2010). The pineal organ is smaller in *gdf6a* morphant embryos, as observed by in-situ hybridization for *crx* transcript and immunofluorescence for Arrestin3a (French, 2010). Analysis of the pineal organ in *gdf6a*$^{-/-}$ mutants with and without P7C3 treatment would perhaps shed some light on the differences in the visual assays we observe. If there is

a defect in pineal function in *gdf6a⁻/⁻* mutants, it may also be rescued by P7C3 treatment and this may be why we only see rescue in the VBA assay.

There is a subset of retinal ganglion cells in the mammalian retina that contain the photopigment melanopsin. These cells send their axons directly to the suprachiasmatic nucleus, the site of the mammalian biological clock, that regulates circadian rhythms (Hattar et al., 2002; Provencio et al., 2002). While mammals have a single melanopsin (*Opn4*), zebrafish have five different types of melanopsin (*opn4xa, opn4xb, opn4a, opn4.1* and *opn4b)*, located in varying cell layers of the retina (Matos-Cruz et al., 2011). These non-photoreceptor light-detecting cells may be involved in VBA, a non-image-forming visual response. P7C3 may be rescuing the function of these cell types in developing *gdf6a⁻/⁻* mutant retinas, allowing the recovery of simple light-detection in VBA, but not the image-forming OMR visual behaviour.

Studies of *crx*-dependent photoreceptor differentiation in zebrafish

Summary of results

All retinal cells are derived from a common population of multi-potent retinal progenitor cells (RPCs). The transcription factor Crx has a crucial role in the specification of photoreceptor cells from RPCs. Lesions in human *CRX* cause retinal degeneration disorders such as LCA, cone-rod dystrophy and retinitis pigmentosa. Our goal was to create a zebrafish *crx* null mutation that could be used as a model for these human disorders and we hypothesized that these fish would be photoreceptor-less (Figures 4.1 and 4.2). Interestingly, the zebrafish *crx⁻/⁻* mutants appeared wild-type and were viable and fertile. The retinal lamination was normal and UV-, red- and green-cones had normal morphology and distribution (Figure 4.4).

Additionally, expression of *crx* target genes such as the opsins (*opn1sw1, opn1sw2, opn1mw1* and *rho*) was comparable to wild-type (Figure 4.5). The expression of transcriptional activators (*nrl* and *nr2e3*) that interact with Crx is also unchanged in the mutant (Figure 4.6). Surprisingly, Crx protein is translated in the mutants (Figure 4.7). This protein is hypothesized to be the result of a secondary start codon in the *crx* transcript and is thought to be non-functional (Figures 4.8 and 4.9). Finally, morpholino-mediated knock-down of the *crx* paralog, *otx5*, reveals a retinal phenotype in the mutants, suggesting that Otx5 is compensating for Crx in the $crx^{-/-}$ mutant (Figures 4.12 and 4.13). This is also supported by the fact that *otx5* and *crx* appear to regulate each others expression, with *otx5* mRNA expression up-regulated in the $crx^{-/-}$ mutants and *crx* mRNA expression up-regulated in the *otx5* morphants (Figure 4.11).

What is the role of otx5 in zebrafish crx mutants?

Through the use of morpholino technologies, we have provided evidence that *otx5* is compensating for the loss of functional *crx* in the mutants. We also provided evidence, from the literature and from our own observations, that morpholino studies may not be entirely accurate. For these reasons we need to identify the role that *otx5* plays in the $crx^{-/-}$ mutants in the context of a genetic model. TALEN-mediated mutagenesis was employed to create an *otx5* mutant zebrafish line with relative ease and speed. The fish line that was generated has a 161 bp deletion in the promoter region of the gene. We predict that mRNA transcription of *otx5* will be reduced or entirely abolished in these mutants. The phenotypic expression of this mutation is yet to be determined.

Recapitulation of the morpho-mutant studies in a fully genetic model is required in order to provide more solid support of our hypothesis.

The groundwork for these studies has been laid out already. A stable $otx5^{+/-}$ carrier line has been established as well as an $otx5^{+/-};crx^{+/-}$ double-mutant line. We hypothesize that homozygous double mutants will phenocopy the morpho-mutant studies, and the double mutants will lose photoreceptor identity.

One of the biological goals of this project was to create a zebrafish mutant line that lacks photoreceptor cells. We predict that this phenotype will be observed in the $crx^{-/-};otx5^{-/-}$ double mutants. With this zebrafish line, we can perform RNA-seq analysis to identify novel components of the transcriptional network that decides photoreceptor cell fate.

What is the role of otx5 in normal retinal development?

Very little research has been performed on the role that *otx5* plays during zebrafish photoreceptor development. The only literature available focuses on its role in the development of the pineal organ. The pineal organ is a photoreceptive neuroendocrine organ responsible for the cyclical production of endocrine and neuroendocrine signals in response to environmental light conditions (Mano and Fukada, 2007). In most non-mammals (such as the zebrafish), the pineal organ contains light-receptive photoreceptors (Ekstrom and Meissl, 2003). Even though *crx* and *otx5* have identical mRNA expression in the pineal organ and retina, it is *otx5* that regulates circadian gene expression in the pineal organ (Gamse et al., 2002). *crx* morpholino does not disrupt the expression of circadian regulated genes, but *otx5* morpholino does (Gamse et al., 2002). Interestingly, the mRNA expression of *otx5* in the pineal remains constant, regardless of the circadian time point examined (Gamse et al., 2002). A constitutively expressed transcription factor like Otx5 regulates circadian gene expression by the action of temporal regulatory factors that bind *cis*-acting regulatory

elements in the promoter of the pineal target genes (Mano and Fukada, 2007). This sequence, called the E-box, is required in addition to the putative Crx/Otx5 binding sites. The temporal regulatory factors BMAL (brain muscle ARNT-like 1) and CLOCK (circadian locomotor output cycles kaput) bind to the E-box and act in cooperation with Otx5 to promote circadian gene transcription (Appelbaum and Gothilf, 2006). Similarly, photoreceptor-specific *cis*-acting regulatory elements have been identified such as the NRE (Nrl responsive element), which is bound by the transcription factor Nrl and works with Crx to promote rod-specific gene expression (Rehemtulla et al., 1996). Additionally, the PINE (pineal negative regulatory element) is required in the blue-opsin gene promoter to repress Crx-driven blue-opsin gene expression in UV-cones, bipolar cells and the pineal organ (Takechi et al., 2008).

To identify if Otx5 actually binds to and promotes mRNA expression from photoreceptor-specific genes, we can test Otx5's ability to interact with transcriptional activators or repressors bound to *cis*-acting regulatory elements. The chromatin immunoprecipitation (ChIP)-loop assay, a variation of chromosome conformation capture (3C) technology, could be utilized to identify these interactions (Simonis et al., 2007). In this assay, chromatin is cross-linked and digested, the protein of interest (Otx5) is immunoprecipitated (with bound DNA pulled down with it), cross-linked DNA fragments are ligated, and high-resolution sequencing of the pulled-down DNA is performed. This may identify *cis*-acting elements that interact with the Otx/Crx DNA binding site (Simonis et al., 2007). Because a zebrafish Otx5 antibody is unavailable, we would have to use a his-tagged Otx5 protein.

What is the role of crx in inner nuclear layer bipolar cells?

crx mRNA and Crx protein do not only localize to the photoreceptor cells, they are also found in a subset of the bipolar cells of the inner nuclear layer (INL; Figure 4.3). In mammals, the INL expression of *crx* is very weak (Bibb et al., 2001; Chen et al., 1997; Furukawa et al., 1997) but this expression is much stronger in the zebrafish INL (Liu et al., 2001). To date, the role of *crx* in the INL remains unclear. In chick, a homeobox gene related to *crx*, called *cbx*, was identified using a human *crx* cDNA probe (Li et al., 2002). This gene is expressed in a small subset ON bipolar cells in the retina. Mis-expression of chick *cbx* in the retina causes a reduction of rod bipolar cells, and loss-of-function results in embryonic lethality. Additionally, the retinas of dying *cbx* loss-of-function animals have an increased number of rod bipolar cells (Li et al., 2002). These data suggest that chick *cbx* expression represses rod bipolar cell fate, allowing the cells to become cone bipolar cells.

Preliminary data performed by an undergraduate student under my supervision investigated whether INL-expressed genes are under the transcriptional control of Crx. mRNA expression of bipolar cell markers (*lin7a, grm6b, gnao1b, vsx1* and *vsx2*) remains unchanged in $crx^{-/-}$ mutants (Louse Upham, personal communication). The expression of bipolar cell-specific genes may vary with the addition of *otx5* MO, as is observed in the photoreceptor cell layer, but this experiment has not yet been performed.

Identification of the type of bipolar cell that expresses *crx* may shed light on its role in the INL. ON bipolar cells can be identified by immunolabeling for Protein kinase c α (Prkca) in zebrafish (Huang et al., 2012). Double immunolabeling for Crx and Prkca may help reveal the identity of the Crx-positive cells in the INL. Additionally, human *CRX* and mouse *Crx* are found in Prkca-positive cells (Hennig et al., 2008).

Transgenic zebrafish lines are available that selectively label sub-types of ON and OFF bipolar cells (Zhao et al., 2009). The bipolar subtypes were identified by their distinct morphology (Connaughton et al., 2004). The *Tg(Gal4-VP16;UAS:eGFP)^{xfz3}* line labels two subsets of bipolar cells, the B_{off}-s1/s3/s5 and B_{on}-s3/s5 types. The *Tg(Gal4-VP16;UAS:eGFP)^{xfz43}* line also labels two subsets of bipolar cells, the B_{off}-s2/s3 and B_{on}-s4 types (Zhao et al., 2009). These transgenic lines may be immunolabeled for Crx protein and screened for co-localization to identify bipolar cell type.

Literature Cited

Agathocleous, M. and Harris, W.A., 2009. From progenitors to differentiated cells in the vertebrate retina. Annu Rev Cell Dev Biol. 25, 45-69.

Appelbaum, L. and Gothilf, Y., 2006. Mechanism of pineal-specific gene expression: the role of E-box and photoreceptor conserved elements. Mol Cell Endocrinol. 252, 27-33.

Arnold, S.J. and Robertson, E.J., 2009. Making a commitment: cell lineage allocation and axis patterning in the early mouse embryo. Nat Rev Mol Cell Biol. 10, 91-103.

Asai-Coakwell, M., French, C.R., Berry, K.M., Ye, M., Koss, R., Somerville, M., Mueller, R., van Heyningen, V., Waskiewicz, A.J. and Lehmann, O.J., 2007. GDF6, a novel locus for a spectrum of ocular developmental anomalies. Am J Hum Genet. 80, 306-15.

Asai-Coakwell, M., French, C.R., Ye, M., Garcha, K., Bigot, K., Perera, A.G., Staehling-Hampton, K., Mema, S.C., Chanda, B., Mushegian, A., Bamforth, S., Doschak, M.R., Li, G., Dobbs, M.B., Giampietro, P.F., Brooks, B.P., Vijayalakshmi, P., Sauve, Y., Abitbol, M., Sundaresan, P., van Heyningen, V., Pourquie, O., Underhill, T.M., Waskiewicz, A.J. and Lehmann, O.J., 2009. Incomplete penetrance and phenotypic variability characterize Gdf6-attributable oculo-skeletal phenotypes. Hum Mol Genet. 18, 1110-21.

Asai-Coakwell, M., March, L., Dai, X.H., Duval, M., Lopez, I., French, C.R., Famulski, J., De Baere, E., Francis, P.J., Sundaresan, P., Sauve, Y., Koenekoop, R.K., Berry, F.B., Allison, W.T., Waskiewicz, A.J. and Lehmann, O.J., 2013. Contribution of growth differentiation factor 6-dependent cell survival to early-onset retinal dystrophies. Hum Mol Genet. 22, 1432-42.

Bakrania, P., Efthymiou, M., Klein, J.C., Salt, A., Bunyan, D.J., Wyatt, A., Ponting, C.P., Martin, A., Williams, S., Lindley, V., Gilmore, J., Restori, M., Robson, A.G., Neveu, M.M., Holder, G.E., Collin, J.R., Robinson, D.O., Farndon, P., Johansen-Berg, H., Gerrelli, D. and Ragge, N.K., 2008. Mutations in BMP4 cause eye, brain, and digit developmental anomalies: overlap between the BMP4 and hedgehog signaling pathways. Am J Hum Genet. 82, 304-19.

Barishak, Y.R., 1992. Embryology of the eye and its adnexae. Dev Ophthalmol. 24, 1-142.

Bedell, V.M., Wang, Y., Campbell, J.M., Poshusta, T.L., Starker, C.G., Krug, R.G., 2nd, Tan, W., Penheiter, S.G., Ma, A.C., Leung, A.Y., Fahrenkrug, S.C., Carlson, D.F., Voytas, D.F., Clark, K.J., Essner, J.J. and Ekker, S.C., 2012. In vivo genome editing using a high-efficiency TALEN system. Nature. 491, 114-8.

Behesti, H., Holt, J.K. and Sowden, J.C., 2006. The level of BMP4 signaling is critical for the regulation of distinct T-box gene expression domains and growth along the dorso-ventral axis of the optic cup. BMC Dev Biol. 6, 62.

Bernardos, R.L., Barthel, L.K., Meyers, J.R. and Raymond, P.A., 2007. Late-stage neuronal progenitors in the retina are radial Muller glia that function as retinal stem cells. J Neurosci. 27, 7028-40.

Bibb, L.C., Holt, J.K., Tarttelin, E.E., Hodges, M.D., Gregory-Evans, K., Rutherford, A., Lucas, R.J., Sowden, J.C. and Gregory-Evans, C.Y., 2001. Temporal and spatial expression patterns of the CRX transcription factor and its downstream targets. Critical differences during human and mouse eye development. Hum Mol Genet. 10, 1571-9.

Biehlmaier, O., Neuhauss, S.C. and Kohler, K., 2001. Onset and time course of apoptosis in the developing zebrafish retina. Cell Tissue Res. 306, 199-207.

Bilotta, J., Saszik, S. and Sutherland, S.E., 2001. Rod contributions to the electroretinogram of the dark-adapted developing zebrafish. Dev Dyn. 222, 564-70.

Blaya, M.O., Bramlett, H.M., Naidoo, J., Pieper, A.A. and Dietrich, W.D., 2014. Neuroprotective efficacy of a proneurogenic compound after traumatic brain injury. J Neurotrauma. 31, 476-86.

Bombrun, A., Gerber, P., Casi, G., Terradillos, O., Antonsson, B. and Halazy, S., 2003. 3,6-dibromocarbazole piperazine derivatives of 2-propanol as first inhibitors of cytochrome c release via Bax channel modulation. J Med Chem. 46, 4365-8.

Bookout, A.L., Cummins, C.L., Mangelsdorf, D.J., Pesola, J.M. and Kramer, M.F., 2006. High-throughput real-time quantitative reverse transcription PCR. Curr Protoc Mol Biol. Chapter 15, Unit 15 8.

Branchek, T. and Bremiller, R., 1984. The development of photoreceptors in the zebrafish, Brachydanio rerio. I. Structure. J Comp Neurol. 224, 107-15.

Burrill, J.D. and Easter, S.S., Jr., 1994. Development of the retinofugal projections in the embryonic and larval zebrafish (Brachydanio rerio). J Comp Neurol. 346, 583-600.

Cajal, S.R., 1972. The structure of the retina, C. C. Thomas.

Cermak, T., Doyle, E.L., Christian, M., Wang, L., Zhang, Y., Schmidt, C., Baller, J.A., Somia, N.V., Bogdanove, A.J. and Voytas, D.F., 2011. Efficient design and assembly of custom TALEN and other TAL effector-based constructs for DNA targeting. Nucleic Acids Res. 39, e82.

Chen, S., Wang, Q.L., Nie, Z., Sun, H., Lennon, G., Copeland, N.G., Gilbert, D.J., Jenkins, N.A. and Zack, D.J., 1997. Crx, a novel Otx-like paired-homeodomain protein, binds to and transactivates photoreceptor cell-specific genes. Neuron. 19, 1017-30.

Connaughton, V.P., Graham, D. and Nelson, R., 2004. Identification and morphological classification of horizontal, bipolar, and amacrine cells within the zebrafish retina. J Comp Neurol. 477, 371-85.

Cremers, F.P., van den Hurk, J.A. and den Hollander, A.I., 2002. Molecular genetics of Leber congenital amaurosis. Hum Mol Genet. 11, 1169-76.

Dahm, R., Schonthaler, H.B., Soehn, A.S., van Marle, J. and Vrensen, G.F., 2007. Development and adult morphology of the eye lens in the zebrafish. Exp Eye Res. 85, 74-89.

Daly, F.J. and Sandell, J.H., 2000. Inherited retinal degeneration and apoptosis in mutant zebrafish. Anat Rec. 258, 145-55.

Danno, H., Michiue, T., Hitachi, K., Yukita, A., Ishiura, S. and Asashima, M., 2008. Molecular links among the causative genes for ocular malformation: Otx2 and Sox2 coregulate Rax expression. Proc Natl Acad Sci U S A. 105, 5408-13.

De Jesus-Cortes, H., Xu, P., Drawbridge, J., Estill, S.J., Huntington, P., Tran, S., Britt, J., Tesla, R., Morlock, L., Naidoo, J., Melito, L.M., Wang, G., Williams, N.S., Ready, J.M., McKnight, S.L. and Pieper, A.A., 2012. Neuroprotective efficacy of aminopropyl carbazoles in a mouse model of Parkinson disease. Proc Natl Acad Sci U S A. 109, 17010-5.

den Hollander, A.I., Biyanwila, J., Kovach, P., Bardakjian, T., Traboulsi, E.I., Ragge, N.K., Schneider, A. and Malicki, J., 2010. Genetic defects of GDF6 in the zebrafish out of sight mutant and in human eye developmental anomalies. BMC Genet. 11, 102.

den Hollander, A.I., Roepman, R., Koenekoop, R.K. and Cremers, F.P., 2008. Leber congenital amaurosis: genes, proteins and disease mechanisms. Prog Retin Eye Res. 27, 391-419.

Donner, A.L., Lachke, S.A. and Maas, R.L., 2006. Lens induction in vertebrates: variations on a conserved theme of signaling events. Semin Cell Dev Biol. 17, 676-85.

Easter, S.S., Jr. and Nicola, G.N., 1996. The development of vision in the zebrafish (Danio rerio). Dev Biol. 180, 646-63.

Ekker, S.C. and Larson, J.D., 2001. Morphant technology in model developmental systems. Genesis. 30, 89-93.

Ekstrom, P. and Meissl, H., 2003. Evolution of photosensory pineal organs in new light: the fate of neuroendocrine photoreceptors. Philos Trans R Soc Lond B Biol Sci. 358, 1679-700.

Elmore, S., 2007. Apoptosis: a review of programmed cell death. Toxicol Pathol. 35, 495-516.

Ethell, D.W. and Buhler, L.A., 2003. Fas ligand-mediated apoptosis in degenerative disorders of the brain. J Clin Immunol. 23, 363-70.

Fantes, J., Ragge, N.K., Lynch, S.A., McGill, N.I., Collin, J.R., Howard-Peebles, P.N., Hayward, C., Vivian, A.J., Williamson, K., van Heyningen, V. and FitzPatrick, D.R., 2003. Mutations in SOX2 cause anophthalmia. Nat Genet. 33, 461-3.

Fernandes-Alnemri, T., Litwack, G. and Alnemri, E.S., 1994. CPP32, a novel human apoptotic protein with homology to Caenorhabditis elegans cell death protein Ced-3 and mammalian interleukin-1 beta-converting enzyme. J Biol Chem. 269, 30761-4.

Fleisch, V.C. and Neuhauss, S.C., 2006. Visual behavior in zebrafish. Zebrafish. 3, 191-201.

French, C., 2010. Patterning the zebrafish visual system requires the actions of Pbx transcription factors, and a downstream growth factor, Gdf6a., Biological Sciences. University of Alberta.

French, C.R., Erickson, T., French, D.V., Pilgrim, D.B. and Waskiewicz, A.J., 2009. Gdf6a is required for the initiation of dorsal-ventral retinal patterning and lens development. Dev Biol. 333, 37-47.

French, C.R., Stach, T.R., March, L.D., Lehmann, O.J. and Waskiewicz, A.J., 2013. Apoptotic and proliferative defects characterize ocular development in a microphthalmic BMP model. Invest Ophthalmol Vis Sci. 54, 4636-47.

Freund, C.L., Wang, Q.L., Chen, S., Muskat, B.L., Wiles, C.D., Sheffield, V.C., Jacobson, S.G., McInnes, R.R., Zack, D.J. and Stone, E.M., 1998. De novo mutations in the CRX homeobox gene associated with Leber congenital amaurosis. Nat Genet. 18, 311-2.

Furukawa, T., Morrow, E.M. and Cepko, C.L., 1997. Crx, a novel otx-like homeobox gene, shows photoreceptor-specific expression and regulates photoreceptor differentiation. Cell. 91, 531-41.

Furukawa, T., Morrow, E.M., Li, T., Davis, F.C. and Cepko, C.L., 1999. Retinopathy and attenuated circadian entrainment in Crx-deficient mice. Nat Genet. 23, 466-70.

Gamse, J.T., Shen, Y.C., Thisse, C., Thisse, B., Raymond, P.A., Halpern, M.E. and Liang, J.O., 2002. Otx5 regulates genes that show circadian expression in the zebrafish pineal complex. Nat Genet. 30, 117-21.

Garcia-Valenzuela, E., Shareef, S., Walsh, J. and Sharma, S.C., 1995. Programmed cell death of retinal ganglion cells during experimental glaucoma. Exp Eye Res. 61, 33-44.

Genini, S., Beltran, W.A. and Aguirre, G.D., 2013. Up-regulation of tumor necrosis factor superfamily genes in early phases of photoreceptor degeneration. PLoS One. 8, e85408.

Gerety, S.S. and Wilkinson, D.G., 2011. Morpholino artifacts provide pitfalls and reveal a novel role for pro-apoptotic genes in hindbrain boundary development. Dev Biol. 350, 279-89.

Gestri, G., Link, B.A. and Neuhauss, S.C., 2012. The visual system of zebrafish and its use to model human ocular diseases. Dev Neurobiol. 72, 302-27.

Glaser, T., Jepeal, L., Edwards, J.G., Young, S.R., Favor, J. and Maas, R.L., 1994. PAX6 gene dosage effect in a family with congenital cataracts, aniridia, anophthalmia and central nervous system defects. Nat Genet. 7, 463-71.

Gosse, N.J. and Baier, H., 2009. An essential role for Radar (Gdf6a) in inducing dorsal fate in the zebrafish retina. Proc Natl Acad Sci U S A. 106, 2236-41.

Hanel, M.L. and Hensey, C., 2006. Eye and neural defects associated with loss of GDF6. BMC Dev Biol. 6, 43.

Hata, A., Lagna, G., Massague, J. and Hemmati-Brivanlou, A., 1998. Smad6 inhibits BMP/Smad1 signaling by specifically competing with the Smad4 tumor suppressor. Genes Dev. 12, 186-97.

Hattar, S., Liao, H.W., Takao, M., Berson, D.M. and Yau, K.W., 2002. Melanopsin-containing retinal ganglion cells: architecture, projections, and intrinsic photosensitivity. Science. 295, 1065-70.

Heasman, J., 2002. Morpholino oligos: making sense of antisense? Dev Biol. 243, 209-14.

Heavner, W. and Pevny, L., 2012. Eye development and retinogenesis. Cold Spring Harb Perspect Biol. 4.

Hennig, A.K., Peng, G.H. and Chen, S., 2008. Regulation of photoreceptor gene expression by Crx-associated transcription factor network. Brain Res. 1192, 114-33.

Hill, R.E., Favor, J., Hogan, B.L., Ton, C.C., Saunders, G.F., Hanson, I.M., Prosser, J., Jordan, T., Hastie, N.D. and van Heyningen, V., 1991. Mouse small eye results from mutations in a paired-like homeobox-containing gene. Nature. 354, 522-5.

Hu, M. and Easter, S.S., 1999. Retinal neurogenesis: the formation of the initial central patch of postmitotic cells. Dev Biol. 207, 309-21.

Huang, Y.Y., Haug, M.F., Gesemann, M. and Neuhauss, S.C., 2012. Novel expression patterns of metabotropic glutamate receptor 6 in the zebrafish nervous system. PLoS One. 7, e35256.

Jadhav, A.P., Mason, H.A. and Cepko, C.L., 2006. Notch 1 inhibits photoreceptor production in the developing mammalian retina. Development. 133, 913-23.

Jia, L., Oh, E.C., Ng, L., Srinivas, M., Brooks, M., Swaroop, A. and Forrest, D., 2009. Retinoid-related orphan nuclear receptor RORbeta is an early-acting factor in rod photoreceptor development. Proc Natl Acad Sci U S A. 106, 17534-9.

Kavsak, P., Rasmussen, R.K., Causing, C.G., Bonni, S., Zhu, H., Thomsen, G.H. and Wrana, J.L., 2000. Smad7 binds to Smurf2 to form an E3 ubiquitin ligase that targets the TGF beta receptor for degradation. Mol Cell. 6, 1365-75.

Kerr, J.F., Winterford, C.M. and Harmon, B.V., 1994. Apoptosis. Its significance in cancer and cancer therapy. Cancer. 73, 2013-26.

Kerr, J.F., Wyllie, A.H. and Currie, A.R., 1972. Apoptosis: a basic biological phenomenon with wide-ranging implications in tissue kinetics. Br J Cancer. 26, 239-57.

Kettleborough, R.N., Busch-Nentwich, E.M., Harvey, S.A., Dooley, C.M., de Bruijn, E., van Eeden, F., Sealy, I., White, R.J., Herd, C., Nijman, I.J., Fenyes, F., Mehroke, S., Scahill, C., Gibbons, R., Wali, N., Carruthers, S., Hall, A., Yen, J., Cuppen, E. and Stemple, D.L., 2013. A systematic

genome-wide analysis of zebrafish protein-coding gene function. Nature. 496, 494-7.

Kikuta, H., Kanai, M., Ito, Y. and Yamasu, K., 2003. gbx2 Homeobox gene is required for the maintenance of the isthmic region in the zebrafish embryonic brain. Dev Dyn. 228, 433-50.

Kimmel, C.B., Ballard, W.W., Kimmel, S.R., Ullmann, B. and Schilling, T.F., 1995. Stages of embryonic development of the zebrafish. Dev Dyn. 203, 253-310.

Koenekoop, R.K., 2004. An overview of Leber congenital amaurosis: a model to understand human retinal development. Surv Ophthalmol. 49, 379-98.

Koike, C., Nishida, A., Ueno, S., Saito, H., Sanuki, R., Sato, S., Furukawa, A., Aizawa, S., Matsuo, I., Suzuki, N., Kondo, M. and Furukawa, T., 2007. Functional roles of Otx2 transcription factor in postnatal mouse retinal development. Mol Cell Biol. 27, 8318-29.

Kooistra, M.K., Leduc, R.Y., Dawe, C.E., Fairbridge, N.A., Rasmussen, J., Man, J.H., Bujold, M., Juriloff, D., King-Jones, K. and McDermid, H.E., 2012. Strain-specific modifier genes of Cecr2-associated exencephaly in mice: genetic analysis and identification of differentially expressed candidate genes. Physiol Genomics. 44, 35-46.

Koshiba-Takeuchi, K., Takeuchi, J.K., Matsumoto, K., Momose, T., Uno, K., Hoepker, V., Ogura, K., Takahashi, N., Nakamura, H., Yasuda, K. and Ogura, T., 2000. Tbx5 and the retinotectum projection. Science. 287, 134-7.

Lele, Z., Bakkers, J. and Hammerschmidt, M., 2001. Morpholino phenocopies of the swirl, snailhouse, somitabun, minifin, silberblick, and pipetail mutations. Genesis. 30, 190-4.

Lemke, G. and Reber, M., 2005. Retinotectal mapping: new insights from molecular genetics. Annu Rev Cell Dev Biol. 21, 551-80.

Lemos, M.C., Harding, B., Reed, A.A., Jeyabalan, J., Walls, G.V., Bowl, M.R., Sharpe, J., Wedden, S., Moss, J.E., Ross, A., Davidson, D. and Thakker, R.V., 2009. Genetic background influences embryonic lethality and the occurrence of neural tube defects in Men1 null mice: relevance to genetic modifiers. J Endocrinol. 203, 133-42.

Li, C.J., Friedman, D.J., Wang, C., Metelev, V. and Pardee, A.B., 1995. Induction of apoptosis in uninfected lymphocytes by HIV-1 Tat protein. Science. 268, 429-31.

Li, C.M., Yan, R.T. and Wang, S.Z., 2002. Chick homeobox gene cbx and its role in retinal development. Mech Dev. 116, 85-94.

Li, Z., Joseph, N.M. and Easter, S.S., Jr., 2000. The morphogenesis of the zebrafish eye, including a fate map of the optic vesicle. Dev Dyn. 218, 175-88.

Liu, A. and Niswander, L.A., 2005. Bone morphogenetic protein signalling and vertebrate nervous system development. Nat Rev Neurosci. 6, 945-54.

Liu, W., Lagutin, O., Swindell, E., Jamrich, M. and Oliver, G., 2010. Neuroretina specification in mouse embryos requires Six3-mediated suppression of Wnt8b in the anterior neural plate. J Clin Invest. 120, 3568-77.

Liu, Y., Shen, Y., Rest, J.S., Raymond, P.A. and Zack, D.J., 2001. Isolation and characterization of a zebrafish homologue of the cone rod homeobox gene. Invest Ophthalmol Vis Sci. 42, 481-7.

Lu, A., Ng, L., Ma, M., Kefas, B., Davies, T.F., Hernandez, A., Chan, C.C. and Forrest, D., 2009. Retarded developmental expression and patterning of retinal cone opsins in hypothyroid mice. Endocrinology. 150, 1536-44.

Luo, D.G., Xue, T. and Yau, K.W., 2008. How vision begins: an odyssey. Proc Natl Acad Sci U S A. 105, 9855-62.

Luo, G., Hofmann, C., Bronckers, A.L., Sohocki, M., Bradley, A. and Karsenty, G., 1995. BMP-7 is an inducer of nephrogenesis, and is also required for eye development and skeletal patterning. Genes Dev. 9, 2808-20.

Ma, A.C., Lee, H.B., Clark, K.J. and Ekker, S.C., 2013. High efficiency In Vivo genome engineering with a simplified 15-RVD GoldyTALEN design. PLoS One. 8, e65259.

Mano, H. and Fukada, Y., 2007. A median third eye: pineal gland retraces evolution of vertebrate photoreceptive organs. Photochem Photobiol. 83, 11-8.

Martinez-Caballero, S., Dejean, L.M., Kinnally, M.S., Oh, K.J., Mannella, C.A. and Kinnally, K.W., 2009. Assembly of the mitochondrial apoptosis-induced channel, MAC. J Biol Chem. 284, 12235-45.

Massague, J., Seoane, J. and Wotton, D., 2005. Smad transcription factors. Genes Dev. 19, 2783-810.

Matos-Cruz, V., Blasic, J., Nickle, B., Robinson, P.R., Hattar, S. and Halpern, M.E., 2011. Unexpected diversity and photoperiod dependence of the zebrafish melanopsin system. PLoS One. 6, e25111.

Meeker, N.D., Hutchinson, S.A., Ho, L. and Trede, N.S., 2007. Method for isolation of PCR-ready genomic DNA from zebrafish tissues. Biotechniques. 43, 610, 612, 614.

Meng, X., Noyes, M.B., Zhu, L.J., Lawson, N.D. and Wolfe, S.A., 2008. Targeted gene inactivation in zebrafish using engineered zinc-finger nucleases. Nat Biotechnol. 26, 695-701.

Mitton, K.P., Swain, P.K., Chen, S., Xu, S., Zack, D.J. and Swaroop, A., 2000. The leucine zipper of NRL interacts with the CRX homeodomain. A

possible mechanism of transcriptional synergy in rhodopsin regulation. J Biol Chem. 275, 29794-9.

Miyazono, K., Kamiya, Y. and Morikawa, M., 2010. Bone morphogenetic protein receptors and signal transduction. J Biochem. 147, 35-51.

Morrow, E.M., Furukawa, T., Raviola, E. and Cepko, C.L., 2005. Synaptogenesis and outer segment formation are perturbed in the neural retina of Crx mutant mice. BMC Neurosci. 6, 5.

Muto, A., Orger, M.B., Wehman, A.M., Smear, M.C., Kay, J.N., Page-McCaw, P.S., Gahtan, E., Xiao, T., Nevin, L.M., Gosse, N.J., Staub, W., Finger-Baier, K. and Baier, H., 2005. Forward genetic analysis of visual behavior in zebrafish. PLoS Genet. 1, e66.

Nasevicius, A. and Ekker, S.C., 2000. Effective targeted gene 'knockdown' in zebrafish. Nat Genet. 26, 216-20.

Neuhauss, S.C., Biehlmaier, O., Seeliger, M.W., Das, T., Kohler, K., Harris, W.A. and Baier, H., 1999. Genetic disorders of vision revealed by a behavioral screen of 400 essential loci in zebrafish. J Neurosci. 19, 8603-15.

Ng, L., Hurley, J.B., Dierks, B., Srinivas, M., Salto, C., Vennstrom, B., Reh, T.A. and Forrest, D., 2001. A thyroid hormone receptor that is required for the development of green cone photoreceptors. Nat Genet. 27, 94-8.

Nicholson, D.W., Ali, A., Thornberry, N.A., Vaillancourt, J.P., Ding, C.K., Gallant, M., Gareau, Y., Griffin, P.R., Labelle, M., Lazebnik, Y.A. and et al., 1995. Identification and inhibition of the ICE/CED-3 protease necessary for mammalian apoptosis. Nature. 376, 37-43.

Nijhawan, D., Honarpour, N. and Wang, X., 2000. Apoptosis in neural development and disease. Annu Rev Neurosci. 23, 73-87.

Nishida, A., Furukawa, A., Koike, C., Tano, Y., Aizawa, S., Matsuo, I. and Furukawa, T., 2003. Otx2 homeobox gene controls retinal

photoreceptor cell fate and pineal gland development. Nat Neurosci. 6, 1255-63.

Nohe, A., Keating, E., Knaus, P. and Petersen, N.O., 2004. Signal transduction of bone morphogenetic protein receptors. Cell Signal. 16, 291-9.

Oh, E.C., Cheng, H., Hao, H., Jia, L., Khan, N.W. and Swaroop, A., 2008. Rod differentiation factor NRL activates the expression of nuclear receptor NR2E3 to suppress the development of cone photoreceptors. Brain Res. 1236, 16-29.

Onichtchouk, D., Chen, Y.G., Dosch, R., Gawantka, V., Delius, H., Massague, J. and Niehrs, C., 1999. Silencing of TGF-beta signalling by the pseudoreceptor BAMBI. Nature. 401, 480-5.

Onwochei, B.C., Simon, J.W., Bateman, J.B., Couture, K.C. and Mir, E., 2000. Ocular colobomata. Surv Ophthalmol. 45, 175-94.

Opferman, J.T. and Korsmeyer, S.J., 2003. Apoptosis in the development and maintenance of the immune system. Nat Immunol. 4, 410-5.

Orger, M.B. and Baier, H., 2005. Channeling of red and green cone inputs to the zebrafish optomotor response. Vis Neurosci. 22, 275-81.

Orger, M.B., Gahtan, E., Muto, A., Page-McCaw, P., Smear, M.C. and Baier, H., 2004. Behavioral screening assays in zebrafish. Methods Cell Biol. 77, 53-68.

Orger, M.B., Kampff, A.R., Severi, K.E., Bollmann, J.H. and Engert, F., 2008. Control of visually guided behavior by distinct populations of spinal projection neurons. Nat Neurosci. 11, 327-33.

Otteson, D.C. and Hitchcock, P.F., 2003. Stem cells in the teleost retina: persistent neurogenesis and injury-induced regeneration. Vision Res. 43, 927-36.

Pant, S.D., March, L.D., Famulski, J.K., French, C.R., Lehmann, O.J. and Waskiewicz, A.J., 2013. Molecular mechanisms regulating ocular

apoptosis in zebrafish gdf6a mutants. Invest Ophthalmol Vis Sci. 54, 5871-9.

Peixoto, P.M., Ryu, S.Y., Bombrun, A., Antonsson, B. and Kinnally, K.W., 2009. MAC inhibitors suppress mitochondrial apoptosis. Biochem J. 423, 381-7.

Peng, G.H., Ahmad, O., Ahmad, F., Liu, J. and Chen, S., 2005. The photoreceptor-specific nuclear receptor Nr2e3 interacts with Crx and exerts opposing effects on the transcription of rod versus cone genes. Hum Mol Genet. 14, 747-64.

Peng, G.H. and Chen, S., 2007. Crx activates opsin transcription by recruiting HAT-containing co-activators and promoting histone acetylation. Hum Mol Genet. 16, 2433-52.

Perrault, I., Rozet, J.M., Gerber, S., Ghazi, I., Leowski, C., Ducroq, D., Souied, E., Dufier, J.L., Munnich, A. and Kaplan, J., 1999. Leber congenital amaurosis. Mol Genet Metab. 68, 200-8.

Pieper, A.A., McKnight, S.L. and Ready, J.M., 2014. P7C3 and an unbiased approach to drug discovery for neurodegenerative diseases. Chem Soc Rev.

Pieper, A.A., Xie, S., Capota, E., Estill, S.J., Zhong, J., Long, J.M., Becker, G.L., Huntington, P., Goldman, S.E., Shen, C.H., Capota, M., Britt, J.K., Kotti, T., Ure, K., Brat, D.J., Williams, N.S., MacMillan, K.S., Naidoo, J., Melito, L., Hsieh, J., De Brabander, J., Ready, J.M. and McKnight, S.L., 2010. Discovery of a proneurogenic, neuroprotective chemical. Cell. 142, 39-51.

Pillay, L.M., Selland, L.G., Fleisch, V.C., Leighton, P.L., Cheng, C.S., Famulski, J.K., Ritzel, R.G., March, L.D., Wang, H., Allison, W.T. and Waskiewicz, A.J., 2013. Evaluating the Mutagenic Activity of Targeted Endonucleases Containing a Sharkey FokI Cleavage Domain Variant in Zebrafish. Zebrafish. 10, 353-64.

Plouhinec, J.L., Sauka-Spengler, T., Germot, A., Le Mentec, C., Cabana, T., Harrison, G., Pieau, C., Sire, J.Y., Veron, G. and Mazan, S., 2003. The mammalian Crx genes are highly divergent representatives of the Otx5 gene family, a gnathostome orthology class of orthodenticle-related homeogenes involved in the differentiation of retinal photoreceptors and circadian entrainment. Mol Biol Evol. 20, 513-21.

Porter, F.D., Drago, J., Xu, Y., Cheema, S.S., Wassif, C., Huang, S.P., Lee, E., Grinberg, A., Massalas, J.S., Bodine, D., Alt, F. and Westphal, H., 1997. Lhx2, a LIM homeobox gene, is required for eye, forebrain, and definitive erythrocyte development. Development. 124, 2935-44.

Portera-Cailliau, C., Sung, C.H., Nathans, J. and Adler, R., 1994. Apoptotic photoreceptor cell death in mouse models of retinitis pigmentosa. Proc Natl Acad Sci U S A. 91, 974-8.

Porteus, M.H. and Carroll, D., 2005. Gene targeting using zinc finger nucleases. Nat Biotechnol. 23, 967-73.

Postlethwait, J.H., Yan, Y.L., Gates, M.A., Horne, S., Amores, A., Brownlie, A., Donovan, A., Egan, E.S., Force, A., Gong, Z., Goutel, C., Fritz, A., Kelsh, R., Knapik, E., Liao, E., Paw, B., Ransom, D., Singer, A., Thomson, M., Abduljabbar, T.S., Yelick, P., Beier, D., Joly, J.S., Larhammar, D., Rosa, F., Westerfield, M., Zon, L.I., Johnson, S.L. and Talbot, W.S., 1998. Vertebrate genome evolution and the zebrafish gene map. Nat Genet. 18, 345-9.

Potts, R.A., Dreher, B. and Bennett, M.R., 1982. The loss of ganglion cells in the developing retina of the rat. Brain Res. 255, 481-6.

Provencio, I., Rollag, M.D. and Castrucci, A.M., 2002. Photoreceptive net in the mammalian retina. This mesh of cells may explain how some blind mice can still tell day from night. Nature. 415, 493.

Ragge, N.K., Brown, A.G., Poloschek, C.M., Lorenz, B., Henderson, R.A., Clarke, M.P., Russell-Eggitt, I., Fielder, A., Gerrelli, D., Martinez-

Barbera, J.P., Ruddle, P., Hurst, J., Collin, J.R., Salt, A., Cooper, S.T., Thompson, P.J., Sisodiya, S.M., Williamson, K.A., Fitzpatrick, D.R., van Heyningen, V. and Hanson, I.M., 2005. Heterozygous mutations of OTX2 cause severe ocular malformations. Am J Hum Genet. 76, 1008-22.

Ranade, S.S., Yang-Zhou, D., Kong, S.W., McDonald, E.C., Cook, T.A. and Pignoni, F., 2008. Analysis of the Otd-dependent transcriptome supports the evolutionary conservation of CRX/OTX/OTD functions in flies and vertebrates. Dev Biol. 315, 521-34.

Raymond, P.A., 1985. Cytodifferentiation of photoreceptors in larval goldfish: delayed maturation of rods. J Comp Neurol. 236, 90-105.

Raymond, P.A., Barthel, L.K., Bernardos, R.L. and Perkowski, J.J., 2006. Molecular characterization of retinal stem cells and their niches in adult zebrafish. BMC Dev Biol. 6, 36.

Raymond, P.A., Barthel, L.K. and Curran, G.A., 1995. Developmental patterning of rod and cone photoreceptors in embryonic zebrafish. J Comp Neurol. 359, 537-50.

Raymond, P.A. and Rivlin, P.K., 1987. Germinal cells in the goldfish retina that produce rod photoreceptors. Dev Biol. 122, 120-38.

Reed, G.H., Kent, J.O. and Wittwer, C.T., 2007. High-resolution DNA melting analysis for simple and efficient molecular diagnostics. Pharmacogenomics. 8, 597-608.

Rehemtulla, A., Warwar, R., Kumar, R., Ji, X., Zack, D.J. and Swaroop, A., 1996. The basic motif-leucine zipper transcription factor Nrl can positively regulate rhodopsin gene expression. Proc Natl Acad Sci U S A. 93, 191-5.

Rhinn, M., Lun, K., Ahrendt, R., Geffarth, M. and Brand, M., 2009. Zebrafish gbx1 refines the midbrain-hindbrain boundary border and mediates the Wnt8 posteriorization signal. Neural Dev. 4, 12.

Riera, M., Burguera, D., Garcia-Fernandez, J. and Gonzalez-Duarte, R., 2013. CERKL knockdown causes retinal degeneration in zebrafish. PLoS One. 8, e64048.

Rinner, O., Rick, J.M. and Neuhauss, S.C., 2005. Contrast sensitivity, spatial and temporal tuning of the larval zebrafish optokinetic response. Invest Ophthalmol Vis Sci. 46, 137-42.

Robinson, J., Schmitt, E.A., Harosi, F.I., Reece, R.J. and Dowling, J.E., 1993. Zebrafish ultraviolet visual pigment: absorption spectrum, sequence, and localization. Proc Natl Acad Sci U S A. 90, 6009-12.

Robu, M.E., Larson, J.D., Nasevicius, A., Beiraghi, S., Brenner, C., Farber, S.A. and Ekker, S.C., 2007. p53 activation by knockdown technologies. PLoS Genet. 3, e78.

Roger, J.E., Hiriyanna, A., Gotoh, N., Hao, H., Cheng, D.F., Ratnapriya, R., Kautzmann, M.A., Chang, B. and Swaroop, A., 2014. OTX2 loss causes rod differentiation defect in CRX-associated congenital blindness. J Clin Invest. 124, 631-43.

Sakuta, H., Takahashi, H., Shintani, T., Etani, K., Aoshima, A. and Noda, M., 2006. Role of bone morphogenic protein 2 in retinal patterning and retinotectal projection. J Neurosci. 26, 10868-78.

Sancho-Pelluz, J., Arango-Gonzalez, B., Kustermann, S., Romero, F.J., van Veen, T., Zrenner, E., Ekstrom, P. and Paquet-Durand, F., 2008. Photoreceptor cell death mechanisms in inherited retinal degeneration. Mol Neurobiol. 38, 253-69.

Sauka-Spengler, T., Baratte, B., Shi, L. and Mazan, S., 2001. Structure and expression of an Otx5-related gene in the dogfish Scyliorhinus canicula: evidence for a conserved role of Otx5 and Crxgenes in the specification of photoreceptors. Dev Genes Evol. 211, 533-44.

Saunders, J.W., Jr. and Gasseling, M.T., 1962. Cellular death in morphogenesis of the avian wing. Dev Biol. 5, 147-78.

Savill, J. and Fadok, V., 2000. Corpse clearance defines the meaning of cell death. Nature. 407, 784-8.

Schmitt, E.A. and Dowling, J.E., 1994. Early eye morphogenesis in the zebrafish, Brachydanio rerio. J Comp Neurol. 344, 532-42.

Schmitt, E.A. and Dowling, J.E., 1996. Comparison of topographical patterns of ganglion and photoreceptor cell differentiation in the retina of the zebrafish, Danio rerio. J Comp Neurol. 371, 222-34.

Schmitt, E.A. and Dowling, J.E., 1999. Early retinal development in the zebrafish, Danio rerio: light and electron microscopic analyses. J Comp Neurol. 404, 515-36.

Schulte, D., Furukawa, T., Peters, M.A., Kozak, C.A. and Cepko, C.L., 1999. Misexpression of the Emx-related homeobox genes cVax and mVax2 ventralizes the retina and perturbs the retinotectal map. Neuron. 24, 541-53.

Sengelaub, D.R., Dolan, R.P. and Finlay, B.L., 1986. Cell generation, death, and retinal growth in the development of the hamster retinal ganglion cell layer. J Comp Neurol. 246, 527-43.

Seo, H.C., Drivenes, Ellingsen, S. and Fjose, A., 1998. Expression of two zebrafish homologues of the murine Six3 gene demarcates the initial eye primordia. Mech Dev. 73, 45-57.

Shen, Y.C. and Raymond, P.A., 2004. Zebrafish cone-rod (crx) homeobox gene promotes retinogenesis. Dev Biol. 269, 237-51.

Shu, X., Zeng, Z., Gautier, P., Lennon, A., Gakovic, M., Cheetham, M.E., Patton, E.E. and Wright, A.F., 2011. Knockdown of the zebrafish ortholog of the retinitis pigmentosa 2 (RP2) gene results in retinal degeneration. Invest Ophthalmol Vis Sci. 52, 2960-6.

Sieber, C., Kopf, J., Hiepen, C. and Knaus, P., 2009. Recent advances in BMP receptor signaling. Cytokine Growth Factor Rev. 20, 343-55.

Silva, E., Yang, J.M., Li, Y., Dharmaraj, S., Sundin, O.H. and Maumenee, I.H., 2000. A CRX null mutation is associated with both Leber congenital amaurosis and a normal ocular phenotype. Invest Ophthalmol Vis Sci. 41, 2076-9.

Simonis, M., Kooren, J. and de Laat, W., 2007. An evaluation of 3C-based methods to capture DNA interactions. Nat Methods. 4, 895-901.

Slee, E.A., Adrain, C. and Martin, S.J., 2001. Executioner caspase-3, -6, and -7 perform distinct, non-redundant roles during the demolition phase of apoptosis. J Biol Chem. 276, 7320-6.

Sohocki, M.M., Sullivan, L.S., Mintz-Hittner, H.A., Birch, D., Heckenlively, J.R., Freund, C.L., McInnes, R.R. and Daiger, S.P., 1998. A range of clinical phenotypes associated with mutations in CRX, a photoreceptor transcription-factor gene. Am J Hum Genet. 63, 1307-15.

Souchelnytskyi, S., Nakayama, T., Nakao, A., Moren, A., Heldin, C.H., Christian, J.L. and ten Dijke, P., 1998. Physical and functional interaction of murine and Xenopus Smad7 with bone morphogenetic protein receptors and transforming growth factor-beta receptors. J Biol Chem. 273, 25364-70.

Srinivas, M., Ng, L., Liu, H., Jia, L. and Forrest, D., 2006. Activation of the blue opsin gene in cone photoreceptor development by retinoid-related orphan receptor beta. Mol Endocrinol. 20, 1728-41.

Stenkamp, D.L., 2007. Neurogenesis in the fish retina. Int Rev Cytol. 259, 173-224.

Su, C.Y., Kemp, H.A. and Moens, C.B., 2014. Cerebellar development in the absence of Gbx function in zebrafish. Dev Biol. 386, 181-90.

Swaroop, A., Kim, D. and Forrest, D., 2010. Transcriptional regulation of photoreceptor development and homeostasis in the mammalian retina. Nat Rev Neurosci. 11, 563-76.

Swaroop, A., Wang, Q.L., Wu, W., Cook, J., Coats, C., Xu, S., Chen, S., Zack, D.J. and Sieving, P.A., 1999. Leber congenital amaurosis caused by a homozygous mutation (R90W) in the homeodomain of the retinal transcription factor CRX: direct evidence for the involvement of CRX in the development of photoreceptor function. Hum Mol Genet. 8, 299-305.

Tait, S.W. and Green, D.R., 2010. Mitochondria and cell death: outer membrane permeabilization and beyond. Nat Rev Mol Cell Biol. 11, 621-32.

Take-uchi, M., Clarke, J.D. and Wilson, S.W., 2003. Hedgehog signalling maintains the optic stalk-retinal interface through the regulation of Vax gene activity. Development. 130, 955-68.

Takechi, M., Hamaoka, T. and Kawamura, S., 2003. Fluorescence visualization of ultraviolet-sensitive cone photoreceptor development in living zebrafish. FEBS Lett. 553, 90-4.

Takechi, M., Seno, S. and Kawamura, S., 2008. Identification of cis-acting elements repressing blue opsin expression in zebrafish UV cones and pineal cells. J Biol Chem. 283, 31625-32.

Taylor, D., 2007. Developmental abnormalities of the optic nerve and chiasm. Eye (Lond). 21, 1271-84.

Tesla, R., Wolf, H.P., Xu, P., Drawbridge, J., Estill, S.J., Huntington, P., McDaniel, L., Knobbe, W., Burket, A., Tran, S., Starwalt, R., Morlock, L., Naidoo, J., Williams, N.S., Ready, J.M., McKnight, S.L. and Pieper, A.A., 2012. Neuroprotective efficacy of aminopropyl carbazoles in a mouse model of amyotrophic lateral sclerosis. Proc Natl Acad Sci U S A. 109, 17016-21.

Tewari, M., Quan, L.T., O'Rourke, K., Desnoyers, S., Zeng, Z., Beidler, D.R., Poirier, G.G., Salvesen, G.S. and Dixit, V.M., 1995. Yama/CPP32 beta, a mammalian homolog of CED-3, is a CrmA-inhibitable protease that

cleaves the death substrate poly(ADP-ribose) polymerase. Cell. 81, 801-9.

Thisse, C. and Thisse, B., 2008. High-resolution in situ hybridization to whole-mount zebrafish embryos. Nat Protoc. 3, 59-69.

van der Sar, A.M., Zivkovic, D. and den Hertog, J., 2002. Eye defects in receptor protein-tyrosine phosphatase alpha knock-down zebrafish. Dev Dyn. 223, 292-7.

Verma, A.S. and Fitzpatrick, D.R., 2007. Anophthalmia and microphthalmia. Orphanet J Rare Dis. 2, 47.

Viringipurampeer, I.A., Shan, X., Gregory-Evans, K., Zhang, J.P., Mohammadi, Z. and Gregory-Evans, C.Y., 2014. Rip3 knockdown rescues photoreceptor cell death in blind pde6c zebrafish. Cell Death Differ.

Voronina, V.A., Kozhemyakina, E.A., O'Kernick, C.M., Kahn, N.D., Wenger, S.L., Linberg, J.V., Schneider, A.S. and Mathers, P.H., 2004. Mutations in the human RAX homeobox gene in a patient with anophthalmia and sclerocornea. Hum Mol Genet. 13, 315-22.

Walther, C. and Gruss, P., 1991. Pax-6, a murine paired box gene, is expressed in the developing CNS. Development. 113, 1435-49.

Wang, K.S., Zahn, L.E., Favor, J., Huang, K.M. and Stambolian, D., 2005. Genetic and phenotypic analysis of Tcm, a mutation affecting early eye development. Mamm Genome. 16, 332-43.

Westerfield, M., 2007. The zebrafish book. A guide for the laboratory use of zebrafish (Danio rerio). 5th ed., University of Oregon Press, Eugene, OR.

Wong, R.O. and Hughes, A., 1987. Role of cell death in the topogenesis of neuronal distributions in the developing cat retinal ganglion cell layer. J Comp Neurol. 262, 496-511.

Wyatt, A.W., Osborne, R.J., Stewart, H. and Ragge, N.K., 2010. Bone morphogenetic protein 7 (BMP7) mutations are associated with variable ocular, brain, ear, palate, and skeletal anomalies. Hum Mutat. 31, 781-7.

Yahyavi, M., Abouzeid, H., Gawdat, G., de Preux, A.S., Xiao, T., Bardakjian, T., Schneider, A., Choi, A., Jorgenson, E., Baier, H., El Sada, M., Schorderet, D.F. and Slavotinek, A.M., 2013. ALDH1A3 loss of function causes bilateral anophthalmia/microphthalmia and hypoplasia of the optic nerve and optic chiasm. Hum Mol Genet. 22, 3250-8.

Ye, M., Berry-Wynne, K.M., Asai-Coakwell, M., Sundaresan, P., Footz, T., French, C.R., Abitbol, M., Fleisch, V.C., Corbett, N., Allison, W.T., Drummond, G., Walter, M.A., Underhill, T.M., Waskiewicz, A.J. and Lehmann, O.J., 2010. Mutation of the bone morphogenetic protein GDF3 causes ocular and skeletal anomalies. Hum Mol Genet. 19, 287-98.

Zarubin, T. and Han, J., 2005. Activation and signaling of the p38 MAP kinase pathway. Cell Res. 15, 11-8.

Zhang, C., Song, Y., Thompson, D.A., Madonna, M.A., Millhauser, G.L., Toro, S., Varga, Z., Westerfield, M., Gamse, J., Chen, W. and Cone, R.D., 2010. Pineal-specific agouti protein regulates teleost background adaptation. Proc Natl Acad Sci U S A. 107, 20164-71.

Zhang, L., Mathers, P.H. and Jamrich, M., 2000. Function of Rx, but not Pax6, is essential for the formation of retinal progenitor cells in mice. Genesis. 28, 135-42.

Zhang, X., Li, S., Xiao, X., Jia, X., Wang, P., Shen, H., Guo, X. and Zhang, Q., 2009. Mutational screening of 10 genes in Chinese patients with microphthalmia and/or coloboma. Mol Vis. 15, 2911-8.

Zhao, X.F., Ellingsen, S. and Fjose, A., 2009. Labelling and targeted ablation of specific bipolar cell types in the zebrafish retina. BMC Neurosci. 10, 107.